ARTIFICIAL INTELLIGENCE
APPLIED TO
BRIDGE DECK RADAR INTERPRETATION

By
DAREL EDWARD MESHER, B.Eng., M.Eng.

A Thesis
Submitted to the School of Graduate Studies
in Partial Fulfillment of the Requirements
for the Degree of
Doctor of Philosophy

McMaster University

ARTIFICIAL INTELLIGENCE

APPLIED TO

BRIDGE DECK RADAR INTERPRETATION

DOCTOR OF PHILOSOPHY (1992)
(Electrical Engineering)

MCMASTER UNIVERSITY
Hamilton, Ontario

TITLE: Artificial Intelligence Applied to Bridge Deck Radar Interpretation

AUTHOR: Darel Edward Mesher, B.Eng., M.Eng. (McMaster University)

SUPERVISOR: Dr. W.F.S. Poehlman

NUMBER OF PAGES: xv, 182

Abstract

The use of ground probing radar for the nondestructive evaluation of structures has been in use for more than a decade. Through the examination of the subsurface reflection waveforms, determinations may be made regarding the profile geometry as well as detecting the presence of structural faults undetectable from surface inspections. Although automated systems have been previously created, the arduous task of interpretation of the large volumes of data produced by these radar surveys are still best handled by human experts.

The research presented in this dissertation details the development of novel techniques which allow an Artificial Intelligence based system to demonstrate comprehensive structural and fault analysis capabilities. Development of an autonomously defined and system trained neural network based radar waveform filter allows reflection event feature extraction. The three-dimensional concept of the bridge structures and the system's ability to accurately model the diverse cross-sections are combined with the neural preprocessed data to allow data abstraction. The positional relationships present in bridge radar surveys are exploited to develop a unique spatiotemporal foundation for analysis. The comprehensive expert system was tested with real bridge radar data and the system results correlate well with human expert analysis.

Acknowledgments

I would like to express my deepest and most sincere thanks to my supervisor and mentor, Skip Poehlman. I simply hope that I will carry with me some of the boundless enthusiasm he has demonstrated during the tenure of this research. I was extremely fortunate to have the insight to approach Skip at the start of my graduate career.

I am also indebted to Dr. Jamie Rossiter for making me accutely aware of the significance of an accurate and intelligent approach to GPR analysis. Many of the subtle interpretation details included in the approach originated from our discussions.

A warm thanks is extended to the team of people lovingly referred to as the *support crew*; Dan Trottier, for rising to all the challenges that I presented him, including perfecting the grey scale conversion routines and some of the most conscientious technical proof reading. Sandy Raiser-Trottier, for doing her best at translating many scribbled fragments into english prose. John Nakamura, for repeating those immortal words "Oh...you can do anything in TEX!" and solving many of the inexplicable typesetting problems (and introducing a few...). And a special thanks to Jorge Ulloa for almost understanding the details which presented the most challenges, and the many discussions that followed.

And of course a loving thanks to my wife, Terry. She provided seemingly endless support and demonstrated boundless patience (in conjuction with all the meticulous proof reading, reference checks and typing). Terry, it only seems like a decade.

A warm acknowldgement is given to Les Davis and Louis Lalumiere of Canpolar

Inc. for enthusiastically snapping my initial attempts at radar interpretation back to reality (to within a first order). The interactions and discussions are deeply appreciated.

An honourable mention must be given to the folks at Sun Microsystems for providing the IPX workstation which allowed the transition of this typesetting nightmare into a reality.

Contents

Abstract iii

Acknowledgments iv

1 Introduction 1

1.1 Background 1

1.2 Current Radar Interpretation 3

1.3 A Multi-Disciplinary Approach to Radar Survey Interpretation 5

1.4 Scope of This Work 7

2 Foundations 8

2.1 Bridge Structures 8

2.1.1 Building Code Development 11

2.1.2 Construction Practices 12

2.1.3 Surface Coatings and Membranes 13

2.1.4 Defect Manifestations 15

2.1.5 Repair Methodology 16

2.2 Radar 17

2.2.1 Radar Backscattering 18

2.2.2 Wave Velocity 20

2.2.3 Material Properties 22
2.2.4 Permittivity Calculation 24
2.2.5 Non-Specular Surfaces 25
2.2.6 Antenna Height Variation 27
2.2.7 Non-Planar Surfaces 29
2.2.8 Air Void Displacement 30
2.2.9 Embedded Steel 32
2.3 Conclusion 34

3 The Inverse Problem **35**
3.1 Introduction 35
3.2 Nonparametric Approaches 37
3.2.1 Steinway at Georgia Institute of Technology 37
3.2.2 Nonparametric Representation Extensions 39
3.3 Parametric Representation 42
3.4 Conclusion 46

4 Expert Systems Approach **47**
4.1 Introduction 47
4.2 Blackboard Systems 49
4.2.1 Control 50
4.3 GPR Bridge Data 52
4.3.1 Data Representation 53
4.3.2 Knowledge Sources 55
4.4 Radar Expert System Design 56
4.4.1 Quantitative Analysis 56
4.4.2 Qualitative Physics 60
4.4.3 Qualitative Model 61

4.4.4 Temporal Reasoning 62
4.4.5 Spatial Reasoning 63
4.4.6 Causal Reasoning 64
4.4.7 Spatial Parameter Thresholds 67
4.4.8 Cross-Sectional Modeling 67
4.4.9 Top-level Agenda Controller 68
4.5 Conclusions 70

5 System Development **72**
5.0.1 System Hardware 72
5.0.2 The Expert System Shell 73
5.0.3 Extensibility 74
5.1 Knowledge Based System 75
5.2 Cross-section Modeling 79
5.2.1 Modeling Procedure 82
5.3 Subsymbolic Data Reduction 86
5.3.1 Peak Detection 88
5.3.2 Sum-Squared-Error Wavelet Classification 90
5.3.3 Neural Network 91
5.3.4 Data Segmentation 99
5.3.5 Layer Detection 101
5.4 Data Alignment 102
5.5 Pre-Analysis 106
5.5.1 Cross-Section Identification 106
5.5.2 Thin Asphalt Layer Events 107
5.5.3 Rough Surface Effects 108
5.5.4 Vehicle Acceleration Effects 110

6 Discussion 113

6.1 Introduction 113

6.2 Modeling Capabilities 113

6.3 MTO Data Analysis System 115

6.3.1 MTO Analysis 117

6.3.2 Expert System Analysis 117

6.4 Spatial and Temporal Analysis 118

6.4.1 Spatial Analysis and Fault Identification 124

7 Conclusions and Recommendations 131

7.1 Summary 131

7.2 Conclusions 132

7.2.1 Recommendations 135

A Ontario Bridge Building Code 138

A.1 Ontario Building Codes; Pre-1958 to Present 138

B Cobbledick Road Bridge-Physical Plan 140

B.1 Physical Specifications 140

C Bridge Radar Data 143

C.1 Raw Data 144

C.2 Segmented Data 148

C.3 Layered Data 152

D Expert System Dialogs 156

E Expert System Inferencing Samples 162

E.1 Cross-Sectional Modeling Output 163

E.2 Acceleration Related Amplitude Analysis 164

E.3 Wheel Rut Related Amplitude Analysis 165

F System Tangle Graphs **166**

List of Tables

2.1 Radius of Curvature for Troughs of Various Widths and Depths . . . 30

List of Figures

1.1 Cross Sectional Model and Radar Reflections 4
2.1 Bridge Constructions by Decade 1900-Present 9
2.2 Province of Ontario Bridge Types 10
2.3 Slab-On-Girder Bridge Structural Components 11
2.4 Common Slab Bridge Configurations 12
2.5 Transmit Waveform and Wide Bandwidth Spectrum 18
2.6 Layered Dielectric Material Structure 19
2.7 Electrical Properties Model 20
2.8 Monopulse Transmit Wavelet 22
2.9 Cantilever Mounted Air-Launch Radar Antenna 29
2.10 Impregnated Concrete Permittivity 31
2.11 Splayed Transmission Line Antenna Illumination Area 33
2.12 Rebar Illumination Based on Antenna Orientation and Placement . . 34
3.1 Incident And Reflected Waves 36
3.2 Georgia Institute of Technology Layered Models 38
3.3 McMaster University Layered Models 40
4.1 Top Level Control Strategy 52
4.2 GPR Data Acquisition Paths 53
4.3 GPR Tiered Data Hierarchy 54
4.4 System Frames and Associated Slots 55

4.5 GPR System Knowledge Bases 56
4.6 Optimum Waveform Deconvolution Sites 57
4.7 Neural Network Peak Classifier 59
4.8 Three Layered Structure 62
4.9 Cell Level Orthogonal Neighborhood 64
4.10 Two Cross-Sectional Waveforms 69
4.11 Top-level controller cell analysis agenda 70
5.1 User Input Session for System Initialization 77
5.2 Cross-Sectional Modeling Operation 81
5.3 Expert System Produced Cross-Sectional Models 85
5.4 Two Step GPR Data Preprocessing Procedure 87
5.5 Peak Detection- Zero Crossing Approximations 89
5.6 Filtered and Peak Detected Radar Line Data 90
5.7 Sum Squared Error Wavelet Classifier 91
5.8 Neural Network Node and Activation Function 92
5.9 Wavelet Sample Points for Neural Network Inputs 94
5.10 Conjugate Gradient Descent Training Error 98
5.11 Segment Search Patterns 100
5.12 Radar Data Segmentation Operation 101
5.13 Layer Module Output 103
5.14 Boundary Radar Reflection Events 104
5.15 Segment Breakpoints used for Data Set Alignment 105
5.16 System Detected Cross-Sections 107
5.17 Thin Asphalt Events 108
5.18 Elevated Surface Amplitude Events 109
5.19 Antenna Displacement Events 112
6.1 Bottom-of-Deck Cross-section Detection 114

6.2 MTO Analysis Error 116
6.3 MTO Radar Analysis Results 118
6.4 Expert System Results: ORIGINAL DATA INTERPRETATION 119
6.5 Expert System Results: WHEEL RUT COMPENSATION 120
6.6 Expert System Results: RUT and ACCELERATION COMPENSATION . . 121
6.7 Expert System Results - Layer Permittivities 122
6.8 Qualitative Reasoning: Layer Dielectric Variations 124
6.9 Qualitative Reasoning: Layer Thickness Variations 125
6.10 Asphalt/Concrete Interface Amplitude Faults 126
6.11 Asphalt/Concrete Interface Position Faults 127
6.12 Rebar Interface Amplitude Faults 127
6.13 Two-Lift Delaminated Asphalt Faults 128
6.14 Expert System Final Analysis: Layer Thickness 129
6.15 Expert System Final Analysis: Layer Permittivities 130
B.1 Cobbledick Road Physical Site Plan- Top view and Data Positions . . 141
B.2 Cobbledick Road Physical Site Plan- Cross-Sections 142
C.1 Cobbledick Road Raw Data Dump (Lines 1 to 3) 145
C.2 Cobbledick Road Raw Data Dump (Lines 4 to 6) 146
C.3 Cobbledick Road Raw Data Dump (Lines 7 and 8) 147
C.4 Cobbledick Road Segmented Data (Lines 1 to 3) 149
C.5 Cobbledick Road Segmented Data (Lines 4 to 6) 150
C.6 Cobbledick Road Segmented Data (Lines 7 and 8) 151
C.7 Cobbledick Road Layered Data (Lines 1 to 3) 153
C.8 Cobbledick Road Layered Data (Lines 4 to 6) 154
C.9 Cobbledick Road Layered Data (Lines 7 and 8) 155
D.1 System Site Configuration Dialog1 157
D.2 System Site Configuration Dialog 2 158

D.3 System Data File Configuration Dialog 159
D.4 System Core Specification Dialog 1 160
D.5 System Core Specification Dialog 2 161
F.1 BRIDGES KB Tangle Graph 167
F.2 DATA KB Tangle Graph 167
F.3 NNET KB Tangle Graph 168
F.4 RADARS KB Tangle Graph 168
F.5 Rule Base Fragment Tangle Graph 169

Chapter 1

Introduction

1.1 Background

Coincidental with the construction of the first engineered structures were the formalization of the methods for their non-destructive evaluation. Many government agencies (including the provincial government of Ontario[1]) are attempting to establish procedures for maintenance of the highway infrastructure. This maintenance strategy includes post-construction evaluation of new bridge decks but is focused primarily on the frequent re-examinations of older structures. Biennial examinations of mature structures are required due to antiquated building codes used during construction and the approach of expected structure life span [MANN83a, MANN83b, MANN83c]. In the past two decades extensive research and development effort has been concentrated on the determination of optimum evaluation techniques for bridge structures. Initial studies investigated a multitude of methodologies for structural evaluation

[1]Much of the factual information presented in the following background sections was obtained through the extensive research and development publications available from Ontario's Ministry of Transportation (MTO) (formerly the Ministry of Transportation and Communications (MTC)). The MTO is an established entity for materials, mechanical and civil engineering research and development and may be considered representative of currently active government highway maintenance agencies.

[MANN82]. The criteria for the ideal test procedure have changed little and were specified in [MANN82] as exhibiting the following properties:

1. independent of deck structure
2. nondestructive
3. performed at the top surface
4. fast
5. inexpensive
6. accurate

Of the examined evaluation methods, radar and infrared thermography[2] (IRT), were recommended for continued development into Ministry of Transportation of Ontario (MTO) operational procedures with the possibility for subsequent field deployment. Thermography efforts were later reduced as a practical method due to IRT's rather limited feasible site temperature window, the inability to generate cross-sectional geometry measurements and extremely slow acquisition speeds [MASL90b]. Radar structural surveys have since become an accepted method of non-destructive evaluation [CANT77, ALON77, CHUN84, MANN85, MASL87, CART86, ROSS89]. Originally manual interpretation was performed by human experts and was extremely tedious. These experts were limited to an inspection of only a small fraction of the total radar data collected. In attempts to automate the interpretation, signal processing systems were created to autonomously analyze the large volumes of data representing a complete bridge radar survey. Relatively small bridge deck surveys (two driving lanes and 50 meters long) typically produce more than 25000 waveforms. It was found that such systems were prone to false alarms [CHUN89], diminishing radar survey credibility as an accurate tool for stand-alone structural evaluation. Due to this deficiency, the MTO views this system as having a diminutive role of providing secondary information. Radar surveys are used in conjunction with conventional

[2]The optical detection of surface temperature variations used for locating voids.

bridge deck surveys when accurate evaluation is required [WOOD91]. Research continues to investigate methods for maximizing the accuracy of radar data interpretation [MASE91].

1.2 Current Radar Interpretation

Ground probing radar analysis, as applied to bridge decks, involves the radiation and propagation of UHF (center frequency typically > 500 MHz) electromagnetic radiation downward into the deck structure and the collection and interpretation of the reflected waveforms. The interpretation of these reflections, obtained at discrete locations forming a grid on the deck surface, yield estimates of the constitutive parameters. These parameters are dictated by a layered cross-sectional model. Conceptually, these cross-sections may be specified as a sequence of layer descriptions which include physical properties (thickness) and electrical characteristics such as permittivity and magnetic permeability. A typical cross-section is shown in Figure 1.1.

The original manual interpretation was performed by human experts and although tedious, was extremely dynamic. These experts were able to adapt and infer complex model variations encountered during interpretation. Prototype signal processing software followed which imposed numerous simplifying assumptions as a trade-off for exhaustive sequential reflection waveform analysis. This software used rudimentary peak detection algorithms and peak amplitude ratios to locate interfaces, approximate parameters and identify anomalies. Extensive refinement of the analytic prototype has been undertaken to increase system accuracy [CHUN90]. The fundamental shortcomings of such a system can be traced to the use of a simplified uniform cross-sectional model. The peril is simply stated: given a valid physical model (N layers of materials m_0, ... ,m_n with thicknesses t_0, ... ,t_n) and the reflection waveform, such systems are capable of rendering the constitutive parameters of interest to the accuracy dictated

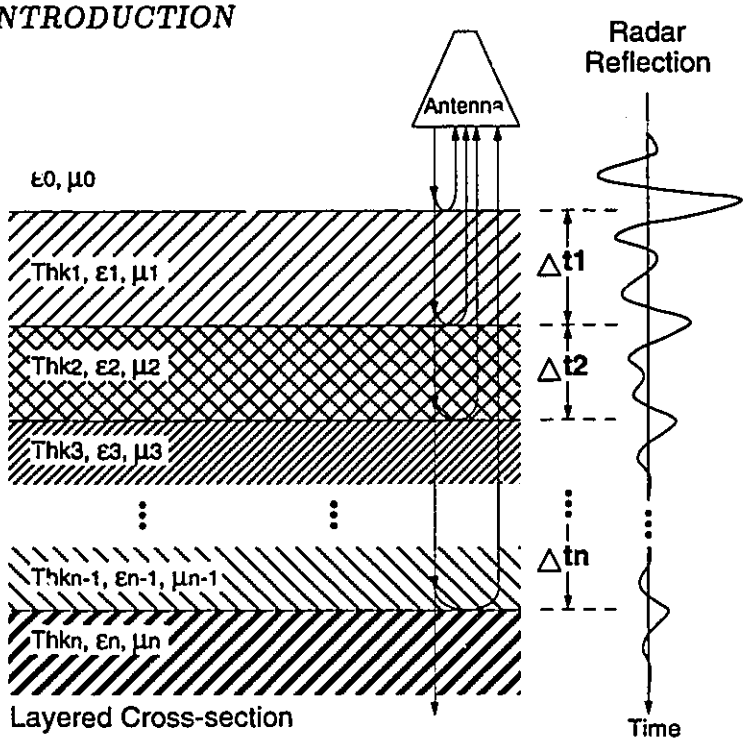

Figure 1.1: Cross Sectional Model and Radar Reflections
Radar reflections are specified by material (permittivity and permeability) and physical parameters (thickness). The reflections of electromagnetic energy are characterized by amplitude and arrival time (Δ t).

by the data gathering process. However, with no such accurate layer and thickness specifications the problem is underdetermined, and using amplitude based calculations has cumulative error effects which propagate through the determination of the remaining parameter estimates.

Using a single uniform model assumption for actual bridge structures is generally invalid. Such a simplistic approach leads to misidentification of interfaces and increased probability of misinterpretation. Independent research identified the limitations of a purely closed form analysis system and increased the depth of interpretation by adding heuristic knowledge. Based on a similar peak detection and amplitude ratio analysis, Maser [MASE86] provided dynamic knowledge-based (KB) refinement to the fundamental inferencing model for particular bridge structures. This enhancement allowed the system to anticipate the expected condition of decks due to age, design and

environmental parameters such as de-icing chemicals [RYEL72, ODRI88, VINC67] and annual vehicular traffic volumes. Although the system was capable of accurate site physical parameter determination and fault identification for simulated data, this KB system again relies on a single-model view of deck structures and is prone to the same misinterpretations for real radar data. Therefore, the radar reflection interpretation problem, as applied to bridge structure analysis with minimal physical verification information, may be generalized as an over-parameterized system identification problem.

1.3 A Multi-Disciplinary Approach to Radar Survey Interpretation

Substantial work has been done by the artificial intelligence community in the area of data interpretation and diagnostic systems [SHOR76, LIND80, DUDA79, BARR82]. Recent advances in qualitative reasoning theory have been adopted to provide a comprehensive framework for data fusion and deep reasoning to address the radar survey and structural analysis problem. The focus of this work addresses the potential of knowledge based systems, incorporating the notion of qualitative problem features and finite inferencing state spaces for the application to problems of over-parameterization. An interpretation task of this complexity requires significant detailed background pseudo-knowledge from diverse engineering disciplines. This domain knowledge includes bridge design, construction practices (both current and historical building codes), materials, signal processing techniques, electromagnetic theory and heuristic insight into bridge deck defect manifestations. The embodiment of multi-disciplinary expertise has been effectively realized through the adaptation of expert system technology. Pioneering work in expert system development for radar

signature analysis [LEE88, MASE86] has demonstrated limited success. However, further extension is required to enhance system capabilities for dealing with the dynamic modeling challenge of practical bridge sites. This work takes a multi-tiered view of the bridge structure which allows inferencing systems to dynamically modify the working cross-sectional model based on the spatial coordinates of the reasoning process. This spatial awareness, combined with the notion of qualitative reasoning, provides the system with reasoning capabilities which facilitate differentiation between model variation and defect manifestations. Further, a combination of both quantitative reasoning, using traditional procedural signal processing techniques, and qualitative reasoning, arising from qualitative modeling of the bridge structures and the related causal relationships, enhance the ability to increase parameter estimate accuracy and identify abnormal deviations attributed to defects. Ideally, inferencing should proceed in a fashion which maximizes unknown parameter estimate accuracy. This progression, determined by both radar site data and site physical data, avoids the pitfalls of arbitrary isolated sequential processing of sampled data.

This interpretation problem should not be mistaken for a simple pattern matching problem: there is no direct mapping of cross-sectional structural geometry to radar reflection waveform (Figure 1.1). Given that the backscatter waveforms are nonunique (nonunique implies in this instance, that many diversified physical situations can generate similar waveforms) it becomes imperative that intelligent interpretation be conducted in conjunction with multi-domain expertise and as much diverse corroborating data as is available or can be extracted. Thus, qualitative relationships provide a means of constraining the under-determined system identification problem to enhance parameter estimation accuracy.

1.4 Scope of This Work

In Chapter 2 the foundations for the structural analysis problem using ground probing radar are addressed. Modern bridge design and cross-sectional diversity issues are presented. Also, the radar backscatter phenomena is presented along with physical and material parameters affecting performance. Chapter 3 develops the notion of the interpretation of radar backscatter waveforms as an undetermined inverse problem. This chapter also presents previous work done on the problem of bridge structure radar analyis. Chapter 4 presents the expert system approach adopted for this work, and introduces a novel qualitative analysis approach to the underdetermined analysis problem. Chapter 5 discusses the system implementation details and the concept of system generated neural network filter used as a foundation for the elaborate system cross-sectional analysis capabilities. Chapter 6 presents system produced analysis results for actual bridge radar data and contrasts the performance with an existing system currently in use. Chapter 7 presents our conclusions and recommendations for areas of further work suggested by this research.

Chapter 2

Foundations

2.1 Bridge Structures

The modeling of bridge structures is very complex and yet, accurate models are essential for correct radar interpretation. Constructed in the last century, many distinct designs still exist and are in daily use. This diversification of design may be attributed not only to continuing improvements in construction materials but also to the fact that it is common in civil engineering for actual design to lag behind detailed structural analysis [OMTC83]. This aspect of civil engineering produces a stepwise refinement of the building codes which govern bridge design and construction. Therefore, any successful examination and modeling must be done in the light of the building codes in effect at the time the structure was designed and constructed. Further, bridge construction is influenced significantly by the environment in which the structure will exist. This reflects a regional dependence on material availability and selection and therefore, ultimately on design [FRAN87]. This subtle diversity forces meticulous modeling efforts and demands caution when analyzing such structures using ground probing radar techniques.

Currently there are in excess of 13,000 bridge structures in the province of Ontario,

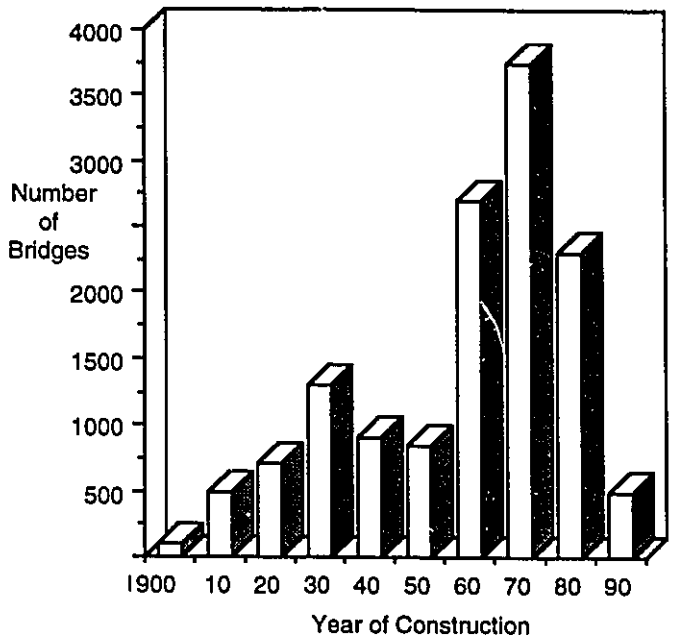

Figure 2.1: Bridge Constructions by Decade 1900-Present

with construction dates ranging over the past 90 years [MANN86a]; this distribution is shown in Figure 2.1. Of these structures some 25% are concrete-slab-on-girder (either steel or prestressed concrete girder) and another 35% are various designs of unsupported concrete slab structures [MANN86a]; see Figure 2.2. Concrete slabs, typically bituminous asphalt covered, represent the design type most prevalent in Ontario and also most amenable to radar surveys. Although of seemingly endless variety, composite bridge structures share common substructures. A slab-on-concrete-girder structure is shown in Figure 2.3. Such a structure may be subdivided, in a macroscopic sense, into the five components shown. These subcomponents may be constructed of different materials and will present different cross-section geometries. Examining the deck cross-sections of Figure 2.3, it is apparent that both the transverse and longitudinal position dramatically effects the observed cross-section. This phenomena is a product of a slab-on-girder design but, more importantly, reflects the American Association of State Highway and Transit O cials (AASHTO) design codes.

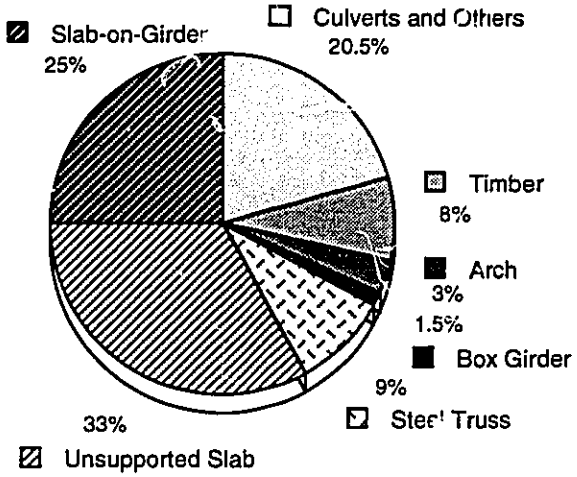

Figure 2.2: Province of Ontario Bridge Types

Ontario presents a unique case of exhibiting a sharp breakpoint in its bridge design code development. Prior to 1978, bridges built in Ontario (as in the rest of North America) followed the AASHTO Load Factor and Working Stress design methods [RICH67]. After that date, Ontario's Ministry of Transportation developed and implemented the far less complex Ontario Highway Bridge Design Code (OHBDC) to reflect realistic provincial bridge loads, vehicle type and traffic volumes [DORT83]. Simplistically, AASHTO design methods involved a detailed load and working stress analysis, typically from first principles, providing a unique design for each new bridge requirement. The OHBDC, based on finite limit states design, endorsed standardized thicknesses and isotropic reinforcing steel placement for slab structure design. Thus, prior to OHBDC introduction, the generalized modeling of reinforcing steel placement for slab bridges is extremely difficult [DORT73]. For the majority of structures in Ontario which are categorized as short and medium span bridges, the common slab configurations are shown in Figure 2.4.

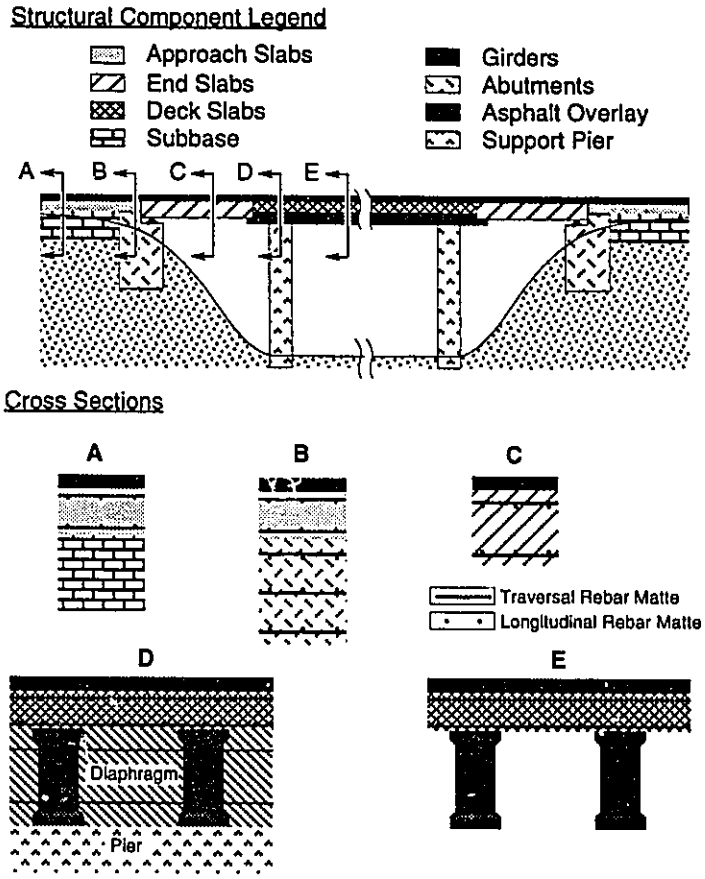

Figure 2.3: Typical Slab-On-Girder Bridge Structural Components

2.1.1 Building Code Development

With the widespread acceptance of prestressed concrete as a bridge design material in the mid-1950's the building code governing construction practices was changed extensively. These changes were motivated by changes in materials, construction techniques and decreasing design tolerances. The construction material and design philosophy effects of these changes are outlined in Appendix A [MANN83a]. This evolution may be characterized by a piecewise refinement of bridge protection and construction specifications until the 1978 definition of the OHBDC.

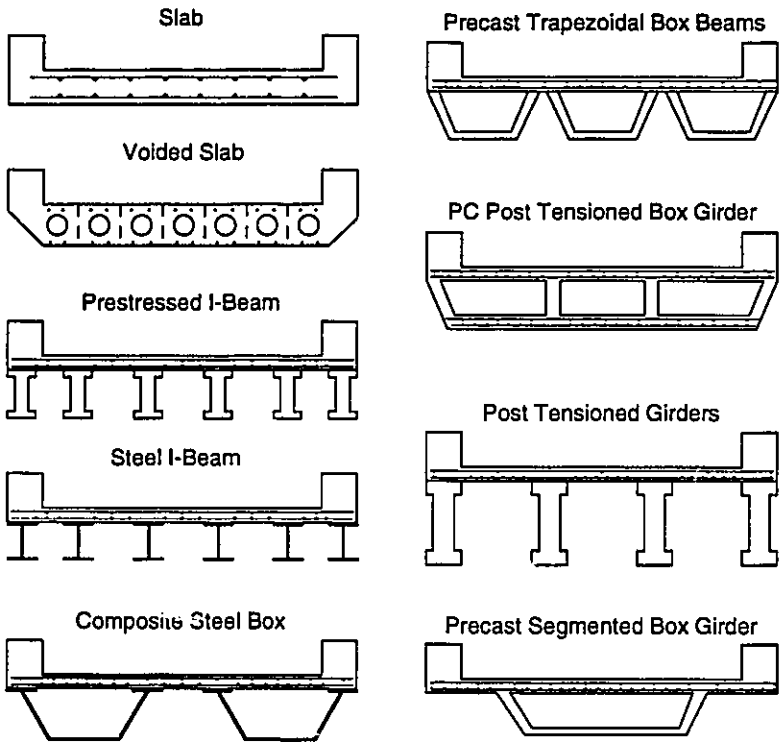

Figure 2.4: Common Slab Bridge Configurations

2.1.2 Construction Practices

Generally, any of the structural subcomponent cross-sections shown in Figure 2.3 may be modeled as a horizontally layered structure. However, additional complexity arises from embedded steel found in the concrete structures. Reinforcing steel is concentrated in two planes, forming upper and lower mattes, containing both longitudinal and traversal steel bars. Prior to the 1978 adoption of isometric steel placement for selected slab structures, the placement of the reinforcing steel was determined by structural load and calculated loading moments [MERL92]. This results in areas, on supported slab structures, with high and low concentrations of both main and

distribution[1] reinforcing steel. Additional reinforcing steel is also present at all subcomponent interfaces in attempts to distribute loads occurring at these joints in the predominantly longitudinal direction. Embedded steel variations also arise in precast construction where wire mesh is used at all longitudinal joints formed between precast segments. Finally, cathodic protection systems found on some bridge structures present many localized subsurface steel concentrations in both primary directions. The effects of this embedded steel on electromagnetic modeling is significant and is discussed in Section 2.2.

As noted in the documented evolution of the building codes, admixtures[2] for concrete are an old and established science. These additives control curing characteristics, air content, moisture permeability and strength properties. Use of glass and metal fibres (up to 120kg/m^3 of concrete) as strength admixtures have also been reported [COPE87]. All admixtures alter the electrical characteristics of the concrete to varying degrees.

2.1.3 Surface Coatings and Membranes

The waterproofing techniques used in Ontario extend from non-existent to the current standard of a rubberized membrane and protection board [SMIT62, CORK64, BLUM72, CORK75]. These waterproofing systems exhibit thicknesses which range from undetectable for the spray barriers, to an approximate maximum of 7 mm for the protection board systems over rubberized membrane. Such a system may be viewed as the addition of another thin lossless dielectric layer to the overall stratified

[1]Main reinforcing steel is typically large in diameter and distributes both the dynamic and static loads throughout the structure. Distribution steel is typically smaller and more dense, used principally to stop stress and temperature crack formation.

[2]Chemical compounds added to concrete to modify characteristics of both the setting process or the long term properties.

model. For all waterproofing systems in use, the top deck surface is either screed finished, floated or mechanically smoothed to eliminate sudden surface discontinuities.

Prior to 1975, several alternative waterproofing methods were evaluated. Of particular significance were the use of water repellent surface impregnants as the first experimental protective mechanism. These coatings proved effective as a hydrophobic barrier by filling the pores of the surface through infiltration into the concrete matrix. The degree of impregnation depended on the surface moisture permeability and was highly variable across the deck surfaces [COPE87]. In areas of high moisture permeability, a 20-30 mm saturation depth was possible. In these areas, air voids present in the concrete would be displaced by the impregnation. Effectiveness of these barrier systems was diminished due to the inevitable cracking which occurs in reinforced concrete after coating and impregnation. The displacement of surface air voids by coating a concrete surface with any material will result in an impregnation layer of increased permittivity as the impregnating substance will have a relative dielectric value greater than air. The effects of the increased surface permittivity will be detected in the interface reflection coefficient. This will be addressed in detail in Section 2.2.

Bituminous asphalt surfacing thickness is extremely variable across a bridge deck. This variability stems both from the original asphalt application and subsequent resurfacings. Bridge structures in Ontario which receive normal daily use are typically resurfaced, on average every 15 to 20 years, along with the adjacent highway [RTAC77]. This rehabilitation may involve either the removal of existing asphalt layers as dictated by deck maintenance requirements or simply the placement of additional asphalt layers. These rehabilitation efforts are not generally recorded at the time of repair and therefore, not known quantitatively from site specifications. This resurfacing technique can result in substantial asphalt wearing course thicknesses on older decks.

All these widely variable aspects of bridge deck cross-sections and material formulation must be considered during the generation of accurate models for structural analysis.

2.1.4 Defect Manifestations

In addition to the difficulty of formulating accurate cross-sectional models for sound deck structures, defects further complicate the modeling process. The layered structure and materials used in the construction of bridge decks promote the formation of various types of structural defects. Defect manifestations may be attributed to the environment to which the structure is subjected, but more importantly to deck construction practices governed by active building codes of the day. These common defects are outlined below [RTAC77];

Cracks In severe service environments, significant cracks (generally greater than 2 mm at the surface of an asphalt covered deck) will determine locations of potential corrosion initiation [FROM72, RYEL72]. Structural cracks provide a mechanism for corrosion, allowing all necessary reagents to be present. As such, surface cracks must be viewed as candidate locations for other more serious defects.

Debonding Debonding is the physical separation of the top asphalt wearing course from the concrete deck slab. Debonding is attributed to inadequate surface preparation or to the use of poor bonding agents prior to asphalt surfacing. The debonded gap may contain either water, a de-icing chemical solution or air, depending on the season. Typical gaps range from less than 1 mm to several mm.

Scaling Scaling is the disintegration of the concrete surface exposed to water and cycles of freezing and thawing. The severity of the scaling is greatly increased

by the presence of aqueous de-icing chemicals, regardless of type. This form of deterioration is not significant if the concrete is sufficiently air-entrained. In the case of proper air-entrained concretes, scaling only arises at areas of poor drainage such as curbs or gutters.

Delamination/Spalling Delamination and spalling represents the most significant form of bridge deck defects. The exposure of the deck to de-icing chemicals which permeate into the concrete surface to initiate corrosion of the top layer of reinforcing steel [NACE72, NACE87]. This corrosion creates lateral stresses within the concrete which may lead to the formation of planar cracks. Deck structures with effective waterproofing membrane systems typically do not develop serious delamination distress. Other corrosion protection strategies (galvanized rebar, epoxy-coated rebar, cathodic protection systems, etc.) also effectively reduce delamination distress.

2.1.5 Repair Methodology

For asphalt related defects (cracking and debonding), repairs are limited to the removal and replacement of the damaged asphalt sections. These repairs are limited to the surface and leave the integrity of the concrete deck structure intact. However, repair of severely scaled or delaminated decks involves the removal of the damaged concrete in the affected area. This removal is extended to include the surrounding chloride saturated concrete to a point where ionic concentrations are at acceptable levels and significant reinforcing steel corrosion is no longer detected. Edges of such areas are typically sawn or disc-cut vertically [CHYC62]. Removal of unsound concrete is done to a level below the top matte of rebar, to minimize the likelihood of future spalls. Patching materials are generally dissimilar to the original concrete mix due to the use of special pastes and admixtures to promote adhesion. Patches are finished

normally to a smooth surface and resurfaced in accordance with methods used for the remaining asphalt layer. Therefore, a repaired concrete deck patch represents a localized area of similar physical cross-sections but typically, with dissimilar electrical properties [CHYC62].

2.2 Radar

Ground penetrating radar (GPR) involves the downward transmission, and subsequent reception of high frequency electromagnetic radiation. Typical GPR systems may be divided into two distinct subgroups; monostatic radars, having a single transmitter/receiver antenna coincident in space and bistatic radars, which utilize space separated transmit and receive antennas. Although there are merits to both strategies [PARR92] commercial systems for bridge deck surveys are predominantly of the air launch monostatic variety. GPR systems are typically designed under contradictory constraints of range and resolution. Narrow pulse widths (in the time domain) enhance resolution by allowing reflections from thin layers to be fully resolved with no inter-reflection interference at a cost of diminished transmit power and therefore, subsurface range. Although pulsed radar used for GPR applications strive for a single cycle ideal, practical systems are plagued by high-speed switching transients and antenna ringing. Therefore, actual transmit wavelets are typically 1.5 cycle sinusoidal waveforms with amplitude diminished time sidelobes. Such a wavelet, and the related wide bandwidth spectrum is shown in Figure 2.5.

For air launch systems, electromagnetic waves leave the antenna and propagate through space. As the propagating wave encounters material of differing electrical characteristics, a portion of the wave energy is reflected at the interface and a portion is transmitted into the material. In the case of layered materials, reflections are

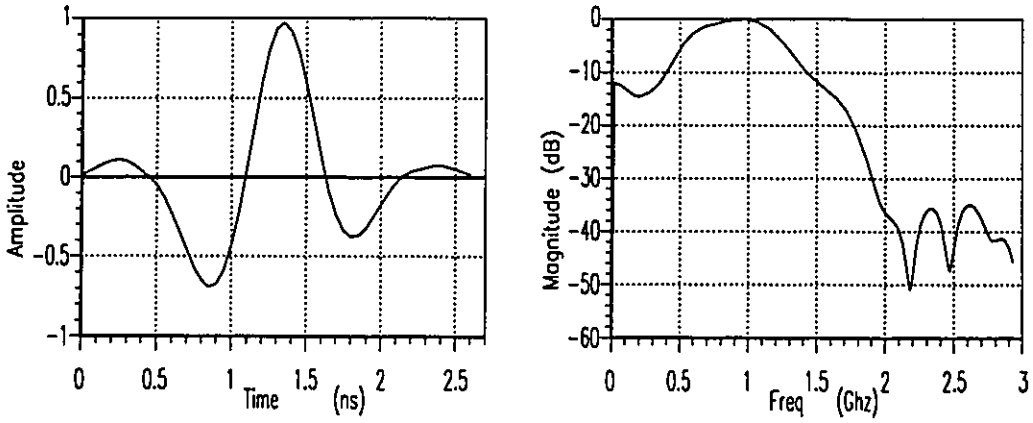

Figure 2.5: Transmit Waveform and Wide Bandwidth Spectrum

produced from each dissimilar interface as the wave propagates through the structure. Therefore, time domain analysis focuses on the amplitude and time of arrival associated with each reflection from dielectric interfaces. This concept embodies the essence of GPR analysis, the identification and classification of observed subsurface interface events.

2.2.1 Radar Backscattering

The reflection of propagating electromagnetic energy is referred to as scattering. In the case of a monostatic antenna system this is further refined to backscattering. Many aspects of reflecting objects affect the detected backscatter associated with radar illumination. These are presented informally, as a basis for later discussions. Sinusoidal time varying electromagnetic waves may be written in the form;

$$E(z,t) = \hat{E}_0 e^{j(\omega t - kz)} \tag{2.1}$$

$$H(z,t) = \hat{H}_0 e^{j(\omega t - kz)} \tag{2.2}$$

where $\hat{E}_0$, $\hat{H}_0$ are the electric and magnetic wave amplitudes (possibly complex), ω is the angular velocity $(2\pi f)$, t is the time dependence, k is the wave number $(2\pi/\lambda)$

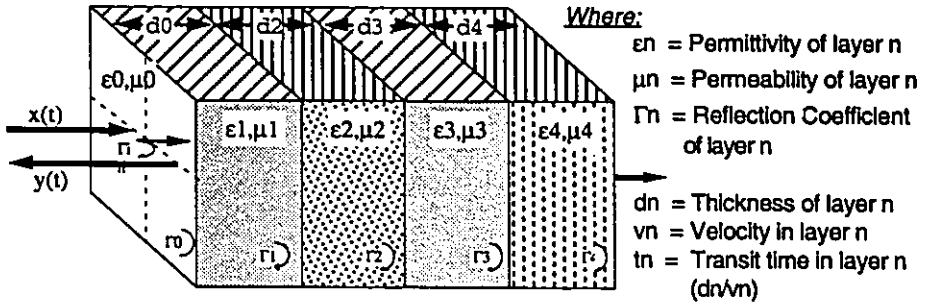

Figure 2.6: A Layered Dielectric Material Structure
A planar layered structure showing reflected waveform produced by incident waveform and reflection coefficients determined at each interface.

and z is the position in the direction of travel. Propagating electromagnetic waves may therefore be described by (2.1) and (2.2) above corresponding with the electric (E) and magnetic (H) fields respectively.

Referring to Figure 2.6 where a plane wave travels from one dielectric material (specified by magnetic permeability μ_1 and permittivity ϵ_1) to another (specified by μ_2 and ϵ_2) a portion of its power is reflected and a portion is transmitted. The reflection and transmission coefficients for normal incidence (quantifying the amount of energy reflected and transmitted) may be determined from the following relationships based on the solution to the one-dimensional wave equation:

$$\rho = \frac{E_r}{E_i} = \frac{\sqrt{\frac{\mu_2}{\epsilon_2}} - \sqrt{\frac{\mu_1}{\epsilon_1}}}{\sqrt{\frac{\mu_2}{\epsilon_2}} + \sqrt{\frac{\mu_1}{\epsilon_1}}} \tag{2.3}$$

$$\tau = \frac{E_t}{E_i} = \frac{2\sqrt{\frac{\mu_2}{\epsilon_2}}}{\sqrt{\frac{\mu_2}{\epsilon_2}} + \sqrt{\frac{\mu_1}{\epsilon_1}}} \tag{2.4}$$

where E_r, E_t and E_i are the scalar magnitudes for the reflected, transmitted and incident electric fields respectively. Therefore rewriting (2.3) and (2.4) for nonmagnetic materials ($\mu_1 = \mu_2 = \mu_0$, where μ_0 is the magnetic permeability of free-space);

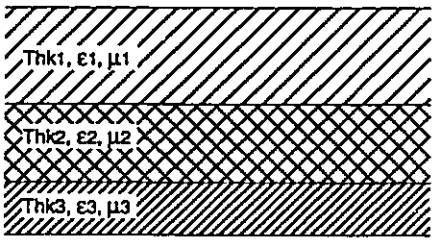

Figure 2.7: Electrical Properties Model
Model properties for a three layered structure of linear and isotropic dielectric materials (thickness, permittivity and magnetic permeability).

$$\rho = \frac{\sqrt{\epsilon_1} - \sqrt{\epsilon_2}}{\sqrt{\epsilon_1} + \sqrt{\epsilon_2}} \tag{2.5}$$

$$\tau = 1 + \rho \tag{2.6}$$

Similarly, given the reflection coefficient, the ratio of dielectrics may be determined;

$$\frac{\epsilon_1}{\epsilon_2} = \left|\frac{(1+\rho)}{(1-\rho)}\right|^2 \tag{2.7}$$

Examining (2.7) it is apparent that the dielectric ratio is extremely sensitive to reflection coefficient measurement error. As most radar analysis systems (detailed next chapter) rely on absolute amplitude measurements for reflection coefficient determination, this error sensitivity is significant.

2.2.2 Wave Velocity

The reflection coefficient determines the amplitude of the backscattered reflection, and wave velocity determines the arrival time of the reflected energy. Examining the layered structure of Figure 2.7 , the electromagnetic velocity in layer$_n$ may be defined as

$$V_n = \frac{C}{\sqrt{(\epsilon_n\ \mu_n)}} \tag{2.8}$$

where C is speed of light in a vacuum, and ϵ_n , μ_n are the relative permittivity and permeability of the layer material. Assuming two layers are isotropic, lossless and nonmagnetic (therefore $\mu_n \approx \mu_0$), the reflection coefficient for the layer$_{n-1}$/layer$_n$ interface may be calculated using (2.5);

$$\rho_{n-1} = \frac{\sqrt{\epsilon_{n-1}} - \sqrt{\epsilon_n}}{\sqrt{\epsilon_{n-1}} + \sqrt{\epsilon_n}} \tag{2.9}$$

The thickness of a layer can therefore be determined by the inter-wavelet delay in the arrival time (Δt_n from Figure 1.1), related to both the layer travel time and the layer velocity. Since the wave must travel twice the layer thickness, the thickness of layer n is defined as;

$$thk_n = \frac{1}{2}\left(Time_{peak_n} - Time_{peak_{n-1}}\right)\ velocity_n \tag{2.10}$$

For the transmit wavelet of Figure 2.8, with a pulse width of 0.92ns (where ns $= 10^{-9}$ seconds), a minimum layer resolution is attained with approximately one pulse width separation. This pulse width, for typical dry bituminous surfacings ($\epsilon \approx 6\,\epsilon_0$, where ϵ_0 is the permittivity of free-space), represents approximately a 60 mm minimum surface layer thickness. This value will decrease with increasing layer permittivity;

$$thk_n = \frac{1}{2}\ \ 0.92(10^{-9})\ velocity_n = \frac{C_k}{\sqrt{\epsilon_n}} \tag{2.11}$$

where C_k is a constant. This demonstrates the desirability of short transmit pulses for thin layer resolution. It should also be noted that layer thicknesses of less than several pulse width separations will result in reflection peak amplitude distortion. This distortion results from the wavelet's time domain sidelobes. The superposition of these sidelobes with the primary pulse peak produces amplitude distortion which is not necessarily negligible. This effect represents a source of amplitude error which can result in cumulative interpretation errors.

Using these fundamental relationships, the stratified layer analysis involves; the

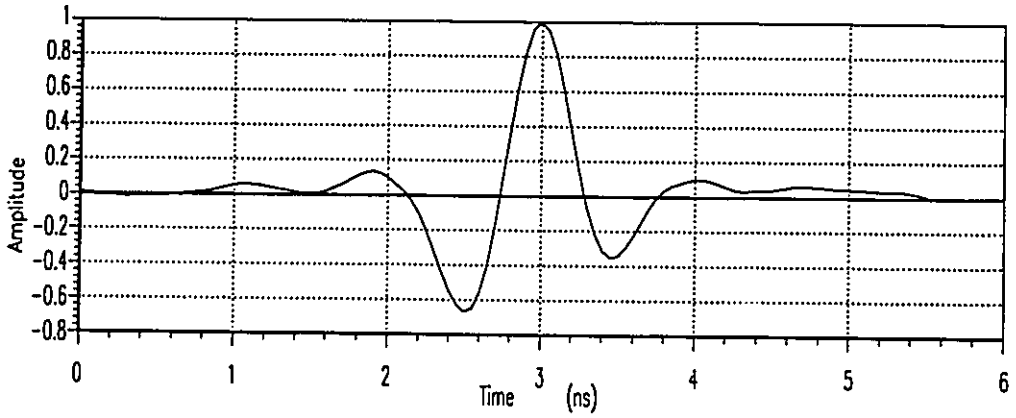

Figure 2.8: Monopulse Transmit Wavelet
Actual monopulse transmit wavelet depicting non-ideal sidelobe phenomena.

location of peaks, the determination of peak amplitudes, the estimation of layer permittivities and the determination of layer thickness from arrival times and layer velocity estimates. Sudden changes in any of these parameters indicate either a physical model change or may be attributed to cross-sectional anomalies.

2.2.3 Material Properties

Effective radar analysis is only possible with a working knowledge of the materials through which the electromagnetic radiation propagates. Such knowledge allows many simplifying assumptions to maintain tractable signal analysis. The basis for these assumptions are stated below.

Losses

As the wave travels through a medium (with the exception of free-space) there will be a reduction in the amplitudes of $E(z,t)$ and $H(z,t)$. For lossy dielectric materials the apparent reflection coefficient is unchanged, however a multiplicative exponential decay term arises. In materials specified by the constitutive parameters (permittivity ϵ and magnetic permeability μ) which are not ideally lossless, the wavenumber must

adopt a complex form

$$k = \frac{2\pi}{\lambda} = \omega\sqrt{\mu\hat{\epsilon}} \tag{2.12}$$

where the complex permittivity $\hat{\epsilon}$ may be defined in terms of material conductivity σ, and real (ϵ) and imaginary (ϵ'') permittivity components

$$\hat{\epsilon} = \epsilon\left(1 + \frac{\sigma}{j\omega\epsilon''}\right) \tag{2.13}$$

therefore

$$k^2 = \omega^2\mu\hat{\epsilon} = \omega^2\mu\epsilon\left(1 + \frac{\sigma}{j\omega\epsilon''}\right) \tag{2.14}$$

This complex term in the wavenumber is referred to as the loss tangent ($\tan\delta = \sigma/\omega\epsilon''$), and allows delineation of materials into high and low loss categories. Typically, non-metallic building and geological materials are essentially non-magnetic ($\mu = \mu_0$, where μ_0 is the magnetic permittivity of free-space) and low loss ($\sigma/\omega\epsilon'' \ll 1$).

Low Loss Case If the conductivity of a material is low such that $\sigma/\omega\epsilon'' \ll 1$ then (2.14) reduces to

$$k = \omega\sqrt{\mu\epsilon}\left(1 + \frac{\sigma}{j\omega\epsilon''}\right) \cong \omega\sqrt{\mu\epsilon} - \frac{j\sigma}{2}\sqrt{\frac{\mu}{\epsilon}} \tag{2.15}$$

Since there is a spatial exponential dependence in the original form of the traveling wave (2.1) the real part of (2.15) is the same as the lossless case. The complex term of (2.15) corresponds with an attenuation due to ohmic losses in conductive materials. For dry construction materials this represents losses of typically less than 10 dB/meter [STEI81]. For materials saturated with water or aqueous de-icing chemical solutions, this loss figure could be increased several orders of magnitude.

Dispersion

Corruption of the original wave shape represents a more severe form of signal distortion. If a material exhibits a wavenumber with a functional dependency on frequency

($k = g(\omega)$), then the material is said to be dispersive. This dependency causes each frequency component of a nonmonochromatic wave to travel at a slightly different velocity. In this case, wide bandwidth signals propagating through dispersive media will become distorted. High resolution radar systems for bridge deck analysis are typically wide bandwidth systems (bandwidths ranging from $\pm 50\%$ of the center frequency for the unit are not uncommon). Such systems will experience severe distortion to the transmit wavelet in a dispersive medium. Although all materials are slightly dispersive, bridge deck construction materials are assumed to be negligibly dispersive.

In addition to construction materials being generally low loss and non-dispersive, two further assumptions are made; these materials do not exhibit constitutive parameters which vary spatially or are a function of applied fields. Therefore, it may also be assumed that construction materials are homogeneous and isotropic. These material property assumptions maintain modeling tractability and are generally accepted for dry low loss geological materials [CHEN82, STOL86, BATH84].

2.2.4 Permittivity Calculation

Using (2.15) provides a relationship for the determination of interface reflection coefficients. For a layered structure as shown in Figure 2.6, unknown permittivities may be determined given interface reflection amplitudes and the incident electric field strength. Assuming E_i is accurately known, (possibly determined by reflection from a large flat conductive sheet placed on the surface) then the surface reflection coefficient, and permittivity (ϵ_2) may be calculated

$$\rho = \frac{E_r}{E_i} \tag{2.16}$$

$$\frac{\epsilon_1}{\epsilon_2} = \frac{1}{\epsilon_2} = \left|\frac{1+\rho}{1-\rho}\right|^2 \tag{2.17}$$

where ($\epsilon_1 \cong \epsilon_0$). Using the transmission coefficient and material loss estimates the next layer's permittivity may be determined. This process may be continued for subsequent layers until reflection amplitudes are reduced to noise levels.

Practical System Limitations

As discussed, reflection-coefficient-based permittivity calculations are extremely sensitive to reflection coefficient perturbations. If reflection coefficient amplitude measurements are susceptible to errors, then all permittivity (and hence thickness) estimates will be in error. Neglecting sampling and quantization errors, the following sections present structurally induced amplitude errors common to practical bridge structures.

2.2.5 Non-Specular Surfaces

The reflection coefficient calculation (2.16) assumes the total specular scattering from the dielectric surface which, in the bridge deck case, is typically the asphalt layer. However, asphalt wearing courses are designed to produce inherently rough surfaces [KAME82] (to provide road traction and skid resistance), and therefore, may introduce diffuse scattering effects [BART53, BECK63, KING59, LONG83]. Typical rough wearing course surfaces are found to have variable gaussian surface height distributions ranging typically from 0.1 to 1 cm from topmost projection to lowermost cavity on the surface (distribution acquired from an actual bridge site). The effect of minute surface height perturbations was investigated by Beckmann and Spizzichino's [BECK63] extensive empirical studies of reflections from rough surfaces. This study was based on data collected from various authors, and lead to the following relationship;

$$\rho_s = R_s \rho_0 \tag{2.18}$$

where ρ_0 is the reflection coefficient of a smooth surface (of known dielectric) and R_s is the narrow bandwidth specular scattering coefficient. For a rough surface with a

gaussian height distribution this coefficient may be approximated by

$$\left(R_s^2\right) = e^{-(\Delta\Phi)^2} \tag{2.19}$$

with

$$\Delta\Phi = \frac{4\pi\,\Delta h}{\lambda} \tag{2.20}$$

for normal incidence. The Δh term represents the standard deviation of the gaussian distribution of heights, which for measured rough asphalt was found to be approximately 0.21, and for smooth limited use sections of the same structure, 0.05 cm. Using these estimates, for a radar with a 1 GHz ($\lambda \approx 0.30$ m) center frequency, the effect of rough surface reflection (with a height variation of 0.21 cm) is approximated below.

$$\left(R_s^2\right) = e^{-\left(\frac{4\pi\,\Delta h}{\lambda}\right)} = e^{-\left(\frac{4\pi\,0.21}{30}\right)} = 0.9169 \tag{2.21}$$

$$(R_s) = 0.9576 \tag{2.22}$$

and for the smooth asphalt surface cited (0.05 cm variation);

$$\left(R_s^2\right) = e^{-\left(\frac{4\pi\,0.05}{30}\right)} = 0.9789 \tag{2.23}$$

$$(R_s) = 0.9894 \tag{2.24}$$

Therefore, for a bridge deck exhibiting the surface height variations shown, (also assuming a typical air/asphalt interface where $\epsilon_{air} = \epsilon_0$, $\epsilon_{asp} = 6.0\ \epsilon_0$ and $\mu_{air} = \mu_{asp} = \mu_0$) this represents a change of the calculated dielectric constant of the asphalt layer of (from (2.5)) ;

$$\rho_{ideal} = \frac{\sqrt{\epsilon_1} - \sqrt{\epsilon_2}}{\sqrt{\epsilon_1} + \sqrt{\epsilon_2}} = \frac{-1.4495}{3.4495} = -0.4202 \tag{2.25}$$

where the negative sign signifies a 180^0 phase reversal between transmit and receive signals. Therefore, for the flat smooth asphalt surface

$$\rho_{smooth} = R_{smooth}\,\rho_{ideal} = 0.9894(-0.4202) = -0.4157 \tag{2.26}$$

$$\epsilon_{apparent} = 5.9\ \epsilon_0 \tag{2.27}$$

For flat rough asphalt surface

$$\rho_{smooth} = R_{rough}\ \rho_{ideal} = 0.9576\ (-0.4202) = -0.4024 \tag{2.28}$$

$$\epsilon_{apparent} = 5.5\ \epsilon_0 \tag{2.29}$$

These conservative estimates indicate the significant effects of the relatively small surface roughness variations on the calculated surface dielectric. The estimation of the rough surface scattering effects are further complicated by the wide bandwidth nature of monopulse radars. While accurate estimates are difficult and prone to error, the effect of variable surface height on the apparent reflection coefficient has been documented by many authors as reported in [BECK63].

2.2.6 Antenna Height Variation

A second phenomena which affects the reflected signal amplitude is antenna height variation. For a one-way far-field (antenna separation $\gg$ wavelength) bistatic configuration, receiver antenna power may be specified as [SKOL90];

$$P_{R_{bistatic}} = \frac{P_T\, G_t\, A_{ant}}{4\pi\ R^2} \tag{2.30}$$

where P_R is the power received, P_T is the power transmitted, G_t is the transmit antenna gain, A_{ant} is the receiving antenna aperture size and R is the transmitter-receiver separation distance. Additionally, for a monostatic radar configuration the backscatter receive power is also related to the scattering area (σ) of the reflecting object. If the antenna to object separation is H then

$$P_{R_{mono}} = \frac{P_t\, G_t\, \sigma\, A_{ant}}{(4\pi)^2\, (H)^4} \tag{2.31}$$

If the antenna is now translated spatially to a position of $H' = (H + \delta)$ then the power received becomes;

$$P'_{R_{mono}} = \frac{P_t G_t \sigma A_{ant}}{(4\pi)^2 (H')^4} \tag{2.32}$$

this represents a change in received power of

$$\frac{P_R}{P'_R} = \frac{\frac{P_t G_t \sigma A_{ant}}{(4\pi)^2 (H)^4}}{\frac{P_t G_t \sigma A_{ant}}{(4\pi)^2 (H')^4}} = \frac{(H')^4}{(H)^4} = \left(1 + \frac{\delta}{H}\right)^4 \tag{2.33}$$

Using (2.33), for an antenna displacement of $+0.1H$ the received power would be reduced by 2.2 dB. For typical air launch GPR systems, the effects of antenna displacement are again somewhat more complex. Rather than operating in the far-field, the surface distance is in the so called intermediate-field ($H \approx \lambda$ in air). Although an exact analytic solution is extremely difficult, the antenna displacement effects have been detected in field experiments.

Displacement Mechanisms

Furthermore, if the same antenna is mounted in a cantilever fashion to a vehicle for the purposes of data collection, then the antenna is prone to height variations due to the road surface undulations or vehicle frame elevation changes due to acceleration/deceleration effects. If a vehicle with a mounted antenna encountered a roadway discontinuity resulting in a variation of the front and rear wheel elevation of x, then antenna displacement from the nominal rest position may be determined from the simple geometric relationship shown in Figure 2.9 (assuming a normal vehicle wheelbase of approximately 4 m and a cantilever distance of 2 m);

$$\frac{x}{4} = \frac{A_d}{6} \tag{2.34}$$

Using (2.34), if surface height changes abruptly by 3 cm then the antenna height will change by 4.5 cm from a nominal rest height of 30 cm. Conversely, a height reduction is produced for a negative discontinuity. These front and rear axle perturbations result

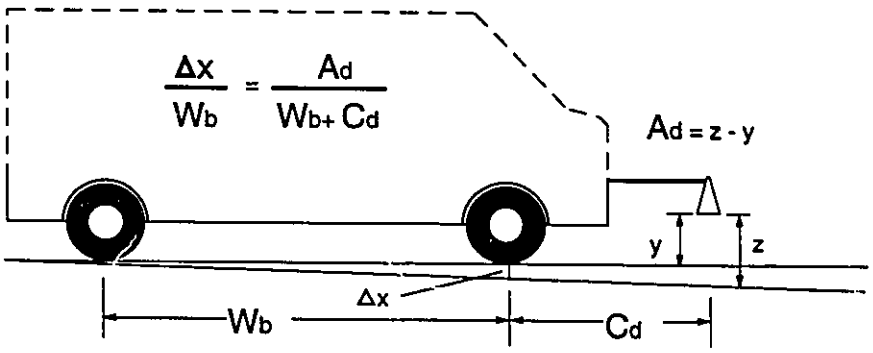

Figure 2.9: Cantilever Mounted Air-Launch Radar Antenna
Cantilever length determines the variation of the antenna from the nominal rest position for a front or rear axle variation.

in complex positive and negative displacements, even if suspension system damping is neglected. These variations will cause variable surface amplitude measurements for a constant surface dielectric, if the road surface is not smooth in a macroscopic sense.

2.2.7 Non-Planar Surfaces

Estimates within the MTO suggest that up to 85% of all wearing coarse bituminous surfaces exhibit some form of wheel track rutting [HAJE86]. This phenomena arises from repeated loading of longitudinal strips on roadways beneath the natural wheel tracks for each driven lane. This compaction and loss of aggregate materials from the asphalt matrix causes the formation of troughs. Typically these troughs are of variable depth, to a worst case maximum of approximately 10 cm measured with a 1.2 meter base line[3]. This represents a radius of curvature in the transversal direction of up to 0.36 m.

When energy strikes a concave surface, the effect is the collimation or focusing of

[3]This technique uses a 1.2 m straightedge placed perpendicular to the wheel rut axis to measure depth.

		Depth (m)		
		0.0	0.05	0.10
Width (m)	1.0	∞	2.5	1.3
	0.5	∞	0.63	0.36

Table 2.1: Radius of Curvature for Troughs of Various Widths and Depths

the reflected waves. The effect of a concave reflection surface at the receive antenna would be equivalent to increasing the scattering area σ in (2.31) when the antenna was centered longitudinally over a concave trough. This increase in receive power would be detected as an increased surface reflection amplitude. The converse is true of convex surfaces, increased scattering losses cause a reduction of received power. Accurate estimation of the concave wheel trough phenomenon is exceedingly difficult for two reasons. Firstly, the actual transversal concave shape is unknown and variable and secondly, the reflection characteristics of nonplanar surfaces are both a function of the surface perturbation height and the incident waveform wavelength with GPR again being typically wide bandwidth [BECK63].

2.2.8 Air Void Displacement

Bulk construction materials, such as concretes and asphalts, are a mixture of many aggregates [YOLL67, RYEL67, PHAN74, DAVY59]. Both materials may be considered to be open celled structures and as such, are moisture permeable [JONE86, NACE83, MARS86]. The local air void content (typically 4-10% by volume for concrete) determines the practical impregnation limit for liquids such as water or silicone solution waterproofing. Estimating the effects of air void impregnation can be done using a relative permittivity calculation formula for binary, homogeneous, isotropic nonconducting media [BEEK67, CALD79, MUSI86] given by;

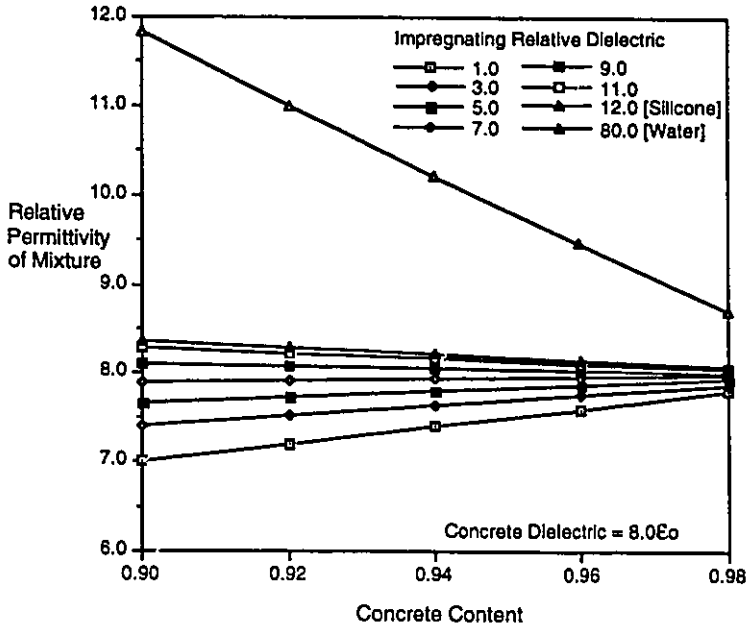

Figure 2.10: Impregnated Concrete Permittivity
Permittivity values calculated from binary dielectric mixture equation (2.35)[MUSI86].

$$\sqrt{\epsilon_m} = r_1\sqrt{\epsilon_1} + (1 - r_1)\sqrt{\epsilon_2} \tag{2.35}$$

where ϵ_1 and ϵ_2 are the permittivities of the mixture constituents, r_1 is the volumetric ratio of constituent 1 and ϵ_m is the permittivity of the resulting mixture. Figure 2.10 shows the mixture permittivity effects of the impregnation of concrete by various substances over a range of air-void content values. An increased permittivity will have the effect of increasing the reflection coefficient for an interface with the impregnated material as the second layer. A second effect of such an impregnation is the formation of a highly non-planar permittivity layer (not related to a physical layer), where the impregnating material concentrations diminish. This impregnating layer thickness is a function of the moisture permeability and as such, is highly variable. Relative humidity will affect the apparent dielectric measure for asphalt and non-waterproofed concrete through water molecule permeation. Although difficult to quantify, these

effects will alter the reflected waveform amplitude and therefore, affect all amplitude derived parameters.

2.2.9 Embedded Steel

As well as reflections from interfaces of dissimilar layers, the placement of steel reinforcing bars (rebars) in concrete presents a conductive reflecting interface to any electromagnetic radiation propagating through the concrete [BOWM69, CHOM86, KNOT85, STON90]. The apparent reflection coefficient is related to the size and orientation of the bar. The concept of radar illumination area is related to antenna beamwidth by;

$$A_I = I_E \, I_H \tag{2.36}$$

$$I_E = H \, tan(\theta) \tag{2.37}$$

$$I_H = H \, tan(\phi) \tag{2.38}$$

where H is the monostatic antenna height above the illuminated surface, the angles θ and ϕ are the electric and magnetic field beamwidths specified from the antenna aperture normal, and I_E and I_H are the beamwidths in the electric and magnetic field directions respectively. This physical situation is shown in Figure 2.11. Typical splayed transmission line antennas of the type commonly used for commercial deck analysis provide E-field beamwidths of 30^0 and an H-field beamwidth of 20^0 [DAVI92]. At an nominal height of 0.30 m, this provides an illumination footprint of approximately 0.4 m by 0.25 m or 0.1 m^2. As the electromagnetic wavefront is focussed as it enters a higher permittivity medium (the wave is bent towards the interface normal), this represents a valid approximation for the dimensions used for rebar illumination calculations. The radar cross-section (scattering width) of a small conducting cylinder (diameter $\ll \lambda$) is only significant for orientations parallel to the electric field

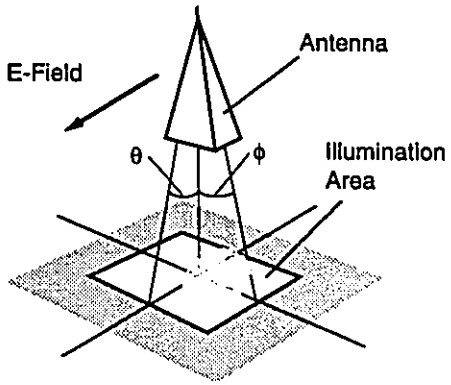

Figure 2.11: Splayed Transmission Line Antenna Illumination Area

[BALA89]. In this configuration, at normal incidence, the scattering width (the effective area per unit length of rebar) may be approximated by;

$$\sigma_{SW} = 2\pi\, r \tag{2.39}$$

where r is the radius of the rebar. Therefore, for a single bar with E-field orientation, and illuminated by a radar with a 0.1 m^2 footprint;

$$\sigma_{REBAR} = I_E\, \sigma_{SW} = 2\pi\, r\, I_E \tag{2.40}$$

$$\rho_{rebar} = \frac{E_{rebar}}{E_i} = \frac{\sigma_{REBAR}}{I_E I_H} \tag{2.41}$$

The modeling of rebar reflection coefficients is complex for bridge decks. With no accurate *a prior* information on the size or placement of the embedded rebar, modeling and analysis must proceed based on the heuristics governing reinforcing steel requirements and placement strategies from bridge design and construction. Rebar densities typically vary (for the 0.1 m^2 illumination area) from no reinforcing steel with E-field orientation to several bars depending on antenna position on the bridge deck (shown in Figure 2.12).

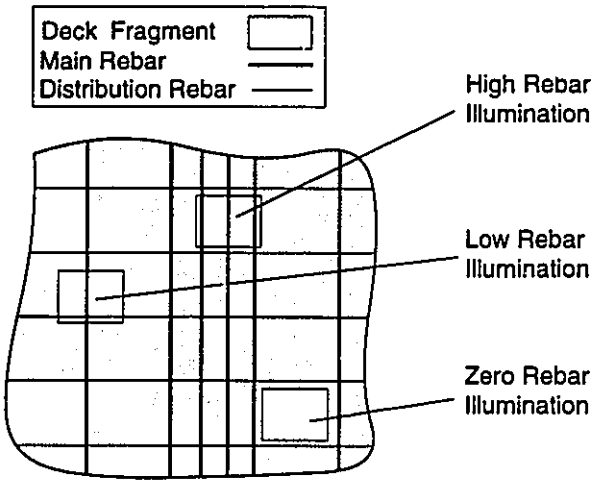

Figure 2.12: Rebar Illumination Based on Antenna Orientation and Placement

2.3 Conclusion

Successful system identification problems may be attributed to sound system models. As presented, the arduous task of system modeling is complicated by both the diversity of bridge structure design and construction and practical limitations on radar amplitude fidelity. In light of these complexities it is obvious that no uniform single model is applicable to actual bridge structures and are best reserved for controlled testbeds of uniform construction. As originally demonstrated in the manual interpretation systems, dynamic modeling based both on observed data and most probable physical structure remains the best system model strategy.

Chapter 3

The Inverse Problem

3.1 Introduction

The inverse problem of determining substrate structure from the backscattered response to probing signals is applicable to many diverse fields. These fields include acoustics, remote sensing, medical imaging, astronomy, radio astronomy and optics (detailed in [BOER81]). In electromagnetic inverse problems, the lossless layered dielectric case is applicable to segmented transmission lines, geophysical layer earth systems or the case at hand, bridge deck analysis [MEND80]. Boerner, Jordan and Kay [BOER81, pp 185] make the following distinction for electromagnetic direct and inverse problems

> Whereas, on the one hand, in the direct problem of electromagnetic scattering total *a priori* information on the size, shape and material constituents of an object, together with the relative geometry of the incident field vector and the object coordinate system, are given and the scattered field vector is to be determined everywhere over the total frequency or time domain; on the other hand, the inverse problem is to reconstruct the

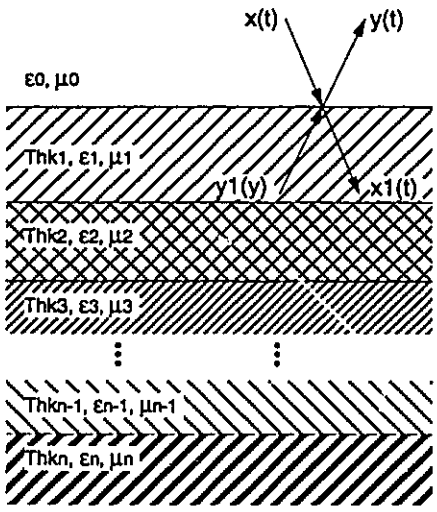

Figure 3.1: Incident And Reflected Waves
The waves are shown here at oblique incidence (rather than GPR case of normal incidence) for ease of illustration.

> size, shape and material characteristics of an *a priori* unknown scattering object from the knowledge of the incident field vector and the resulting scattered field data.

A single interface for a structure of n layers is depicted in Figure 3.1. An electromagnetic plane wave at normal incidence x(t) represents the input and y(t) represents the ideal output from the system. As shown in Section 2.2.1 at normal incidence, reflection coefficients arise at each interface from the solution of the one dimensional wave equation. Therefore, the response of the system to the input stimulus contains information about layer travel times and reflection coefficients. This represents the inverse problem, given the input signal x(t) and the observed response y(t), determine the system structural geometry (layer thickness and permittivities).

System Identification or inverse problems may be considered fundamentally as modeling endeavors. This modeling involves both physical and mathematical model generation. As discussed in Chapter 2, even with fundamental simplifying assumptions (isotropic, homogeneous and non-dispersive) the physical modeling task for

bridge decks is complex. Relying on physical model foundations, mathematical modeling applied to inverse problems is of two types, non-parametric and parametric representations.

Non-parametric representations of layered media rely on convolutional sum models. As presented by Robinson [ROBI67, ROBI75], the proposed summation model to describe the output signal y(k) is;

$$y(k) = \sum_{i=1}^{K} \mu(i)x\ (k-i) \tag{3.1}$$

where $y(k)$ is the output, k represents time t_k, $m(i), i = 0...k$ is the sampled input and $\mu(i), i = 1, 2...$ is the reflection coefficient sequence. It is assumed that the observed output sequence has an additional noise term, $v(k)$ as in (3.2).

$$y^{'}(k) = y(k) + v(k) \tag{3.2}$$

Since (3.1) is a convolution, various deconvolution methods can be used for deriving the localized refiection coefficient $\mu(k)$ sequence. As well as predictive deconvolution methods developed by Robinson [ROBI67] other methods such as homomorphic and Kalman filtering are available. These deconvolution methods are less effective for wide bandwidth signals and thin layer resolution (introducing multiple overlapping internal layer reflections) as reflection amplitude is distorted due to superposition of the multiple reflections.

3.2 Nonparametric Approaches

3.2.1 Steinway at Georgia Institute of Technology

Original work done at Georgia Institute of Technology (GIT) by Steinway *et al.* investigated the feasibility of radar applied to void detection beneath pavement [STEI81].

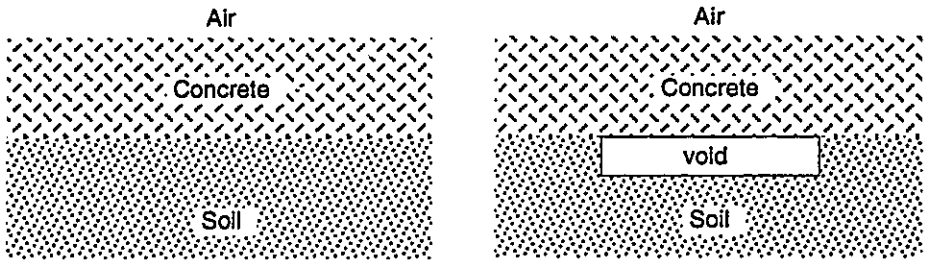

Figure 3.2: Layered Structures Modeled at Georgia Institute of Technology

This innovative and extensive research suggested the applicability of radar for subsurface profiling and defect identification. Detailed convolutional models were developed for parameter estimation based on two and three layer physical models, shown in Figure 3.2. For the two layer model;

$$y(t) = \rho_1\, x(t) + \rho_2[1-\rho_1^2]\, x(t-\tau) + \rho_1\rho_2^2[1-\rho_1^2]\, x(t-2\tau) \tag{3.3}$$

$$= \sum_{k=1}^{3} r_k\, x(t-\tau_k) \tag{3.4}$$

where the terms of the summation represent the surface reflection (reflection coefficient = ρ_1, and two-way travel time = 0), the concrete/soil reflection (reflection coefficient = ρ_2, and two-way travel time = τ) and the second reflection from within the concrete layer (reflection coefficient = $\rho_1\rho_2$, and four-way travel time = 2τ) with coefficient derived from reflection and transmission relationships (2.30). Deconvolution was done with *a priori* physical model knowledge and peak mapping using approximate dielectric values for each layer. The development of this system led to the formalization of the following concepts;

1. The estimation of layer permittivity and thickness from measured reflection coefficients.
2. The distinction of two separate void thickness discrimination mechanisms;
   - time of arrival methods for voids having two-way travel times greater than the transmit pulsewidth.
   - amplitude relationships for interfering reflections due to thin layers.

3. The recognition of the effects of layer losses on amplitude based decisions and the related investigation of temperature and moisture effects on concrete layer attenuation.
4. Adoption of a uniform physical model (for all isometric test slab cases) to allow background subtraction for anomaly/defect recognition.
5. The identification of internal radar hardware related reflections and the concept of useful signal to noise levels.

The physical modeling done was valid for the particular GIT testbed, consisting of an extensively studied and carefully constructed concrete slab with sections containing isometric reinforcing steel. Rarely is such exact *a priori* physical data available during practical bridge deck evaluation. These specific-model-derived peak amplitude to layer thickness relationships are not valid in the general case of unknown rebar placement or concrete losses. However, with this structural knowledge available, the effective layer travel times were hard coded into the GIT deconvolution analysis (3.4). Most algorithmic simplifications adopted at GIT can be attributed to hardware limitations imposed by available personal computers in 1980. Although not applicable to general bridge analysis, this work represents the foundation for many present day deck and roadway analysis systems.

3.2.2 Nonparametric Representation Extensions

Carter at McMaster University

Extensions to this work have been done at McMaster University by Carter *et al.* [CHUN84, CART86]. With the advent of more powerful personal computers and data sampling hardware, efforts were focused on generalizing the work done at GIT. The models developed by Carter *et al.* were again a convolution sum with a more complex physical model typical of bridges constructed in Ontario after 1978. This model is shown in Figure 3.3. For a three layer physical model, the observed response

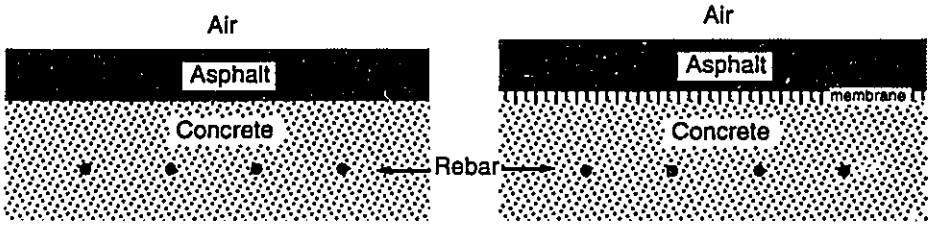

Figure 3.3: Layered Structures Modeled by Carter at McMaster University

(disregarding secondary reflection effects) may be given as;

$$y(t) = \rho_1\ x(t) + \rho_2[1-\rho_1^2]\ k_1\ x(t-\tau_a) + \rho_3[1-\rho_2^2][1-\rho_1^2]\ k_2\ x(t-2\tau_c) \qquad (3.5)$$

$$= \sum_{k=1}^{3} r_k\ x(t-\tau_k) \qquad (3.6)$$

where the terms in the convolution summation are the surface reflection (with two-way travel time = 0) the asphalt/concrete reflection (with two-way travel time = τ_a), and the concrete/air reflection (with two-way travel time = τ_c). New to the GIT model is the addition of the constants k_1 and k_2 representing unexplained losses at each of these interfaces. Through data analysis of common bridge structures, empirical values were obtained for the loss correction terms. Although not reported here, empirical data observations lead to a derivation of thresholds which are incorporated in fault detection algorithms based on specific waveform peak amplitudes. This scheme tracks bipolar peak values generally assumed to represent specific interfaces and flags faulted areas when the detected values exceed the empirical thresholds. The magnitude of the threshold violation determines the identity of one of a number of possible faults. Much like the original GIT system, this method relies on a single uniform model assumption for the entire structure. Using this technique, sudden changes to the physical model are interpreted as defects. The uniform model assumption also significantly reduces the sophistication of the deconvolution mechanism. Given a user specified physical model description, the system establishes nominal layer propagation

times. In terms of (3.5) this determines approximations for τ_a and τ_c and represents reduced parameterization of the inverse problem (through the assumption of localized *DELAY* parameter values).

Use of this scheme produced many spurious fault detections, which were subsequently minimized through averaging and cluster analysis. As stated, any changes in the physical model are identified simply as faults. In the case of isometric rebar slabs (seen in bridges constructed after 1978), the rebar model is acceptable and matches the GIT isometric assumptions. However, for non-isometric rebar slabs, high and low concentration rebar sections would be identified as defective. This work represented the first step towards a generalized empirical system.

Maser and Infrasense

Intelligent system additions were added to the basic ratio fault detection scheme by Maser at Infrasense [MASE86, MASE91]. The notable enhancements included background domain knowledge, in the form of environmental parameters, annual vehicle traffic, structural faults, age, and typical model variations based on structure type. Carter *et al.* highlight the perils of misinterpreted bridge structures in [CHUN89] due to incorrect physical models (arising from case histories). A structure thought to have a single lift of asphalt was discovered to have multiple unrecorded layers. This feasible *second-lift of asphalt* model variation is addressed by the system developed at Infrasense. A second noticeable extension of the Infrasense system is the modeling of moisture permeation based on binary mixing relationships for dielectric materials. In this way, high moisture contents may be correctly identified during data analysis. However, the underlying uniform model assumption and ratio threshold detection scheme causes the system to be inherently as prone to error with practical bridge structures as the previous approach.

3.3 Parametric Representation

Sometimes referred to as model-based, parametric representations for the inverse scattering problem has been, and still are, widely studied [COEN81, GAUN81] (detailed in [MEND80]). This approach models wave motion in layered media as two oppositely traveling waves. These two signals, referred to as the downgoing (right traveling) and upgoing (left traveling) waves, provide an elegant and succinct mathematical model for multilayered systems.

For transmission line models (representative of lossless layered media) the following relationships apply:

$$\begin{bmatrix} W_R(n+1,t) \\ W_L(n,t) \end{bmatrix} = \begin{bmatrix} \phi_1(k_n)D_n & \phi_2(k_n) \\ k_n D_n & \phi_3(k_n) \end{bmatrix} \begin{bmatrix} W_R(n,t) \\ W_L(n+1,t) \end{bmatrix} \tag{3.7}$$

where $\phi_1(k_n) = \phi_3(k_n) = (1-k_n^2)^{1/2}$ and $\phi_2(k_n) = -k_n$ and D_n represents the layer$_n$ propagation delay operator.

Assuming the system is causal, $(W(n,t) = 0, t < 0)$ then (3.7) may be written in the same form as the non-parametric representation

$$W_R(n+1,t) = (1-k_n^2)^{1/2}\ D_n\ W_R(n,t) - k_n\ W_L(n+1,t) \tag{3.8}$$

$$W_L(n,t) = k_n\ D_n\ W_R(n,t) - (1-k_n^2)^{1/2}\ W_L(n+1,t) \tag{3.9}$$

Reformulating (3.8 and 3.9) using the following substitution $T_n = (1-k_n^2)^{1/2}$ and adopting an implied time dependence $(W_R(n,t) = W_R(n))$ for notational simplicity. Then solving (3.8 and 3.9) for primary reflections only, given a three layer model,

$$\begin{aligned} W_L(0) &= k_0 D_0 W_R(0) + T_0 W_L(1) \\ W_R(1) &= T_0 D_0 W_R(0) + \cdots \\ W_L(1) &= k_1 D_1 W_R(1) + T_1 W_L(2) \\ W_R(2) &= T_1 D_1 W_R(1) + \cdots \\ W_L(2) &= k_2 D_2 W_R(2) + T_2 W_L(3) \\ W_R(3) &= T_2 D_2 W_R(2) + \cdots \\ W_L(3) &= 0 \end{aligned} \tag{3.10}$$

where $\cdots$ indicates high order reflection terms. Therefore, solving for $W_L(0,t)$ as a sum and expanding

$$W_L(0) = k_0 D_0 W_R(0) + T_0[k_1 D_1[T_0 D_0 W_R(0)] + T_0 T_1[k_2 D_2[T_1 D_1[T_0 D_0 W_R(0)]]]] \tag{3.11}$$

$$W_L(0) = k_0 D_0 W_R(0) + k_1 T_0^2 D_1 D_0 W_R(0) + k_2 T_0^2 T_1^2 D_0 D_1 W_R(0) \tag{3.12}$$

$$W_L(0) = \rho_0\, x(t-\tau_0) + \rho_1(1-\rho_0^2)\, x(t-\tau_0-\tau_1) + \rho_2(1-\rho_0^2)_1(1-\rho_1^2)\, x(t-\tau_0-\tau_1-\tau_2) \tag{3.13}$$

which, for the lossless transmission case, reduces to the same form as the non-parametric case (this sum only considers primary reflections).

The elegance of parametric cowave model inverse techniques is further enhanced by Bruckstein and Kailath through the development of two iterative methods for local parameter determination (in this case local reflection coefficient k_n) [BRUC87]. Of these two methods, the *Layer Peeling* method is highlighted here.

Given the relationship (3.7);

$$\begin{bmatrix} W_R(n+1,t) \\ W_L(n,t) \end{bmatrix} = \Sigma(k_n, t) \begin{bmatrix} W_R(n,t) \\ W_L(n+1,t) \end{bmatrix}$$

and

$$\begin{bmatrix} W_R(n+1,t) \\ W_L(n+1,t) \end{bmatrix} = \Theta(k_n,t) \begin{bmatrix} W_R(n,t) \\ W_L(n,t) \end{bmatrix}$$

and assuming the existence of a function $\mathcal{F}\{\ \}$ such that

$$k_0 = \mathcal{F}\{W_R(0), W_L(0)\} \tag{3.14}$$

then

1.

$$k_0 = \mathcal{F}\{W_R(0), W_L(0)\}$$

2.

$$[W_R(n+1,t)W_L(n+1,t)] = \Theta(k_n,t)\,[W_R(n,t)W_L(n,t)] \tag{3.15}$$

Steps (1) and (2) above are repeated until

$$k_n = \mathcal{F}\{W_R(n), W_L(n)\} \tag{3.16}$$

is below reliable signal to noise ratios.

Although seemingly ideal, Bruckstein and Kailath recognized the following serious limitation of either technique (paraphrased from [BRUC87] below);

> Not all inverse scattering problems are solvable using techniques with no *a priori* physical model knowledge. There are many physical models which present the same responses for a variety of local parameters. This represents situations which do not present a one-to-one mapping of local parameters to observed response.

Further complication stems from errors which arise from the $\mathcal{F}\{\ \}$ function. In practice, this relationship relies on the ratio of incident to reflected wavelet amplitudes to

determine the reflection coefficient k_n. As indicated in Section 2.2.1, time overlapped reflections, transmit pulse time sidelobes and reflection and propagation losses cause errors in the observed amplitudes which are then propagated cumulatively through the remaining k_{n+1} calculations. Both the nonparametric and parametric representations rely on an accurate physical model. Examining the inverse problem with a more generic view, the observed response will rely fundamentally on three parameters;

1. layer thickness
2. layer permittivity
3. propagation losses (both material and interface induced)

Therefore, associated with parameter estimates using inverse techniques is the notion of observed output reliability. As noted by both Carter and Maser, structure evaluation is enhanced when the scope of the analysis is broadened beyond a single waveform. Current purely analytic approaches ignore substantial heuristic knowledge and causal relationships allowing the determination of reasonable parameter confidence. Incorporating this wealth of untapped information substantially increases the derived parameter reliability. Adding symbolic analysis to the analytic approach thereby allows the assessment process to include concepts such as *fully resolved reflection wavelet* or *corrupted multiple reflection wavelet* prior to extracting and incorporating a peak amplitude. Similarly, sudden reflection pulse position variations, implying a sudden layer thickness change, are not physically possible on visibly smooth decks built using standard construction practices. A multi-tiered expert system approach allows heuristic physical information (some in the form of rule-based common sense as above) to migrate downwards for inclusion in physical parameter estimation, which represents a significant improvement in the deck evaluation process. This approach, demonstrated here, develops an entire analysis procedure anthromorphically and automatically, which closely mimics the operation of a human expert in assimilating many forms of knowledge, both analytic and heuristic.

3.4 Conclusion

Inverse problems are characterized by under-determination. Current systems either rely on physical model approximations and assumptions to determine material properties or assume material properties to determine the physical variations. In the case of a single uniform isometric structure, such systems prove to be acceptable. However, these approaches have been demonstrated as unacceptable in the general case. Expert systems allow a multi-leveled approach to guide analytic reasoning steps indicating the parameters most appropriately responsible for the observed responses.

Chapter 4

Expert Systems Approach

4.1 Introduction

Artificial Intelligence (AI) represents an area of computer science which has matured over the last 35 years. The focus on developing intelligence for difficult reasoning tasks has led to many successful so-called 'Expert Systems'. Expert systems research and applications may be roughly separated into two classes;

1. problems of interpreting data to analyze a phenomenon [data analysis]
2. problems of finding the most appropriate solution under problem constraints [problem solving]

Original expert systems demonstrated the effectiveness of the application of artificial intelligence technology to broad areas within these classifications. Until recently, computing hardware limitations have restricted the applicability of AI techniques to problems with small working data sets. Several notable applications in the area of signal analysis, found in published literature, are highlighted below.

- DENDRAL and Meta-DENDRAL [1964-1970] Originally proposed by Joshua Lederberg in 1964, the DENDRAL algorithm applied heuristics to the enumeration of possible molecular structures given the constituent atoms. The Meta-DENDRAL project extended this to automatically infer rules given mass spectrometry data and the corresponding human expert analysis. This rule inference capability represents inductive machine learning [LIND80].

- HEARSAY I & II [1971-1976] The HEARSAY project is one of many continuous speech-understanding projects funded by Defense Advanced Research Projects Agency (DARPA). Originally limited to the chess playing domain (HEARSAY I), this project was expanded to include a working vocabulary of 1011 words. Operation of this system was limited to the interpretation of short burst audio sequences [BARR86].
- HASP/SIAP [1972-1976] Another DARPA funded project, the HASP/SIAP system interprets continuous sonar signals with the intention of identifying enemy submarine signatures. This project addressed the issues of incorporating human expert knowledge for recognition, and the importance of temporal relationships (highlighting the time variability of sonar signals) and the application of meta-knowledge from related domains (such as the average speed of vessels) [BARR86].
- AISD [1986] AISD is a comprehensive expert system developed for subsurface radar data interpretation. The interpretation task is limited to the sequential processing of individual radar reflections. Using this sequential method, extremely large data sets are accommodated incrementally. This singular approach does not exploit the inherent positional information contained in typical detailed GPR surveys. This system also incorporates substantial related domain meta-knowledge [MASE86].

Of the highlighted expert system projects, only the HASP/SIAP system incorporated explicit temporal relationships found in the observed data. This temporal analysis was limited to the observation time of the sonar echo data. In GPR analysis tasks, data sets exhibit both a time-of-arrival temporal aspect and a strong spatial relationship between neighbouring data observations. This combination of intelligent spatial and temporal analysis is currently unexplored in published literature.

Well designed expert systems may be distinguished from conventional programs in several important aspects and as such, may be recognized as applications which:

- reason with symbolic domain specific knowledge. Although not restricted to symbolic knowledge, expert systems rely on domain modeling as well as quantitative data.
- use domain specific knowledge in the form of heuristics. These causal (predicate and conclusion) relationships and meta-knowledge represent common sense and expertise shared by those familiar with the domain.
- provide both asynchronous and procedural execution capability. Asynchronous reasoning can involve production rules, and procedural code may be used for control or embedded algorithmic operations.
- demonstrate a strong distinction between inferencing and control operations. Expert systems typically have control strategies which are distinctly isolated from the symbolic reasoning.

- are flexible and extensible. Most expert systems are modular and allow extension or refinement through simple additions or modifications.
- provide an elevated performance level at the specific task.

In order to attain these conceptual goals, expert systems require three fundamental components:

- Knowledge: domain expertise
- Data: problem set data
- Control: mechanism to apply knowledge to data

The specification of the functionality and structure of these components produce specific expert system architectures and implementations which define various problem solving models.

4.2 Blackboard Systems

A problem solving model is a methodology for presenting knowledge and controlling the inferencing steps which lead to a solution. Of the endless variety of existing modeling strategies used in expert system applications [BARR86], the blackboard model presents a highly structured example of opportunistic problem solving. All the systems described in Section 4.1 use a blackboard modeling strategy. Expert system components for blackboard system implementation consist of:

1. Knowledge sources; the rules and heuristics required to solve the problem.
2. The blackboard; a repository for global problem and state data which are incrementally modified to move to a solution.
3. Control; in addition to conventional inferencing control, in large data problems, a top-level control element allows focusing of the knowledge sources to monitor and react to a subset of the blackboard data.

Blackboard (BB) systems are data structures which present data defining the problem state to the monitoring knowledge sources (KS). In production rule systems these KS's would consist of rules. When a particular observed system state is detected

by a sensitive knowledge source (a KS designed to recognize that state), the KS reacts and modifies the blackboard. This new state may then invoke other observing KS's to react. Therefore, the KS's are *triggered* by state space opportunities to which they are sensitive. These condition-reaction events describe the blackboard reasoning methodology.

The size of the blackboard reflects the size of the problem state space. As the blackboard size increases, the performance of the knowledge source monitoring process is diminished due to the obvious increase in state space scope. As the problem size increases there are two methods of maintaining KS response performance. The first approach uses an additional top-level control unit to provide a mechanism to limit the active KS monitoring/sensitivity space. In extremely large blackboard systems, monitoring the entire state space presents a prohibitively resource intensive approach, therefore a control strategy which focuses the KS monitoring activity to particular regions will improve performance. A second approach overcomes the large state space problem by reducing the active blackboard size. This logical extension alters the monolithic blackboard concept by adopting a divide and conquer philosophy. By subdividing large tasks into natural subdomains, a hierarchy of similar blackboards (or blackboard panels) is possible. Using this strategy, specialized knowledge sources are able to limit the scope of surveillance and improve overall system performance. Although focused on the smaller blackboards, these specialized KS's are free to modify the state space of neighbouring blackboard panels as well as a top-level or global blackboard. This distributed reasoning allows locally triggered knowledge sources to influence the global state space.

4.2.1 Control

As indicated, in order to achieve efficient inferencing for large systems, supplemental control procedures are necessary. For such systems, two levels of control are common;

- top-level application specific control constructed explicitly as part of the expert system.
- knowledge source control (inference engine).

In typical production rule systems (characterized by the use of IF-THEN rule structures), the control paradigms are restricted to forward and backward chaining. Commonly referred to as data-driven reasoning, forward chaining exhaustively determines the consequence of all observed and applicable data. For large data spaces, forward chaining represents an extremely costly approach. On the other hand, backward chaining represents a goal-driven or hypothesis proving approach. Given a hypothesis, backward chaining systems examine only predicates required to assert the desired conclusion. Backward chaining is more efficient; however, all consequences of a given data state may not be realized. Most complex knowledge source controllers (or inference engines) allow the combination of both methodologies to maximize application efficiency.

Top-level control structures are required in situations where data set size prohibits the use of inference engine control mechanisms as the overall control strategy. As implied, these controllers are application specific; a typical configuration is shown in Figure 4.1. For large state space inferencing using a fragmented blackboard approach, a blackboard panel agenda controller explicitly selects the focus of the inference engine KS application. Using the scheme shown in Figure 4.1, the system blackboard modifications, arising from local reasoning, is fedback to the controller to allow possible updates to the established blackboard panel agenda.

As presented, the blackboard model provides a means of effectively encapsulating large and disjoint data sets for inferencing using multiple and possibly unrelated knowledge sources. This description applies directly to GPR bridge survey interpretation problems.

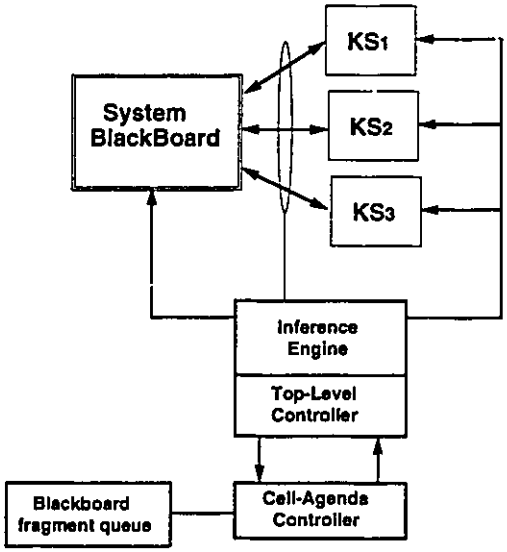

Figure 4.1: Top Level Control Strategy

4.3 GPR Bridge Data

GPR survey analysis may be characterized as a data intensive interpretation procedure. This assessment arises from the volumes of raw radar data produced from typical GPR surveys. In the case of bridge decks, the complete survey is truly 3-dimensional. Reflection data is typically collected in transversal lines at densities of 10-20 reflections/meter with 4 or 5 lines per driven lane. Figure 4.2 shows the coverage of a typical bridge structure survey. The exploded view of the small section of bridge deck in Figure 4.2 indicates the 3-dimensional aspect of the radar data. Each radar waveform has deck surface coordinates (transversal and longitudinal position), as well as a depth dimension derived from the reflection data. This positional nature to the deck data presents an opportunity to establish spatial and temporal relationships between data elements. This novel aspect of the data analysis will be explored in Section 4.4.2.

It is apparent from Figure 4.2 that complete bridge deck surveys extend to include structural sections beyond the actual deck slab. This feature of the bridge deck data

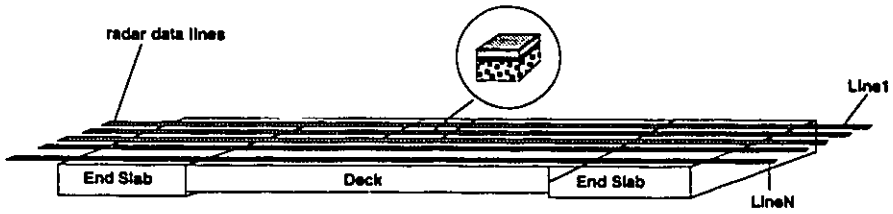

Figure 4.2: GPR Data Acquisition Paths
Typical bridge radar profiling involves multiple parallel longitudinal lines. These lines ideally cover both the driven and curb lanes in a uniform fashion.

provides logical data segmentation heuristics.

4.3.1 Data Representation

The GPR data acquisition method and the structural subcomponent nature of bridge construction lend themselves to a tiered data structure. A hierarchical structure proves ideal for the fragmented blackboard concept. As with a solitary blackboard system, this tiered data structure can contain both static and dynamic problem data as well as state information for system reasoning. The physical arrangement depicted in Figure 4.2 suggests the data structure shown in Figure 4.3. This structure has both physical and abstract data types, the BRIDGE, LINE, SEG, and WAVE nodes represent physical entities or structures and CELL is an abstract node construct.

Frame-based Data

The top-down nature of this structure provides a mechanism for efficient data sharing. Using a frame-based data structure [MINS75], data placed at one node of the hierarchy may be accessed at all lower levels by *reference*. The reference mechanism provides access to the data without the overhead of multiple copies of these potentially large substructures. This code/data reuse feature and class-subclass links are inherent in frame-based systems. Exploiting these attributes, frames present a cohesive unit for

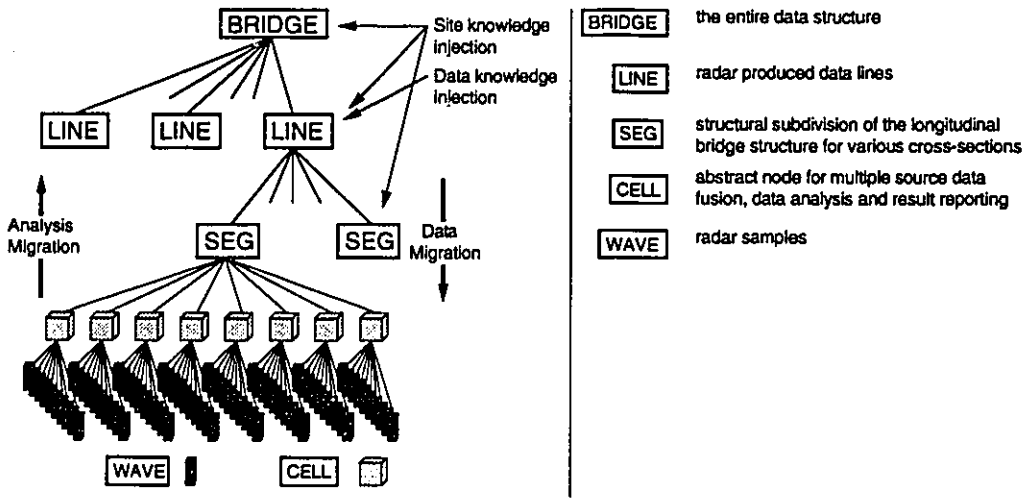

Figure 4.3: GPR Tiered Data Hierarchy

node representation. Associated with each frame unit can be any number of object parameters, referred to as slots. Slots may contain data or procedural code (methods) which operate on the unit in an object-oriented fashion. For the GPR data structure shown, Figure 4.4 highlights each frame type and the fundamental slot specifications. For a typical GPR survey of a small bridge deck, the hierarchical data structure contains approximately 5000 nodes with the majority created at the WAVE level. Further, the slots in a frame-based structure comprise both the static and dynamic background used for inferencing, these environments represent the system blackboard. With the proper top-level control algorithm each node may be selected as the current inferencing point, thereby restricting knowledge source application and dramatically improving knowledge base inferencing speed.

Examination of both the physical site survey (Figure 4.2), and the frame description (Figure 4.4), allows the realization of the spatial nature of the GPR data. Given valid surface coordinates and a properly aligned data set, the node based data structure allows the determination of neighbouring nodes corresponding to physical

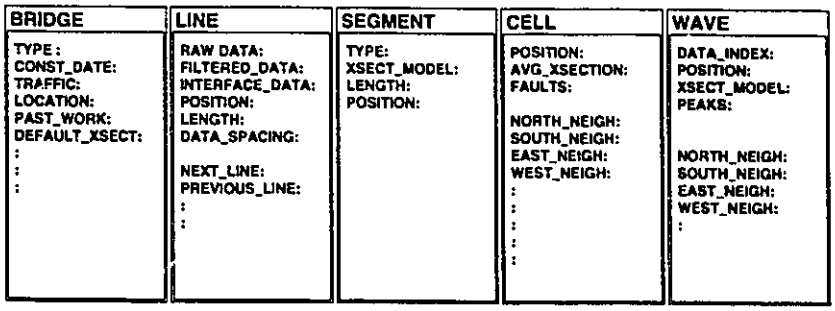

Figure 4.4: System Frames and Associated Slots
General format for slots associated with system data structures comprising the distributed blackboard.

neighbours. The cartesian nature of the data set allows the definition of a four node neighbourhood for all nodes below the LINE level. These may be arbitrarily defined as [NORTH,SOUTH,EAST,WEST] with NORTH representing the direction of travel of the data acquisition process. Using this spatial awareness, through the notion of a neighbourhood, there exists a method of defining a spatial deviation for any local parameter in the direction of any neighbouring nodes. Extending this concept to the temporal aspect of radar reflections (detailed next section), then relative time derivatives are also possible.

4.3.2 Knowledge Sources

The inherent domain diversity for the bridge deck radar interpretation problem is particularly well suited to an expert system approach. Experts skilled in the art of bridge deck GPR analysis subconsciously incorporate knowledge in the areas of electrical, civil, mechanical engineering and material science. Without the necessary background knowledge and practical radar interpretation experience, successful interpretation is impossible. Effective expert data analysis systems must contain equally diverse knowledge in the form of knowledge bases containing procedural, causal (rules)

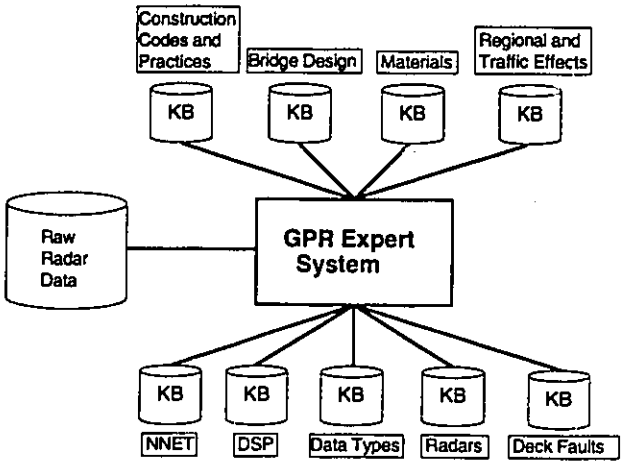

Figure 4.5: GPR System Knowledge Bases

and declarative information. This expertise was amassed through knowledge engineering efforts in the various domains. The resulting system knowledge bases are shown in Figure 4.5. Using the same frame-based structure for knowledge encapsulation as the system data structures, allows a logical knowledge base hierarchy which also exhibits subclass specialization and code/data reuse.

4.4 Radar Expert System Design

Having defined the blackboard system architecture as it applies to the bridge GPR problem, the design details of such a system will now be discussed.

4.4.1 Quantitative Analysis

Numerical GPR Data Analysis is based on the lossless layered structure physics developed in Section 2.2.1. Based on the time convolution-sum relationship;

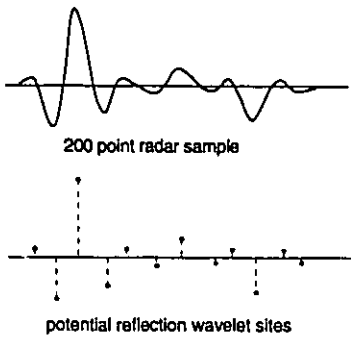

Figure 4.6: Optimum Monopulse Waveform Deconvolution Sites
For monopulse radar, uncorrupted interface reflections will be characterised by a peak in the reflected waveform. These peaks represent candidate locations for expensive deconvolution operations.

$$y(t) = \sum_{i=1}^{N} \mu(i)\, x(t - \tau_i) \tag{4.1}$$

Deconvolution allows the estimation of reflection coefficients which may be used to derive layer thickness estimates. Deconvolution ideally reduces the convolution sequence to impulses with a magnitude equal to the reflection coefficient for that layer. A time-domain deconvolution process is transmit wavelet dependent, and represents the bulk of the preprocessing effort for the entire system. Conventional deconvolution algorithms rely on various filtering or homomorphic processing operations. Both approaches require expensive time/frequency domain transformations. These classical approaches are not generally accurate for physical situations without *a priori* cross-sectional information.

Selective Deconvolution

Rather than blindly applying these deconvolution methods to entire N-point radar reflection waveforms (which would require two operations to deconvolve both positive and negative wavelets) a more efficient approach was sought.

Given the reflected waveform of Figure 4.6, and assuming that the layers are thick

enough for primary peak resolution, then candidate pulse reflection points exist only at locations of peaks and valleys. Therefore, the number of candidate deconvolution points for the given wavelet reduces to typically less than 10 for a 4 layer structure. A simple method for peak detection uses a differentiating filter to map peak locations into zero crossings. The peak detector operates on N-point waveforms in kN operations, where k is the filter length [BLAC90]. This filter length parameter also controls detector peak sensitivity. These candidate locations then require a wavelet recognition operation to identify valid peaks. For each candidate location, using a sum-squared-error classifier (Σerr^2) the following steps are required:

1. determine polarity and offset of candidate peak
2. scale transmit wavelet (x_{ideal})
3. calculate difference $\Delta = \Sigma(x_{ideal} - x_{test})^2$
4. IF ($\Delta >$ threshold) THEN (not valid interface) ELSE (valid interface)
5. next candidate

This method relies on the assumption that the interface reflection is an undisturbed replica of the transmit wavelet. This assumption is only valid for sufficiently thick layer structures, not generally valid for bridge structures. An alternate approach was developed for this expert system.

Neural Net Approach

Rather than using the classical mean-sum-squared-error similarity criterion, a neural net filter was developed for candidate wavelet classification [AMAR67, HECH87]. The classifier is a multiple input, three output feed forward network. Under expert system control the neural network classifier is trained based on data parameters (sample rate), and the originating radar unit signal-to-noise figure. The expert system generates training sets for the two valid reflection wavelet classes (positive and negative wavelets) and a collection of wave fragment shapes (forming the third detection class

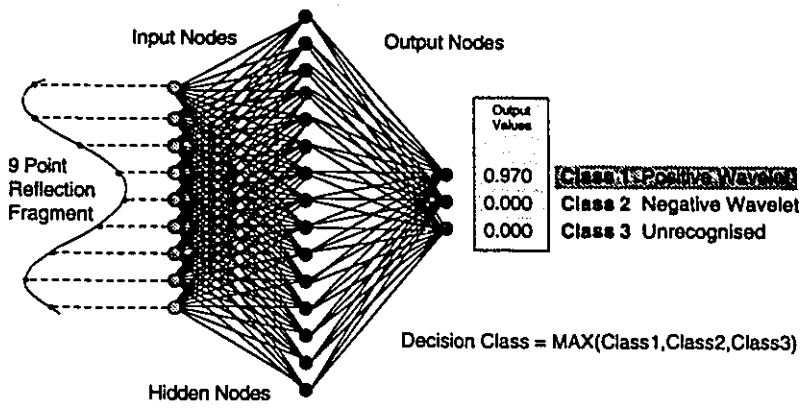

Figure 4.7: Neural Network Peak Classifier
A three layer feedforward network topology may be defined by a connected INPUT, HIDDEN and OUTPUT layer. The number of output nodes corresponds with the number of output CLASSES. The network shown here has a [9-15-3] topology.

of invalid waveshapes). This network topology is shown in Figure 4.7. Inputs for the network are selected heuristically based on sample spacing and transmit wavelet shape. Input number and location (integer offset) are selected to most closely capture the wavelet shape. Training is performed by the system using a conjugate gradient descent variant to the traditional backpropagation method. This training scheme is extremely fast and contains non-convergence detection. In the improbable event that the training set does not converge, the system increases the number of hidden nodes, re-randomizes the intial weight conditions and retrains. Using this approach, the system typically produces a trained neural classifier in less than 70 iterations of a single training session with no observed training requiring more than one increase in hidden layer nodes. The trained network weights are compiled dynamically into a standalone classifier function for use by the expert system driven deconvolution operation. The benefits of using the network classifier are highlighted by the ability to generalize non-ideal reflected wavelet shapes. If a wavelet is partially distorted, the neural classifier is able to correctly identify the positive wavelet shape, whereas a mean-sum-squared-error classifier may well exceed the identification threshold. This generalization characteristic is significant for the bridge deck problem where slightly

distorted reflections are common.

Classification of network output is trivial, each output node produces a value which ranges from [0 to 1]. The most active output represents the network classification [positive wavelet, negative wavelet, unknown]. Therefore, no decision threshold is required, the classifier simply selects the most active output node. However, in practice, the additional constraint that the winning output must exceed 0.5 is imposed. For all outputs < 0.5 it is assumed that the network is undecided and the classification becomes INVALID. Using the neural classifier, the sampled N-point waveform is reduced to a probable interface impulse sequence. This represents the base level abstraction (the transformation of raw data to probable interface sequences) for the expert system, and is used as a foundation to model and align the data structures. The details of the wavelet classification technique will be examined in Chapter 5.

4.4.2 Qualitative Physics

Qualitative physics is an area of artificial intelligence which deals with reasoning qualitatively about the behavior of physical systems. Qualitative physics differs from traditional physics approaches in that reasoning is performed at a more abstract level. This abstraction embodies qualitative characteristics of the behavior of the physical system under scrutiny. The use of qualitative physics allows common-sense analysis to be applied to physical situations when detailed numerical parameters are not easily determined, or simply not available.

The qualitative physics of physical systems represents a substantial amount of research from deKleer and Brown at Xerox Palo Alto Research Center and Forbus at Massachusetts Institute of Technology. The power of formalizing the common-sense knowledge associated with a physical system is the realization of a mechanism for ambiguity resolution. Without this resolution capability, underdetermined systems have only two courses of action; either assert unsubstantiated assumptions to resolve

the ambiguity, or eliminate the possibility of error by avoiding decisions. deKleer and Forbus present two different approaches to physical system modeling. In Forbus's Qualitative Process Theory [FORB83, FORB84], the notion of a physical process is the model primitive, whereas in de Kleer and Brown's ENVISION system [DEKL79, DEKL84A, DEKL84B, DEKL84C], they model a physical system as devices having components with interconnections. The model presented here for the layered bridge deck structure most closely resembles the latter, with layer entities and interlayer links representing interfaces.

4.4.3 Qualitative Model

Paramount to the success of qualitative reasoning and the definition of causal (cause and effect) relationships is the formulation of the domain model. For physical systems, these models require both detailed structural and behavioral knowledge. The ontological primitives necessary for the bridge deck model are restricted to LAYERS and REFLECTION COEFFICIENT interconnections. The structure knowledge for the system at the qualitative level is limited to the physical arrangement of the layers. This physical arrangement and the related layer properties determine the connecting reflection coefficient. Hence, this behavioral knowledge for the physical system may be derived from the associated classical physics relationships. These relationships are outlined below;

Assuming the following notation:

$\epsilon_n \equiv$ permittivity of the n^{th} layer (layer$_n$)
$\rho_n \equiv$ reflection coefficient between layer$_{n-1}$ and layer$_n$
$v_n \equiv$ velocity in layer$_n$
$thk_n \equiv$ thickness of layer$_n$
$time_n \equiv$ time of arrival for reflection$_n$
$[+] \equiv$ qualitative value denoting an increase
$[0] \equiv$ qualitative value denoting a steady state

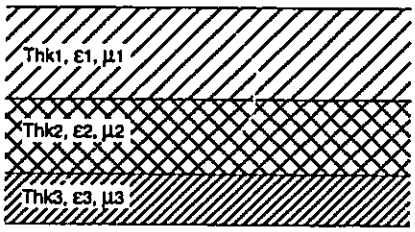

Figure 4.8: Three Layered Structure

$[-] \equiv$ qualitative value denoting a decrease
$\rightsquigarrow \equiv$ implies or asserts

Using the above notation and assuming the layered structure of Figure 4.8 , the following behavioral knowledge may be extracted from the physical model and formalized.

Permittivity - Velocity Relationships

1. $\epsilon_n \equiv [+] \rightsquigarrow v_n \equiv [-]$
2. $\epsilon_n \equiv [0] \rightsquigarrow v_n \equiv [0]$
3. $\epsilon_n \equiv [-] \rightsquigarrow v_n \equiv [+]$

Permittivity - Reflection Coefficient Relationships

$$\epsilon_n \equiv [+] \rightsquigarrow |\rho_n| \equiv [+] \quad ; [\epsilon_n > \epsilon_{n-1}]$$
$$\epsilon_n \equiv [+] \rightsquigarrow |\rho_n| \equiv [-] \quad ; [\epsilon_n < \epsilon_{n-1}]$$
$$\epsilon_n \equiv [0] \rightsquigarrow |\rho_n| \equiv [0] \quad ;$$
$$\epsilon_n \equiv [-] \rightsquigarrow |\rho_{n+1}| \equiv [-] \quad ; [\epsilon_n > \epsilon_{n+1}]$$
$$\epsilon_n \equiv [-] \rightsquigarrow |\rho_{n+1}| \equiv [+] \quad ; [\epsilon_n < \epsilon_{n+1}]$$

From the behavioral knowledge a wealth of useful causal relationships may be derived. These causal relationships rely on spatial and temporal reasoning concepts. Prior to formalizing these relationships, definitions for spatial and temporal reasoning must be established.

4.4.4 Temporal Reasoning

Systems which deal with model dynamics are forced to acknowledge temporal dependencies in data. Radar data represents a temporal or time-of-arrival relationship for

each of the reflections arising from dielectric discontinuities. Repeated here is the convolution sum representing layered structure reflections:

$$y(t) = \sum_{i=1}^{N} \mu(i) x(t - \tau_i) \tag{4.2}$$

where the time-of-arrival of interface$_n$ is τ_n. Traditional numerical analysis of the radar data relies on reflection arrival times to estimate layer thickness. Qualitative dynamics extends this dependency by considering time derivatives, the change in time of the reflection events for spatially related reflections. These time derivatives include absolute variations (the variation of reflection$_n$ arrival time with respect to time = 0; or τ_0) and also relative variations between any two interface reflections (τ_m - τ_n).

4.4.5 Spatial Reasoning

As discussed in Section 4.3, bridge GPR surveys represent a 3-dimensional data set; (abscissa ordinate) pairs indicating surface position, as well as interface arrival times representing depth values. Therefore, for any position on the structure there may be associated a neighbourhood. Based on the neighbourhood concept is the capability to generate spatial derivatives for any physical parameter of interest.

Assuming there exists some local parameter of interest k in $CELL0$, then for any neighbourhood (in the case shown in Figure 4.9, the neighbourhood is orthogonal consisting of cells [CELL1 ,CELL2 ,CELL3 ,CELL$_4$]) the directional spatial derivatives may be calculated (based on an intercell spatial displacement of δc_n);

$$\frac{\delta k_n}{\delta c_n} = \frac{k_0 - k_n}{\delta c_n} \tag{4.3}$$

Associating physical significance to these spatial derivatives allows the formulation of causal relationships regarding the positional variation of parameter k. Without considering the entire bridge structure and thereby viewing each data set (the LINE variables in the physical model, shown in Figure 4.3) as a fragment of the entire

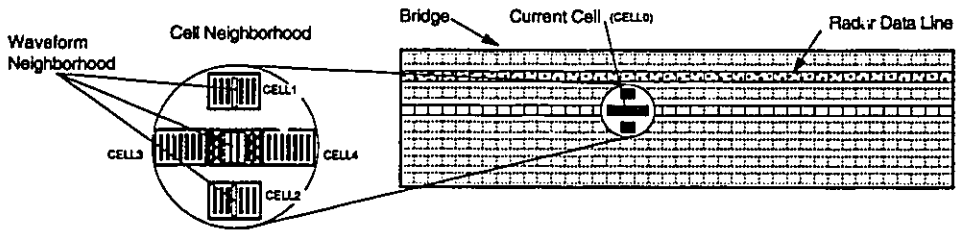

Figure 4.9: Cell Level Orthogonal Neighborhood

problem set, these spatial derivatives would not be available. Spatial derivatives contain substantial qualitative reasoning potential.

4.4.6 Causal Reasoning

Combining the behavioral knowledge with temporal and spatial reasoning provides the foundation of the qualitative physics approach towards the solution of the bridge radar and the related underdetermined inverse problem. The available causal relationships may now be developed, using the notation presented in Section 4.4.3;

Thickness

The effects of layer_n thickness variation on time of arrival for interface reflection_{n+1} and all subsequent layers (ie. $layers_{n+1:M}$):

$$thk_n \equiv [+] \rightsquigarrow time_{n+1:M} \equiv [+]\,;\, |\rho_{n+1:M}| \equiv [0]$$
$$thk_n \equiv [-] \rightsquigarrow time_{n+1:M} \equiv [-]\,;\, |\rho_{n+1:M}| \equiv [0]$$

Permittivity

Again, assuming the three layered structure where $(\epsilon_{n-1} < \epsilon_n < \epsilon_{n+1})$:

$$\epsilon_n \equiv [+] \rightsquigarrow v_n \equiv [-]\,;\, time_{n+1:M} \equiv [+]\,;\, |\rho_n| \equiv [+]\,;\, |\rho_{n+1}| \equiv [-]$$

$$\epsilon_n \equiv [-] \rightsquigarrow v_n \equiv [+]\,; time_{n+1:M} \equiv [-]\,; |\rho_n| \equiv [-]\,; |\rho_{n+1}| \equiv [+]$$

Observed Radar Data Relationships

For observed site radar data the inverse form of these qualitative relationships are functions of only amplitude and reflection arrival time. These relationships, in the form used for rule system inferencing are presented here. Where $\Delta_d Amp_n$ and $\Delta_d time_n$ are the spatial derivatives of the amplitude and time-of-arrival of interface$_n$ in the direction d in a neighbourhood about the current inferencing point.

Radar Data Thickness Rules

IF

1. $\Delta_d Amp_n \equiv [0]$
2. $\Delta_d time_{n:M} \equiv [+]$
3. $\Delta_d time_n < \Delta time_{limit}$
4. $\Delta_d model \equiv [0]$

THEN

$\Delta_d thk_{n-1} \equiv [+]$

where predicate [4] above indicates there was not a model change in the d direction. Conversely, if [2] above showed a cascading decrease:

IF

1. $\Delta_d Amp_n \equiv [0]$
2. $\Delta_d time_{n:M} \equiv [-]$
3. $\Delta_d time_n < \Delta time_{limit}$
4. $\Delta_d model \equiv [0]$

THEN

$\Delta_d thk_{n-1} \equiv [-]$

Radar Data Permittivity Rules

For an increasing dielectric layered structure (where $\epsilon_{n-1} < \epsilon_n < \epsilon_{n+1}$)

IF

1. $\Delta_d Amp_n \equiv [-]$
2. $\Delta_d Amp_{n+1} \equiv [+]$
3. $\Delta_d time_{n+1:M} \equiv [-]$
4. $\Delta_d model \equiv [0]$

THEN

$\Delta_d \epsilon_n \equiv [-]$

And

IF

1. $\Delta_d Amp_{n-1} \equiv [+]$
2. $\Delta_d Amp_n \equiv [-]$
3. $\Delta_d time_{n+1:M} \equiv [+]$
4. $\Delta_d model \equiv [0]$

THEN

$\Delta_d \epsilon_n \equiv [-]$

These rules assume the amplitude and time-of-arrival of reflection waveforms are not severely corrupted by interreflection interference caused by multiple reflections or thin layers. A change to the relative permittivity relationship for this consecutive layer structure (indicating a physical model change) would alter the observed reflection coefficient changes according to the qualitative relationships established in Section 4.4.3. These qualitative relationships produce straightforward derivations for layer permittivity increase and decrease rules to reflect the new physical model.

4.4.7 Spatial Parameter Thresholds

Spatial derivatives also provide a mechanism to establish limit relationships to indicate a possible model class violation (for bridge decks this implies either a cross-section change or defects). Defining the spatial derivatives for the primary parameters of the GPR inverse problem allows the definition of limits defined by practical physical structures:

$$\left|\frac{\Delta Amp_n}{\Delta c_n}\right| \rightsquigarrow \left|\frac{\Delta \epsilon_n}{\Delta c_n}\right| < \epsilon_{limit} \tag{4.4}$$

$$\left|\frac{\Delta time_n}{\Delta c_n}\right| \rightsquigarrow \left|\frac{\Delta thk_n}{\Delta c_n}\right| < thk_{limit} \tag{4.5}$$

where both thresholds (ϵ_{limit} and thk_{limit}) are functions of sample separation (Δc_n), the particular layer (type, material, condition) and radar footprint.

Thickness variation threshold (thk_{limit}) is a far more rigid threshold than the permittivity variation threshold (ϵ_{limit}). Building codes determine acceptable thickness tolerances for various cross-sectional layers. For decks built after 1978, a suitable heuristic threshold is:

$$thk_{limit} = \frac{2.5\ cm}{meter} \tag{4.6}$$

which is valid for the top surface of concrete deck slabs away from formwork joint or seam locations [MERL92]. Using these qualitative causal relationships as rule foundations allows reasonable ambiguity resolution when faced with inferencing decisions with multiple degrees of freedom.

4.4.8 Cross-Sectional Modeling

A significant advantage to multidomain knowledge based systems is the seamless interaction of unrelated expertise to solve a global problem. This interaction is highlighted by the system ENVISIONMENT module. As indicated, bridge GPR surveys

typically encounter many different cross-sections. The envisionment process combines the knowledge of the current bridge structure's possible cross-sections with radar and electromagnetic expertise to construct a collection of cross-section templates or models for the particular bridge structure being surveyed.

This modeling process uses the current radar transmit waveform (defined by the source radar used to produce the GPR data), the electromagnetics convolution-sum definition of the direct problem, the bridge cross-section specifications and typical material parameters to generate cross-sectional units (data structures) and representative waveforms. The cross-sectional models provide the system with a data interpretation foundation by establishing nominal values for expected reflection amplitudes and time-of-arrival parameters. This cross-sectional reflection envisionment also provides a means for the system to accurately distinguish between structural model changes in the actual data. By comparing the similarity of various cross-sectional returns as time domain waveforms, the system can decide on various digital signal processing (DSP) strategies for the accurate identification of embedded structural events. Figure 4.10 depicts waveforms for two juxtaposed structural components. The system would elect to use a sudden concrete/air reflection in the highlighted zone for model change detection. For juxtaposed cross-sections not exhibiting such a model change, the cross-sectional similarity is used to advantage to locate short spatial discontinuities representing structural joint steel concentrations. This emulates the human expert top level model recognition process.

4.4.9 Top-level Agenda Controller

As discussed in Section 4.2.1, large blackboard based data analysis systems typically incorporate top-level control strategies to enhance inferencing performance. The highest level inference control strategy used by the radar interpretation system is driven by two complementary directives:

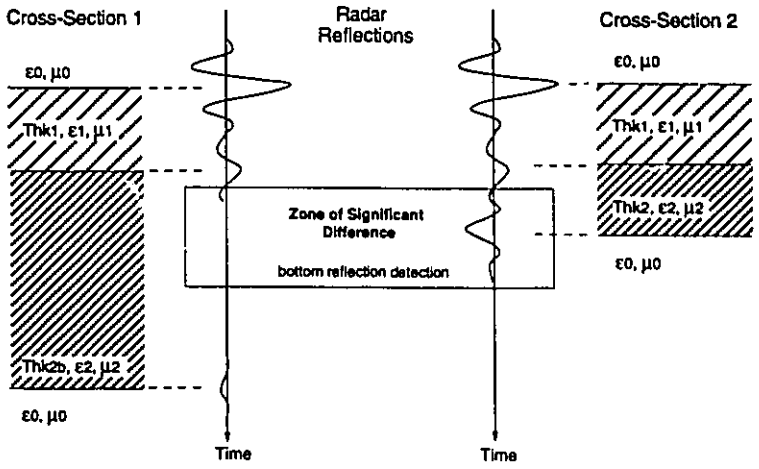

Figure 4.10: Two Cross-Sectional Waveforms

1. Inference performance: Expert system inferencing during [WAVE] and [CELL] level analysis need only be concerned with a neighbourhood spatially arranged around the current system reasoning point. Knowledge source monitoring of the entire bridge data structure would be fruitless and computationally prohibitive.

2. The desire to maximize estimated parameter reliability: As local parameter derivation for the inverse problem suffers from assumption based reasoning limitations for all locations where the exact physical dimensions of the cross-section are not known, reasoning should begin where these dimensions are known.

In conjunction with GPR data acquisition, the current bridge evaluation methods include taking core samples from several locations on the bridge deck structure. These locations indicate locations where 100% reliable cross-sectional dimension data exists. Using the cell agenda control algorithm, these represent the starting points for bridge analysis. Subsequent cells are selected by minimizing the Euclidean distance to the core locations. This strategy causes inferencing to ripple outward from the core locations much like ringlets emanating from a point source in a smooth pond. Figure 4.11 shows the cell level agenda for a simple slab which has two core locations.

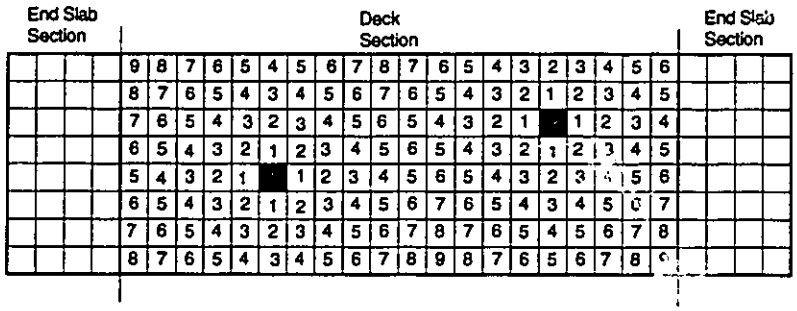

Figure 4.11: Top-level controller cell analysis agenda
This figure shows the cell processing agenda for the Deck slab of a three section structure based on the specification of the physical core sample locations (the shaded cells).

Structural joints represent boundaries to this strategy. All inferencing remains within the boundaries of a structural component prior to moving onto the next. In this way, at points where the physical dimensions are known, the material permittivities may be determined with maximum reliability. As the cell distance increases away from the cored cells, the qualitative analysis for resolving multiple parameter (layer thickness and permittivity) variation ambiguity becomes paramount.

4.5 Conclusions

Expert system methods elegantly assimilate several reasoning paradigms for use on the GPR analysis problem;

1. Multiple diverse knowledge sources are effectively combined, and efficiently interact using a blackboard architecture.
2. Qualitative reasoning principles can be applied to both the spatial and temporal aspect of the problem to provide formal derivations of unknown parameter relationships based on physical and practical assumptions.
3. Quantitative techniques may be intelligently applied for preprocessing and data enhancement.
4. Top level control structures are incorporated to enhance performance by restricting the scope of system inferencing.
5. Conventional inference engine methods to combine both data and goal driven reasoning.

The following chapter presents the implementation of these fundamental concepts to formulate an unique automated interpretation system for bridge deck GPR data which significantly enhances the consistency and precision of generated results.

Chapter 5

System Development

As indicated in Section 4.1, the application of Artificial Intelligence techniques requires a framework of interpretation as most significant problem tasks are context sensitive. An expert system implementation provides such a framework for the flexible combination of many diverse signal and symbolic processing methodologies. This framework is presented in detail here for the GPR interpretation problem, with specific results based on actual GPR data acquired from a concrete slab-on-girder bridge deck. The structural details of the actual bridge site are given in Appendix B, and the raw digitized data are presented in graphical form in Appendix C.

5.0.1 System Hardware

The development and implementation of the expert system was done on a Texas Instruments microExplorer. At the time of acquisition, the microExplorer represented the state-of-the-art for symbolic LISP machines. Using LISP machines for large intelligent system development is attractive for several reasons;

- native virtual memory support at the operating system level. The microExplorer operating system supports large virtual memory spaces to a maximum of 128 Mbytes. The configuration used to develop the GPR expert system had

100 Mbytes virtual memory (limited by secondary mass storage size) and 12 Mbytes physical memory.

- high performance 1120x826 pixel graphics display in conjunction with LISP based Common Windows, an object-oriented windowing environment.
- hardware level support for the LISP language. The Explorer provides machine language support for compiled LISP at the microcode level. Additionally, the microExplorer system uses a tagged memory architecture to reduce the overhead of garbage collection arising from dynamic memory LISP environments.

The virtual memory space consideration was particularly significant for the large data sets produced by GPR surveys. Manipulating entire bridge data sets can require more than 30 Mbytes for all forms of data storage (including raw, filtered, and processed data structures). The ability to keep all data sets on hand during reasoning was a high priority for the platform/environment selection process. Another benefit of choosing a LISP machine is the availability of high performance expert system development shells.

5.0.2 The Expert System Shell

Expert system shells provide a high level language interface to the task of constructing expert system applications. The shell used for this GPR system development was the Knowledge Engineering Environment (KEE) from Intellicorp[KEE88]. The KEE product is one of a select few expert system development environments capable of managing and reasoning on problems of the size presented by GPR bridge analysis. The Bridge Deck System creates more than 6000 units (frames) during the course of reasoning and even for KEE, this presents some interface and display related problems. The sheer size of the hierarchical bridge data structure caused corrupted graphical displays and annoying display related delays. These problems were limited to display aesthetics and in no way impaired the operation of the inferencing system. KEE also provides several benefits for large system development;

- a comprehensive environment; KEE provides a rich environment for system development, which includes context sensitive editors, full function debuggers,

interface building tools and most importantly, an open architecture.

- multiple reasoning paradigms; KEE provides support for any combination of either of the following AI paradigms:
  - **RULES** KEE provides conventional induction based reasoning using production rules (IF *predicate* THEN *conclusion*), as well as deduction based reasoning using deduction rules (WHILE *predicate* BELIEVE *conclusion*). Using deductive reasoning, when *predicate* is asserted, then *conclusion* is asserted. Thereafter, if *predicate* is retracted, the system automatically retracts *conclusion*. In the KEE system, *predicates* and *conclusions* may reference any LISP function or object.
  - **FRAMES and INHERITANCE** Frames represent the lowest level building blocks of an object based system, inheritance allows superclass (parents) attributes (slots and facets) to be carried down to subclasses (children) in the hierarchy. The inheritance of frame attributes is accomplished by *reference* and therefore minimizes data and code replication.
- a fully integrated mouse based graphical user interface with programming access to extensive windowing functionality.
- object oriented programming including message passing and methods.
- external LISP language support.
- multiple feature inferencing system: the KEE environment provides support for

  rule grouping: KEE allows the creation of logical subsets of rule classes. This capability increases reasoning performance by limiting rule application and search scope. Without this feature all rules must be examined each time a new fact is added to the system.

  rule priorities: the ordering of the invocation sequence for rules and rule subclasses.
- various inferencing strategies; KEE provides the ability to intermix forward and backward reasoning within the same inferencing thread. This provides efficient navigation of potentially large rule bases.

5.0.3 Extensibility

It should be stressed that KEE provides seamless support for extension. A developer need only create the LISP code necessary to provide application specific functionality. Once compiled and loaded these functional modules can be invoked by any other system operation. In this way, numeric or algorithmic code may be effortlessly embedded in rules and the inferencing process. This capability was used throughout the radar analysis system.

5.1 Knowledge Based System

Using the KEE/LISP environment, a multi-domain expert system was created for GPR signal analysis. The application consists of eight knowledge bases processed by a separate rule base (actual KB tangle graphs establishing unit and rule hierarchical relationships are included in Appendix F).

The prototype implementation consists of 6000 lines of LISP source code and approximately 250 rules to encapsulate basic system reasoning as well as the detailed reasoning knowledge for a single bridge type. Although the current system presents an expansive framework for the GPR expert system analysis approach, detailed development and completeness for the prototype were restricted to the interpretation of a particular bridge type (multiple section, asphalt covered concrete slab on prestressed-girders) using a particular radar unit (air-mounted, constant flare-angle horns). This does not represent a limitation to the techniques presented here, as the system development was approached from a modular design standpoint. To accommodate different entities (specifically bridge types, radar units, data formats and new construction materials) only specialization of the appropriate hierarchical knowledge base is required. Additionally, the modularity inherent in expert systems allows the substitution of system knowledge and rule bases to modify the applicable area of expertise and application.

All development was done under the enormous diversity which is the KEE system. Initial design efforts vehemently avoided conventional procedural code for initialization and control functions, adopting instead *expert systems* methods. As such, there is no overall controlling code for the system, rather the blackboard paradigm is exploited to enable rule-based system operation. As facts are asserted and added to the system blackboard, various rule bases react and cause subsequent system initializing side effects and further assertions. This reasoning chain propagates until all reasoning

and data interpretation is complete.

For this system, the processing may be separated into five essentially sequential operations;

- Initialization
- Configuration
- Pre-analysis
- Data analysis and inferencing
- Result extraction

Each of these operations will be introduced here and discussed in detail in subsequent sections. During the detailed discussion of the system implementation, methodology limitations and improvements will be presented.

Initialization

The system initialization phase allows the user to interact with the system through a graphical interface to specify site specific background facts required for further inferencing. For the current system this initialization includes:

- bridge type selection and age.
- physical dimensions including the number of driven lanes.
- visible deck joints and apparent surface distresses [including cracks, potholes, patches] and structural anomalies such as drainage grates, support piers and girder diaphragms.
- bridge environment, vehicle traffic estimates, salt applications, previous maintenance and deck rehabilitation (asphalt resurfacings).
- core sample location and descriptions.
- subjective operator input such as surface Pavement Condition Index[1].
- source radar unit.

As the operator selects the various options and specifications the facts are asserted and added to the global blackboard. A portion of a sample user input session is shown in Figure 5.1.

[1]PCI represents a surface condition rating from 0, indicating extremely poor surface, to a maximum of 5, indicating a smooth, generally excellent condition surface. The PCI index scheme is a rating technique developed and used by MTO and radar data collection operators are typically capable of rendering a PCI rating of a surface by casual visual inspection.

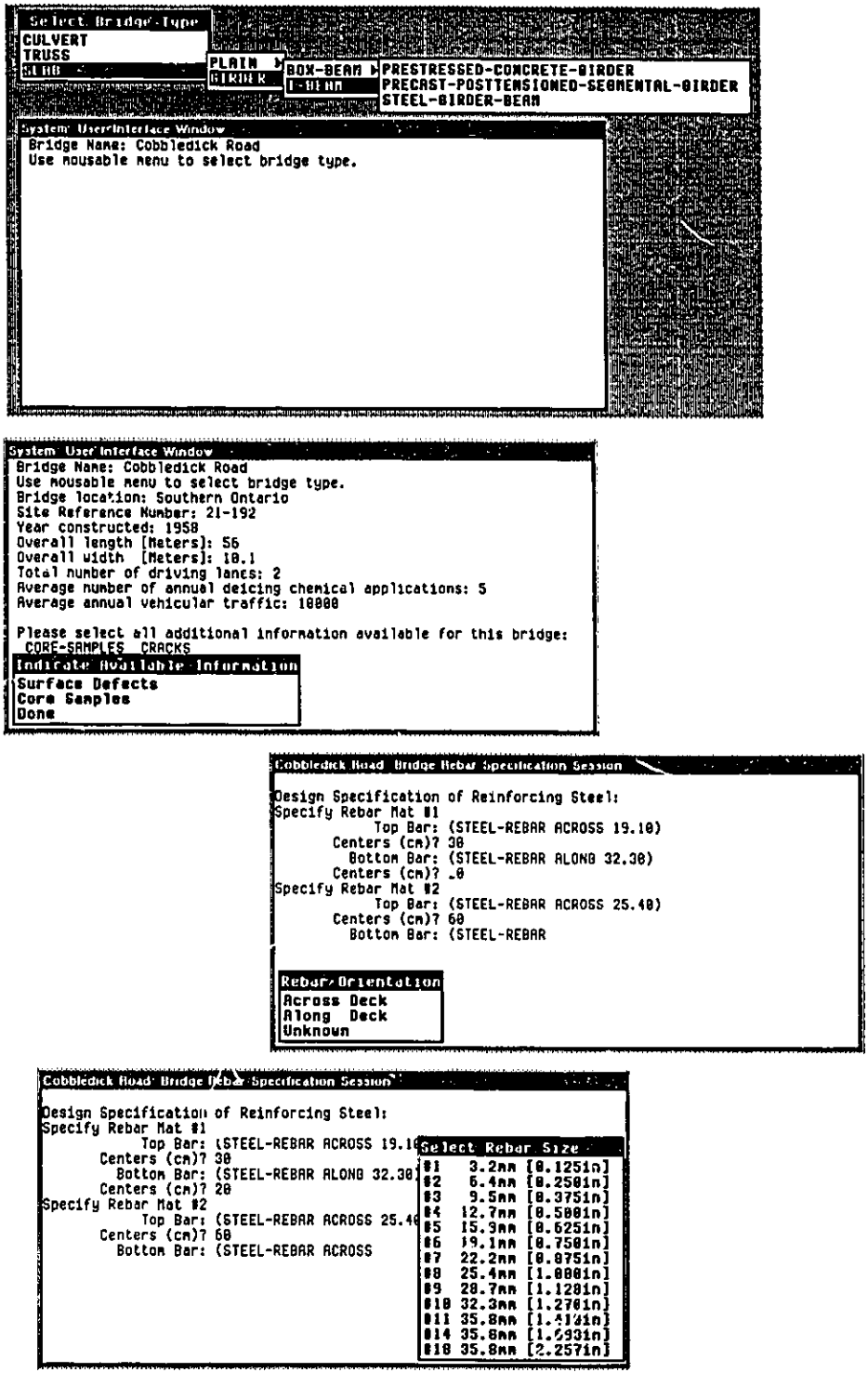

Figure 5.1: User Input Session for System Initialization

Configuration

After physical site specification, the system prompts the user for data file specification, and the associated deck location where the data was located. As each file is loaded by the system, the external data format is converted to an internal floating point representation. Simultaneously, the data is filtered (detailed in Section 5.3.1 below) and construction of the hierarchical structure for the bridge is performed. The appropriate data translation is selected by the data rules, based on the selected input data type (these conversions involve digitized data format translations such as word length and order translations).

Pre-analysis

Prior to the actual data interpretation the system performs various levels of pre-analysis generating substantial data condition metaknowledge. This analysis identifies and tags the associated CELL structure of areas on the deck structure which exhibit user identified surface distresses (cracks, patches, etc.) and identify driven lane related amplitude variations and the possibility of thin asphalt areas. The final phase of the pre-analysis provides the system data inferencing operation with an optimized data cell analysis agenda, identifying the sequence for data analysis which optimizes qualitative rule application and thereby increases inferencing reliability. Each of these operations are discussed in detail in following sections.

Data Analysis

Cell and waveform level inferencing comprise the bulk of the expert system processing effort. The data interpretation provides numerical interpretation of the radar data based on system generated cross-sectional models and results in physical layer estimates and identification of suspected areas exhibiting physical distress. This physical

distress identification arises from locations with unexplained interface anomalies or unique qualitative physics and spatial variation based physical system violations.

Result Reporting

This prototype system restricts output generated to the extraction of numerical layer specifications for all CELL units in the BRIDGE hierarchy. Bridge fault reporting is produced by the extraction of the affected CELL fault slots.

5.2 Cross-section Modeling

Cross-sectional modeling represents a mapping of the underlying structure of the user specified bridge design type to a detailed layer structure. As originally suggested, this modeling represents the foundation for successful data interpretation. Modeling includes nominal material, dielectric, and thickness properties. The default values are extracted from the system BRIDGES design and MATERIAL knowledge bases and building code details included in the system rule bases. During model reasoning the system creates a unit for each possible cross-section arising from the active bridge type. Each bridge design included in the BRIDGES KB contains a slot specifying the possible cross-sections encountered for the particular design type. These cross-sections are specified as multi-level lists referred to here as (XSECT_LIST), where each entry in XSECT_LIST represents a typical structural cross-section for the given bridge type. The possible cross-section list concept may be illustrated by way of an example. Consider the possible cross-sections for a concrete slab-on-girder design (as presented in Appendix B):

(ROADWAY, APPROACH, ABUTMENT, UNSUPPORTED.ENDSLAB, ENDSLAB,
DECK.ON.AIR, DECK.ON.GIRDER)

The XSECT_LIST structure allows concise encapsulation of relative position, bridge component necessity and identification information for bridge design cross-sections. The DEFAULT.CROSS-SECTION slot for concrete-slab-on-girder design fully specifies:

((ROADWAY | NIL)
(APPROACH | NIL) (ABUTMENT | NIL) (ENDSLAB | UNSUPPORTED.ENDSLAB)
(DECK.ON.AIR | DECK.ON.GIRDER)
(ENDSLAB | UNSUPPORTED.ENDSLAB) (ABUTMENT | NIL) (APPROACH | NIL)
(ROADWAY | NIL))

Therefore, the system identifies the possibility of a maximum of nine and a minimum of three *different* cross-sections arising during inferencing. Each sublist presents alternate choices to the system, with **NIL** indicating the possible absence of that particular segment during interpretation. The cross-sections specified in the XSECT_LIST must exist in the CROSS-SECTION KB, otherwise an *unknown cross-section* error will result. The ordinal arrangement of the default cross-sections slot is significant, and indicates the fixed arrangement of bridge subcomponents as the structure is examined sequentially in a longitudinal direction (this eliminates impossible juxtaposed cross-section possibilities such as sequential ABUTMENT/ABUTMENT cross-sections). The use of a list structure (the native data structure for LISP) is an efficient method for storing and manipulating the default structure. As new bridge structures are added to the BRIDGES KB then any new cross-sections contained within the new definition must be added to the CROSS-SECTION KB.

The second phase of modeling combines these generic cross-sectional definitions with knowledge derived from the RADAR KB for the radar unit responsible for producing the input data files and modeling procedures for direct wave solution to the layer media problem. The modeling process is shown in Figure 5.2.

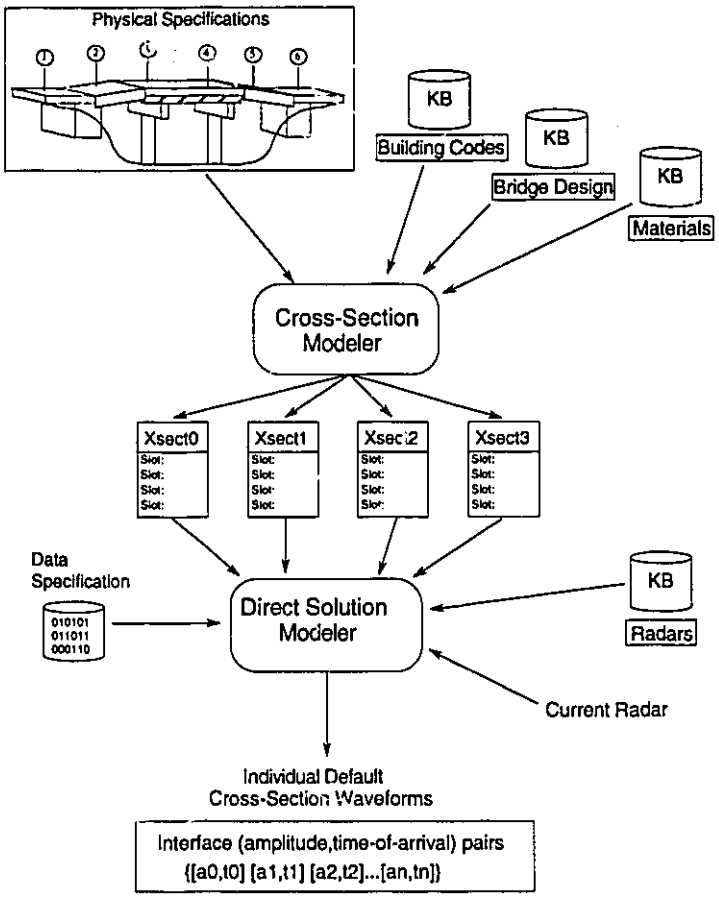

Figure 5.2: Cross-Sectional Modeling Operation

The system modeling operation combines physical site with data and radar unit specifications to produce models for the various cross-sections of the structure. The Modeling module output is a list of amplitude and delay pairs representing each interface reflection.

5.2.1 Modeling Procedure

The system proposes an intelligent modeling scheme for the bridge structures which is responsible for:

1. formally defining default cross-sections and layer/interface (amplitude, time-of-arrival) reflection pairs for the entire bridge surface according to site specifications.
2. identifying essential cross-sections and optional alternates where they exist. This allows the system to anticipate and identify valid model changes during reasoning.
3. allowing the expert system to conduct more elaborate inferencing in the form of preliminary structural analysis prior to detailed data set interpretation

The procedure used by the XSECT KB modeling module uses a direct wave solution incorporating the matrix form of the transmission line parametric model for layered structures presented in Section 3.3. This relationship is repeated here for convenience;

$$\begin{bmatrix} W_R(n+1,t) \\ W_L(n,t) \end{bmatrix} = \begin{bmatrix} \phi_1(k_n)D_n & \phi_2(k_n) \\ k_n D_n & \phi_3(k_n) \end{bmatrix} \begin{bmatrix} W_R(n,t) \\ W_L(n+1,t) \end{bmatrix} \tag{5.1}$$

where

$\phi_1(\rho_n) = \phi_3(\rho_n) = (1-\rho_n^2)^{1/2}$ and $\phi_2(\rho_n) = -\rho_n$

$\rho_n = \frac{\sqrt{\epsilon_n}-\sqrt{\epsilon_{n+1}}}{\sqrt{\epsilon_n}+\sqrt{\epsilon_{n+1}}}$

and attenuation effects, velocity and reflection delays for layer$_i$ are given by,

$atten_i = e^{2\alpha\ thk_i}$

$vel_i = \frac{C}{\sqrt{\epsilon_i}}$

$delay_i = \frac{2\ thk_i}{vel_i}$

Using this relationship, the modeling proceeds with site specific parameters supplied by the system KB's including;

- default material properties from the MATERIALS KB, ($\epsilon_i, \alpha_i \equiv$ layer$_i$ permittivity and attenuation (dB/m))

- physical parameters from the site specification, (thk$_i \equiv$ layer$_i$ thickness)
- CURRENT_RADAR parameters from the RADAR KB, ($W_{R0} \equiv$ incident radar amplitude, and radar footprint)

And for N multiple reflections between a three layered structure ([layer$_j$ layer$_k$ layer$_l$] and where ρ_{jk} is the reflection coefficient between layer$_j$ and layer$_k$);

$$W_{Li} = W_{Ri}(-\rho_{jk})^{N-1}\rho_{kl}^{N}(1-\rho_{jk}^{2})e^{2^{N}\alpha thk_i}$$

$$T_l = T_k + \frac{2^{N}thk_k}{v_k}$$

Also included in the modeling strategy are embedded rebar effects for each cross-section based on radar footprint and rebar specifications (density and placement) determined from building code rules and bridge type. The modeling operation determines the total steel rebar scattering width using a thin wire approximation and calculates the reflected energy based on incident energy and illumination area (detailed in Section 2.2). This reflected energy is subtracted from the incident energy to approximate the transmitted energy through the rebar matte.

$$Rebar_{ref} = W_{Rinc}\,\sigma_{REBAR}$$

$$Rebar_{xmt} = W_{Rinc} - Rebar_{ref}$$

Using these relationships the (amplitude A_i (given as W_{Li} above), and time-of-arrival T_i) sequences may be generated for each of the default cross-section units. The reflection modeling process is performed until the reflection amplitude is below CURRENT_RADAR noise levels or the time-of-arrival is outside the data observation window defined by the data set.

By examining these models the system can extract probable magnitude, polarity and time-of-arrival for each interface defining a cross-section. Further time-of-arrival analysis allows the system to acknowledge sections of structures where full wavelet resolution is not probable. Thin layers thickness variation can introduce interwavelet

distortions and affect observed wavelet peak amplitude. Identifying this scenario allows the system to flag structures as being layer thickness sensitive for calculations derived from interface reflection amplitudes (such as material permittivity).

For a monopulse radar with data sampling rates of 54 pS and a concrete slab-on-girder (a nominal cross-section of 100mm asphalt over 180mm concrete) bridge structure constructed in 1958, the system produces the cross-sectional models shown in Figure 5.3. The system produced internal layer structures for these models are presented in detail in Appendix E. The accurate and extensive intelligent modeling capabilities of this system represent a significant advancement for accurate radar data interpretation.

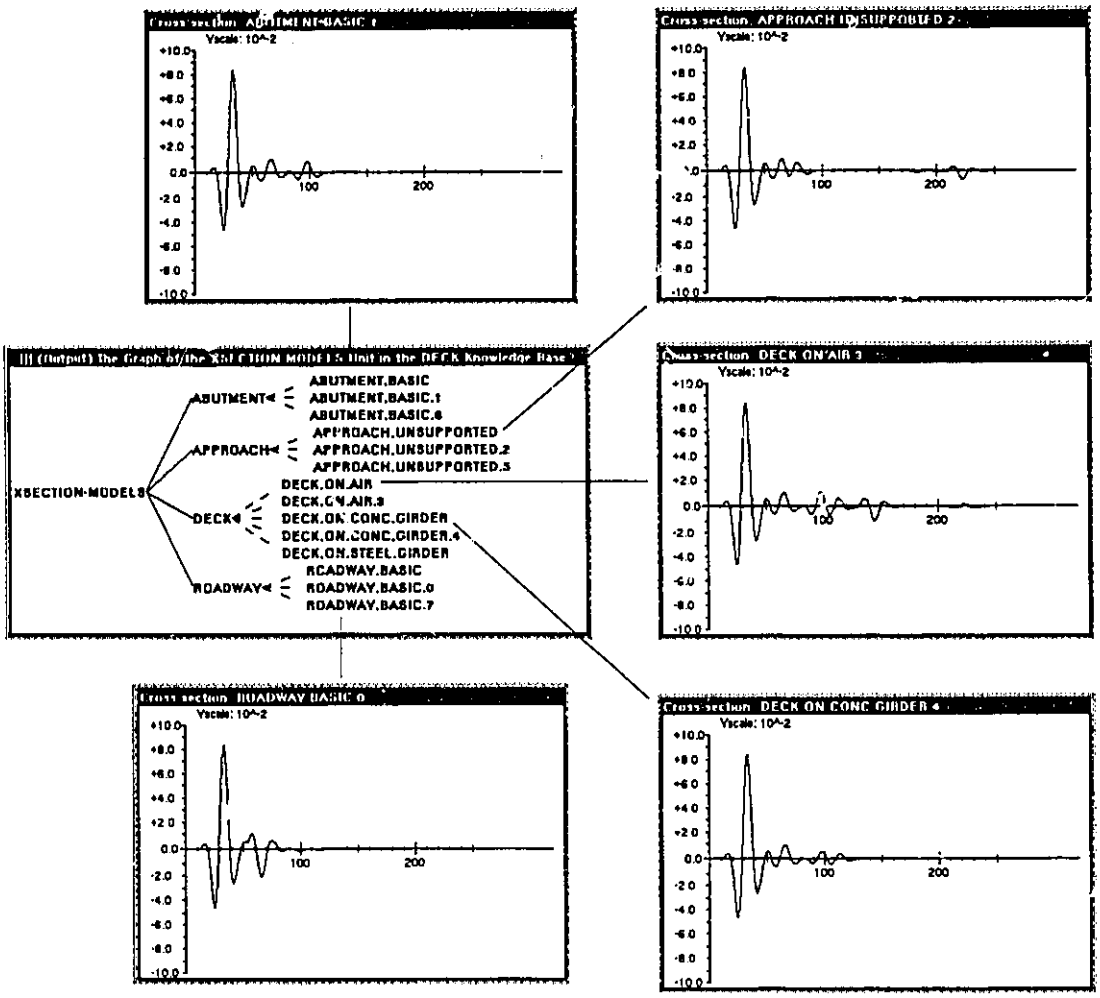

Figure 5.3: Expert System Produced Cross-Sectional Models
The system modeling output for the various cross-sections of a SLAB-ON-GIRDER structure. The horizontal axis scale is measured in CURRENT RADAR sample-time intervals.

5.3 Subsymbolic Data Reduction

The data produced by GPR procedures may be described as discrete time-series data, and typically contains far more raw data than information. This observation and the recognition that AI systems excel at symbolic and logical operations [ANTO91] led to the realization that a non-symbolic level was required to preprocess the raw GPR data. This was approached cautiously to avoid the pitfalls of such systems which rapidly become focussed on algorithmic preprocessing and retain only an insignificant amount of intelligent reasoning [ROSS91, LEE87]. Therefore, the preprocessing was concentrated at the raw data processing level, manipulating the data into a form amenable to an abstract reasoning system. Ideally, this subsymbolic process would act on the discrete time-series data achieving maximum levels of raw data reduction while preserving all information content.

Detailed study reveals that primary information sources in GPR data consist of amplitude and time-of-arrival for each interface reflection. This realization lead to the notion of the ideal preprocessing operation; a two port process where time-series data is given as input and interface reflections, classified by amplitude and time-of-arrival, are produced as output. In practice the accuracy of such preprocessing is hindered by noise and thin layer reflection interference. A second practical consideration is the computational expense associated with the operation. In the framework of expert system based analysis, low computational cost and less analytically efficient processing is preferred to high cost and higher efficiency preprocessing. This may be interpreted as a decision to relax critical classification efforts during preprocessing. Such a philosophy allows algorithmic preprocessing to focus on data reduction and not on interpretation.

The resulting preprocessed data set is viewed by the system as auxiliary data which

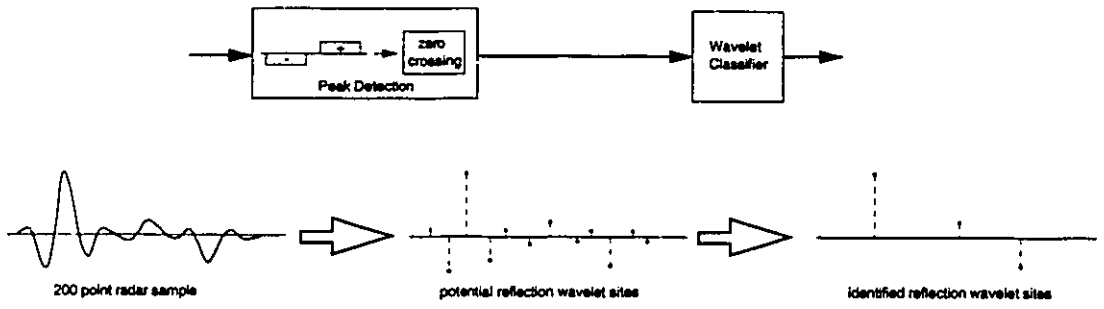

Figure 5.4: Two Step GPR Data Preprocessing Procedure
The system incorporates a zero-crossing based peak detector operation followed by a waveform classifier in order to accomplish the raw data abstraction moving from digitized data to high likelihood interface reflections.

augments the overall symbolic interpretation. This ancillary nature to the preprocessed data implies a limited expenditure of total system processing time be allocated for reflection interface processing. Based on these considerations, the requirements of a suitable preprocessing procedure were identified as:

- maximize the retrieved information content.
- identify and extract significant interface reflection peaks from the backscatter data.
- being capable of high noise immunity.
- be insensitive to minor reflected wavelet distortions.
- minimize processing time and resulting data set size.

Due to extreme radar data set sizes, all levels of system processing speed were of constant concern. In order to maintain reasonable pre-processing performance, a two step approach was adopted which capitalizes on physical characteristics of reflected data. The procedure involves the crude (and correspondingly fast) identification of all candidate interface locations in the time-series data, and the subsequent classification of each of these candidates. The candidate identification step consists of the definition of a reflected wavelet characteristic which is both consistent and recognisable in the data. For a monopulse triplet this is defined as the primary peak.

In the monopulse case, a simple heuristic for interface identification relies on the initial recognition of a substantial primary peak in the backscatter data. This

significant peak identification provides a reduced number of candidate locations for reflected wavelet classification as detectable interfaces *only* occur when some form of peak is detected. The candidate location technique reduces the number of test locations in the GPR bridge data from each of the input sample points (typically greater than 200) to less than 20. This represents the first preprocessing operation of peak detection. The second step provides binary wavelet classification (TRUE: wavelet detected, and FALSE: unknown pulse shape). This two step approach is shown in Figure 5.4. Based on the ideal reflected wavelet shape derived from the CURRENT_RADAR transmit pulse slot in the RADAR KB, this operation compares the actual wavelet to the ideal. Therefore, the second process represents a wavelet correlator. Based on these requirements, two different approaches were investigated during system development;

- a least mean of squared errors similarity measure and threshold routine.
- a neural network classifier.

5.3.1 Peak Detection

During classification method assessment, the peak detection operation was identical for both the neural network and sum squared error approaches and provided substantial data reduction. Although many peak detection algorithms exist, the technique adopted incorporates a differentiating filter which maps peaks into zero crossings. This filter is convolved with the input data stream to produce the filtered derivative.

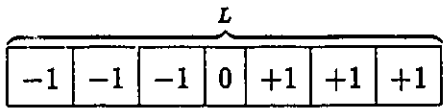

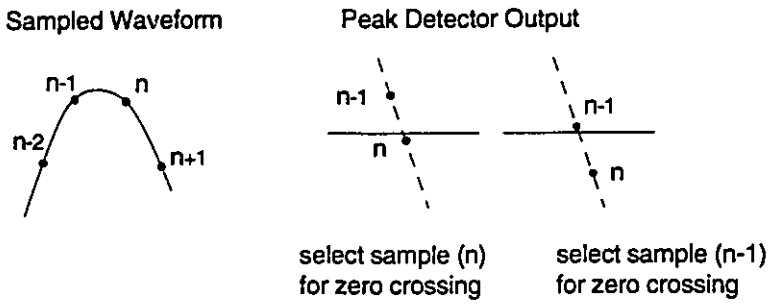

Figure 5.5: Zero Crossing Approximations Arising From Sampled Data
In order to reduce time-of-arrival approximations, the peak detection routine selects the closest zero crossing point (shown in the two cases at right).

In addition to simplicity (and hence low computational overhead) this filtering technique provides the additional benefit of allowing system selection of the filter length parameter L, which controls data smoothing prior to peak detection. The filter length heuristics are based on data set noise figures and desired peak sensitivity. Typically, this parameter varies between 3 and 9. A consequence of longer filter lengths can see a dramatic increase in peak detection time and the oversight of faint interface reflections. The discrete nature of the sample data requires added complexity to the zero crossing selection. For sharp peaks the zero crossing detection involves a decision based on the closest crossing point; this reduces time-of-arrival interpretation errors (Figure 5.5). The output from the peak detector (amplitude scaled impulse sequence) is used by the wavelet classification operators.

The effectiveness of this simple filter technique at peak detection is shown in Figure 5.6. The original 108,000 samples (arising from 540, 200 point waveforms) have been reduced by more than an order of magnitude to less than 10,000 peaks. As mentioned previously, this peak detection is performed during the data load and translation operation as the data is read from mass storage into the system. During this data loading operation, each sample point is converted into the internal floating point format, and the filtering operation is done concurrently at minimal expense.

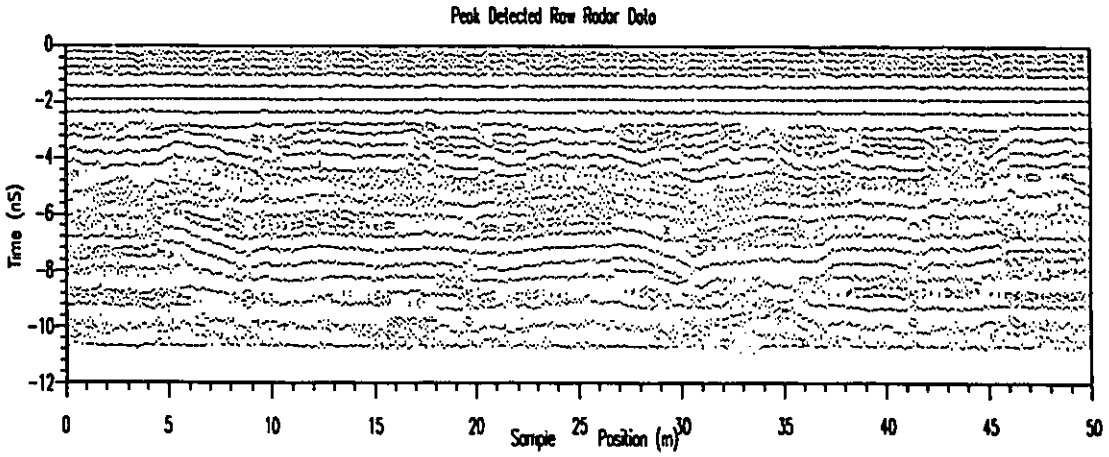

Figure 5.6: Filtered and Peak Detected Radar Line Data

5.3.2 Sum-Squared-Error Wavelet Classification

Using the peak locations, the radar transmit pulse obtained from the global blackboard is scaled and the difference taken from the raw data about the peak location. This difference is compared with a system generated threshold. Although fast, this classifier is prone to wavelet noise and the inability to distinguish significant signal distortion. Figure 5.7 shows two wavelets which produce almost identical sum-squared-error values. The wavelet on the left represents a *shape* distortion which should ideally produce a much greater error when classified by a wavelet shape classifier. In use, the threshold selection was found to be highly data dependent and system heuristics were biased towards selecting inappropriate peaks rather than missing valid peaks. Optimum operation of this classifier was accomplished by user intervention for threshold selection.

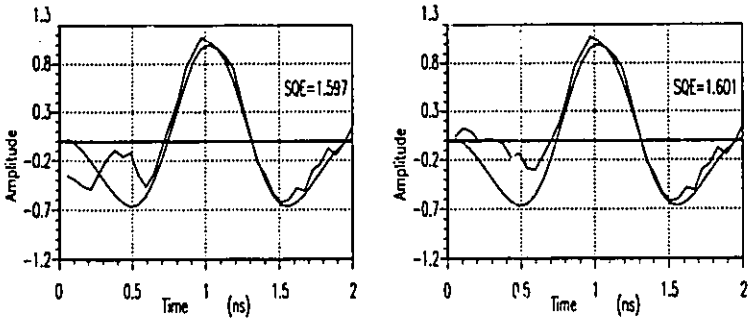

Figure 5.7: Sum Squared Error Wavelet Classifier

5.3.3 Neural Network

Feed-Forward Networks

Neurocomputing and neural networks first demonstrated effectiveness at character pattern classification in 1957 with the Mark I Perceptron [HECH90]. Neural networks are defined as [HECH90, pp 3];

> ... a parallel distributed information processing structure consisting of **processing elements** ... connected by unidirectional signal channels called **connections.** Each processing element has a single output connection that branches ... to as many collateral connections as desired each carrying the same signal - the **processing element output signal.** The processing element output signal can be any mathematical type desired. The information processing that goes on within each processing element can be defined arbitrarily with the restriction that it must be completely local; that is, it must depend only on the current values of the input signals arriving at the processing element via impinging connections ...

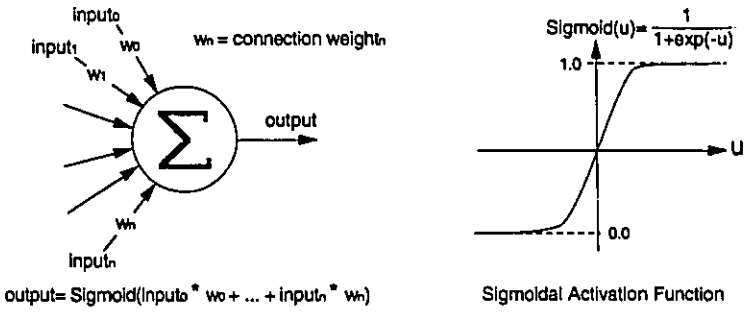

Figure 5.8: Neural Network Processing Node and Sigmoidal Activation Function
Each node in a neural network has a number of weighted inputs which are summed and used as input to the nodes activation function. For the networks used in the system, the activation function was sigmoidal. The output from each node is used as input to subsequent layers, in a fully connected fashion.

Typical topologies for neural networks involve three cascading layers referred to as input (the network input signals), hidden, and output (the unique network classifications). The addition of the hidden layer units allows networks to provide functional mapping for spaces of arbitrarily large dimension. A macroscopic view of such a three layer network is depicted in Figure 4.7.

Activation functions for each processing element (or node) found in feed-forward networks should be bounded and differentiable over the entire possible input range [GROS88, PAO89]. Also, activation functions should be monotonic (to avoid network oscillation associated with small network input perturbations) and have large input and limited output dynamic ranges [LIPP87]. One such activation function is the *sigmoidal* function, an example is shown in Figure 5.8.

The shape of the *sigmoidal* function is significant, the lower asymptotic limit provides small random input (considered to be noise) insensitivity. Once this threshold has been exceeded the system responds nearly linearly until the upper asymptote is reached. Therefore the *sigmoidal* function provides a limited output dynamic range with noise insensitivity.

The combination of many processing units into a connected network allows the mapping of complex input spaces to a binary output classification space (ie. output of [0,1]). Through the addition of multiple output nodes a feedforward network is capable of simultaneous multiclass input classification. This type of network responds by activating the output node most closely related (through network training) to the current input signal (vector) and may be thought of as a multiple matched filter implementation.

Wavelet Identification

Several key issues led to the development of a feed-forward network for wavelet identification. Firstly, the recognition of the distortion effects of backscattered wavelets from layered structures, and the ability of feed-forward networks to generalize functional [CUN85] and non-linear [BARH89, GULA87] mappings. Secondly, the adoption of an enhanced conjugate gradient descent neural network training algorithm [POWE77] which typically reduces training times by several orders of magnitude. This increased performance made the practical aspects of dynamic training of small networks possible and their embedded use attractive. Finally, in a LISP machine environment, as procedural code is created it can be compiled and loaded into the system inferencing environment dynamically, thereby allowing subsequent invocation as an executable module. In order to generate a usable neural network, the expert system must:

- define a network topology
- generate a complete training set
- compile and load the trained executable module.

Topology

The network topology defines the number of input nodes (representing wavelet data sample points), the number of output nodes (representing the number of unique

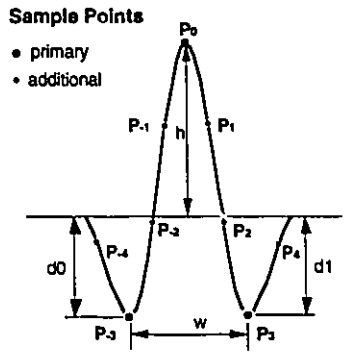

Figure 5.9: Wavelet Sample Points for Neural Network Classifier Inputs
The monopulse wavelet shape may be defined by the primary peak amplitude (h), tail amplitudes (d_0 and d_0) and tail separation (w).

classifications for the network) and the number of nodes in the hidden layer (the nodes responsible for input/output space mapping). The overall concern with repeated uses of a sigmoidal activation function neural network is the performance decrease with increasing node count. This forms the underlying motivation in topology definition.

The expert system relies on input data and radar transmit wavelet shape (defined by parameters d0,d1,w and h in Figure 5.9) to define the input node requirements. According to the Nyquist sampling theorem [OPPE75], the information content of an arbitrary signal may be retained through the sampling process if the sample rate is selected to be at least twice the highest frequency component of the signal. For sinusoidal transmit wavelets produced by monopulse radars with *a priori* main peak location information, the ideal sample points for shape characterization are shown in Figure 5.9 (labeled PRIMARY $[P_{-3}, P_0, P_{+3}]$). In practice, layered structures can produce reflection interference effects thereby distorting the reflected wavelets. Successful wavelet detection may be improved by additional sampling points.

The system uses raw data sampling rates to heuristically define the optimum number and placement of sample points. The sample rate and transmit wavelet shape define integral offset sampling points which most closely attain the ideal points of Figure 5.9. Use of neural network based classification led to sample rates for monopulse

wavelets of three times the sample rate suggested by Nyquist. This over sampling decision arose from the examination of the misidentification cases for undersampled wavelets. The errors were consistently attributed to generalizations caused by main peak distortions. The addition of the P_{-4} and P_4 sample points ensure the classification of wavelets rather than simple peak classification.

Using these sampling heuristics and given a 1.1 GHz transmit pulse with a peak separation of 0.92nS and an effective radar sample rate of 50pS/sample, then the integral sampling position offsets for the points labeled in Figure 5.9 are determined to be:

$$[P_{-4}, P_{-3}, P_{-2}, P_{-1}, P_0, P_1, P_2, P_3, P_4] = [-12, -9, -6, -3, 0, 3, 6, 9, 12]$$

Conversely, if the transmit wavelet was determined to be multiple cycles, then the number of input samples (and hence the minimum number of network input nodes) would be appropriately increased to sample the elongated reflection wavelet. Practical application of the neural classifier suggested the use of two sample points between peak and trough, to detect primary peak shape distortions. Without this *peak shape sensitivity* wavelet selectivity is reduced. Output node topology is straightforward, the network requires a single output node for each network classification. The valid classifications for wavelet detectors are [POSITIVE NEGATIVE INVALID].

The final topology definition requirement is the number of hidden layer nodes. Published literature [LIPP87] indicates a valid empirical choice for generalized complex non-linear mappings is 2.0 times the number of input nodes. However, the wavelet classification scenario presented by the GPR system is somewhat restricted in complexity. The network input is spatially fixed with the centre input node aligned with the peak sample position determined by the peak detection routine. A second

simplification arises from the normalization of the input sequence based on overall wavelet amplitude. This normalization eliminates the requirement for the network to classify amplitude variations. Therefore, for the more simplistic, normalized and spatially centered wavelet classification problem, the number of network hidden nodes may be reduced. In practice the number of hidden nodes is initially set to be one greater than the number of input nodes. This (9-10-3) topology (as shown in Figure 4.7) represents a practical trade-off between classification speed and performance.

Training

Once the network topology has been defined, attention is focused on network training. The conjugate gradient descent algorithm represents an error corrected supervised learning strategy. These methods use the deviation between the actual network output value and the desired output to update the internode connection weights in the direction which reduces the deviation (representing classification error). Using a least mean squared error (F( )) goal for neural network training [RUME86b, RUME86a, LIPP87].

$$\mathrm{F}(\mathbf{w}) = \lim_{N \to \infty} \sum_{i=1}^{N} (y_k - y'_k)^2$$

where y_k is the desired output, y'_k is actual output, N is the number of input vectors, and w are the connection weights. Network training involves the optimization of the weights w to minimize F( ). Typical neural network weight space optimization techniques use the method of steepest descents to minimize the observed F( ) (Perceptron learning rule, Widrow-Hoff or delta rule, and back propagation all use this technique [GROS88, RUME86b]). The problem with steepest descent is the repetitive use of $-\nabla \mathbf{F}$ to reduce F( ) (where F( ) is of quadratic form) in typically small incremental steps to avoid oscillations. A more effective method of optimization would

be the traversal of this weight space in directions which are not only conjugate to the old gradient but also to all previous gradients. Optimizations of this form are termed conjugate gradient methods [POWE77] and have been adopted to dramatically improve the performance of neural network training.

Supervised learning methods present input/output classification pairs from a representative sample of the problem universe for each output class. Therefore, to accomplish network training the expert system must produce a training set containing examples for each of the three output classes (representing [positive, negative and invalid] wavelets). The system generates the training set (T_{set}) using the radar transmit wavelet (W_t) under the following relationships:

$$T_{set} \doteq \left\{ \overbrace{D_0\left(W_t + n\right)}^{positive}, \overbrace{D_0\left(-W_t + n\right)}^{negative}, \overbrace{\overline{D_0}\left(\overline{W_t} + n\right)}^{invalid} \right\}$$

where D_0 is a distorting operator and n is additive white gaussian noise with amplitude equivalent to the estimated radar data SNR. The random distorting operator D_0 produces wavelet tail distortion (modifying parameters $d0$ and $d1$ of Figure 5.9) to provide the neural network with a basis for generalization.

The generation of the training set is greatly simplified by the input wavelet offset correction and normalization. Offset correction forces input peak offset to zero and normalization imposes;

$$P_0 - \max\left(|P_3|, |P_{-3}| \right) = 1$$

where P_{-3}, P_0, P_3 are the primary wavelet sample points of Figure 5.9. This method eliminates the difficulty in producing a network which is position and amplitude sensitive. A side effect of this normalization is the ability to bypass network classification

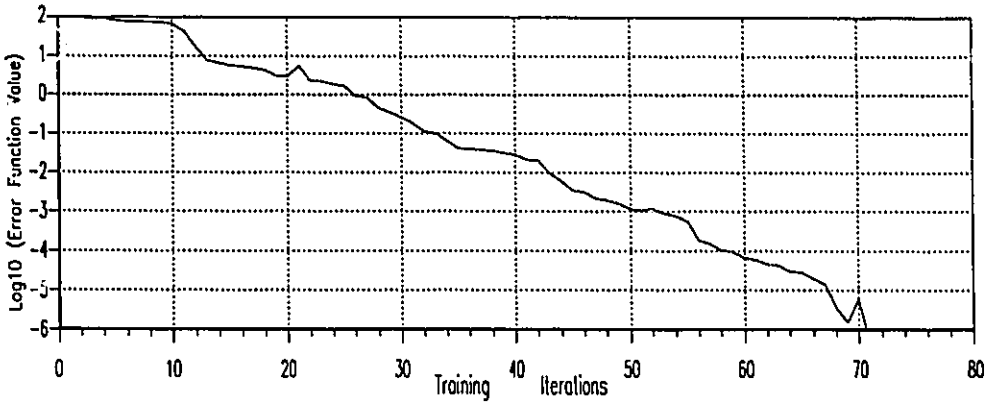

Figure 5.10: Conjugate Gradient Descent Output Error for a Typical Training Session

for peaks not exceeding some system imposed minimum amplitude limit. The training sets generated by the system are arbitrarily created to contain 450 training samples, representing 150 of each classification. The number for each output classification is identical to avoid biasing the network's generalization and the total number represents an acceptable training time. Typically, training requires less than 70 classify-update iterations of the entire data set for a total sample set classification error F( ) of less than 1E-6 (the convergence rate for a typical training session is shown in Figure 5.10). The conjugate gradient descent training method incorporates non-convergence detection, if a network training session fails to converge the system detects the failure and halts. The expert system responds by incrementing the number of hidden nodes, re-randomizing the network weights and retraining. This method guarantees convergence. The trained weight matrix is then compiled into an executable global function for use during data classification. This neural network classifier provides a threshold independent classification scheme which is able to generalize, thereby enabling enhanced distorted wavelet recognition.

In this fashion, a dynamic network topology (based on radar selection and input data sample rates) and training set generation allows the autonomous creation of multiclass pattern classification neural networks. Conventional network training methods lack the performance, and non-convergence detection necessary for the dynamic network definition, training and compilation for embedded classification modules used by expert systems. This represents both an exciting and novel approach to dynamic filter generation under expert system control. The effectiveness of the neural classifier may be seen by comparing Figure 5.6 with Figure 5.12, the contrast is striking.

5.3.4 Data Segmentation

Following the wavelet classification preprocessing operation, it is desirable from a data interpretation standpoint to further increase the reasoning level of the wavelet data. A natural abstraction for bridge structure analysis is the definition of interface layers. This data structure realization may be accomplished by data segmentation and intelligent layering operations. Through segmentation, the individual nature of the bridge deck wavelet peak events are consolidated into single dimension vectors referred to as LINE *segments*. These segments are then analysed and combined into a contiguous sequence forming a line interface layer. Using spatial position information for each radar data line allows the two dimensional concatenation of interface layers into interface surfaces for the bridge structure.

Input for the segmentation module are line wavelet data sets, these sets consist of amplitude and time-of-arrival pairs for all detected wavelets (one such set is shown in Figure 5.6). Peak events are combined horizontally (corresponding to a direction of data sampling) to form contiguous interface segments. The segmentation algorithm is peak position and amplitude dependent. Only close proximity peaks (in a time-of-arrival sense) of similar amplitude may be considered to belong to the same

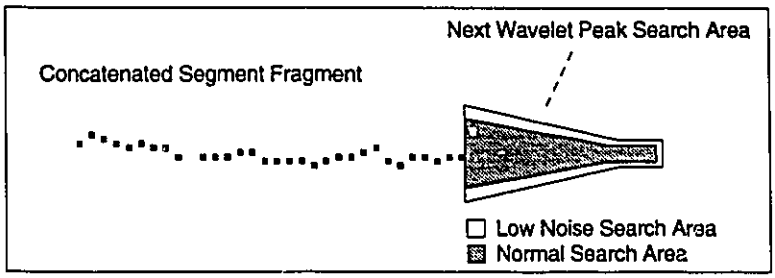

Figure 5.11: Segment Search Patterns
The system uses a variable search area to locate the next peak in a segment sequence. Given the segment fragment above (the black sample position bins), the peak search area is shown. The search region would be restricted to the lightly shaded area for higher noise raw data. In the case of less noisy data, this search region is broadened, allowing increased peak displacement offsets which are compensated for by greater expected peak similarity.

interface segment [AMIN87]. Under Expert System control the amplitude and positional thresholds are based on the desired degree of generalization. Low noise data allows the expert system to restrict amplitude variations and increase offset thresholds. The variable segment search areas are shown in Figure 5.11. The success of this technique can be attributed to the wavelet classification modules effectiveness at removing all but the the most significant wavelets from the peak data sets.

The segmentation algorithm identifies all candidate peaks in the current segment scan area and adheres to the following prioritized selection rules given a choice of multiple candidate peaks.

IF

1. only a single candidate peak with comparable peak amplitude, select it.
2. the closest peak (Euclidean distance) has comparable amplitude, select it.
3. two peaks with comparable amplitudes, with comparable Euclidean distances, choose peak with later time-of-arrival (representing a deeper interface).
4. peak amplitude similarities are marginal, and the Euclidean distance is large - end segmentation process for that segment.

The segment selection process imposes a physical restriction limiting peak selection to only a single peak for each observation (sample) position.

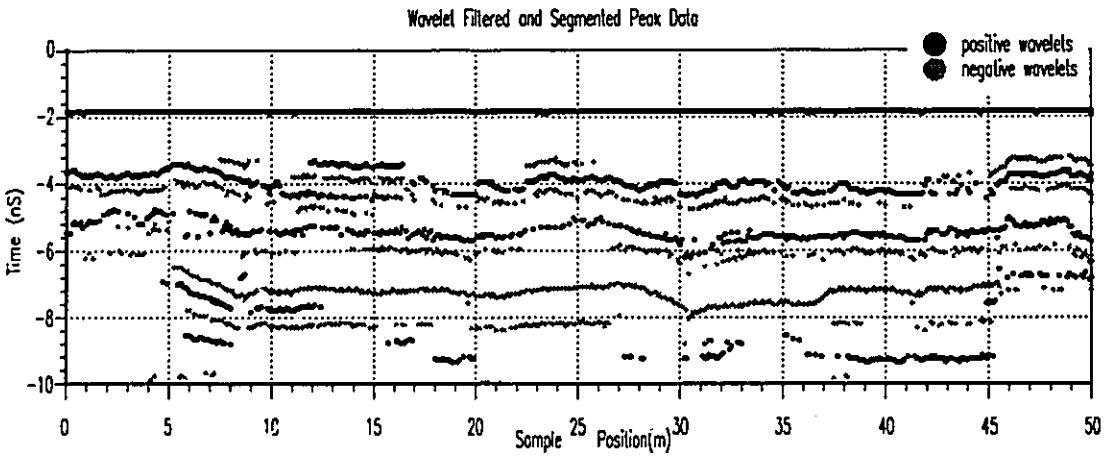

Figure 5.12: Segmentation Operation Applied to Radar Data
Segmentation output for peak detected LINE3 radar data. This data set shows the data reduction due to data peak filtering and neural based wavelet classification.

In this fashion, the system concatenates peaks into segments. Segments must have more than 2 peaks (selected as representing less than half of the radar footprint) to be retained, this eliminates any spurious segment occurrences. Figure 5.12 shows the result of the peak segmentation process for the data in Figure 5.6. The amplitude/position search and selection combination is found to be effective for segmenting wavelet peaks given the distinct primary peak nature of this monopulse radar data.

5.3.5 Layer Detection

Following peak segmentation, these layer interface fragments are consolidated into layer structures. Using a segment characterization scheme and bridge structure cross-sectional knowledge, similar segment fragments are combined into layers. Based on segmented data sets (Figure 5.12), the system individually characterizes each segment to identify candidate concatenation sequences. These characteristics include, average segment amplitude, average segment position and segment start and end positions. By using average amplitude and position values and cross-section models, the layering operation can successfully overcome typical peak variation at segment fringes

to combine appropriate segments. Segment concatenation is done to all individual transverse data lines. Radar specific rules govern the removal of segments which represent false segments rather than physical interface layers. For the monopulse radar transmit wavelet, opposite polarity wavelets (with respect to the primary peak) can be expected before and after a larger primary peak at a distance equal to one-half the pulsewidth. Using this type of CURRENT_RADAR specific reasoning supplied by the RADAR KB, many of the incorrect layers can be identified and removed. The success of the intelligent cross-section based layering strategy is demonstrated by the uncluttered residual radar data shown in Figure 5.13. Each of the distinct horizontal layer segments corresponds to a significant interface (asphalt surface [≈2ns], asphalt/concrete [≈4ns], rebar matte [≈5.5ns] and bottom of deck [≈7ns]).

The expert system then combines the generated bridge XSECT models with the layered data to perform initial structure inferencing, this represents the structural preanalysis and will be detailed in Section 5.5. This inferencing identifies top level site information disparities. These include; multiple unreported lifts of asphalt (detected by extended top layer thickness estimates based on default asphalt permittivities or the appearance of anomalous intra-layer reflections) and identification of data line classifications based on model type and known bridge cross-sections. This preanalysis creates global blackboard-warning flags and tags appropriate cell structures with current cross-section types.

5.4 Data Alignment

For systems that incorporate positional (both absolute and relative) information into data analysis, proper data alignment is critical. Radar data recorded in the field rely on the GPR vehicle data collection process starting at precisely the same longitudinal position for each transverse data set recorded. This accurate data alignment was not

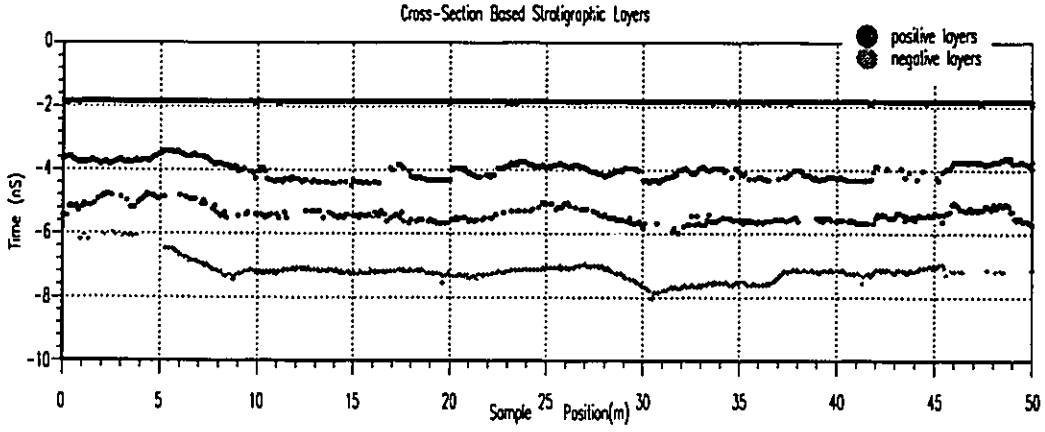

Figure 5.13: Intelligent Layer Module Output
The primary interface data produced by the cross-sectional layering routines. These interfaces represent: (top to bottom) asphalt surface, asphalt/concrete, embedded rebar, and bottom of deck.

generally considered, with data sets exhibiting a substantial lack of individual data line registration (See raw data sets in Appendix C).

This prevalent variable offset characteristic of existing data sets led to the addition of intelligent data alignment rules. The data alignment process relies on both the peak detected data and the detailed cross-sectional model for the bridge structure. Analysis of the juxtaposed cross-sectional models allows the system to choose the most appropriate method for structure boundary determination. The current system implementation uses any combination of the following techniques (as illustrated in Figure 5.14):

- metallic surface joint detection; causing high amplitude surface reflections not exceeding the spatial displacement consistent with physical joints.
- multiple layer discontinuities; spatially confined interface discontinuity, aligned for all cross-sectional layers.
- specific layer detection; for vastly dissimilar juxtaposed cross-sections, the anomalous feature is used to identify structure boundaries (as is the case for bottom of deck concrete-air interface reflection).

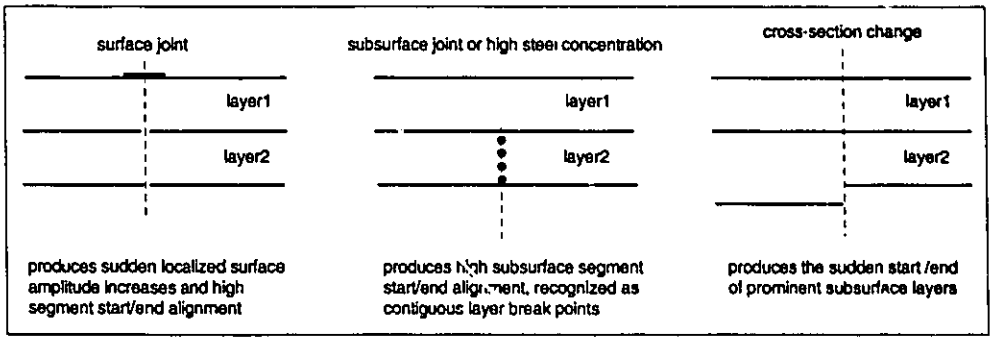

Figure 5.14: Boundary Radar Reflection Events used for Data Alignment Operations

The detection of these events is used in conjunction with the physical bridge site specifications to properly identify the structural boundaries. The physical dimensions for the bridge allow registration of the individual alignment operation results. Such ancillary physical event alignment data is shown in Figure 5.15.

In practical settings, complications arise using this alignment strategy with the appearance of unknown and yet significant amplitude reflection events. For normal structures, support piers[2] and girder diaphragms[3] represent localized occurrences of high reinforcing steel concentrations. These steel concentrations appear during data alignment analysis, to be structural discontinuities leading to unexplained subsurface joint events. This scenario was added to the data alignment rule base by enforcing physical data alignment for all alignment strategy results. The system resolves alignment ambiguity by enforcing physical specification corroboration for the final offset decision.

In cases where pier and diaphragm locations are known, they are included in the physical dimensions. This information is also added to the cell blackboard panels to

[2]Piers represent any support mechanisms for the bridge structure, including pilings and transverse beams. At these points the internal bending moment forces are at a maximum, forcing high reinforcing steel concentrations.

[3]Diaphragms are stabilizing transverse members placed between girders to added flexural strength. Diaphragms are formed as an integral part of the deck structure and present increased reinforcing steel concentrations.

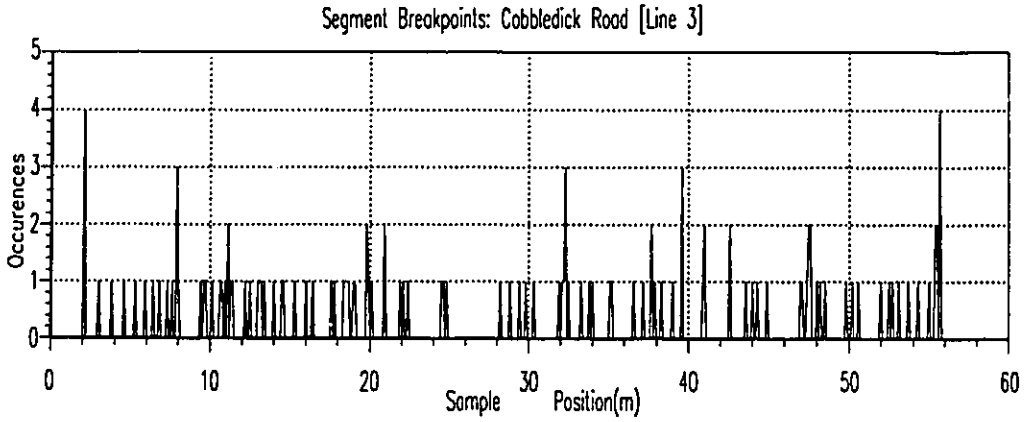

Figure 5.15: Segment Breakpoints used for Data Set Alignment

allow cell level interpretation to identify pier and diaphragm effects.

This overall alignment strategy will fail in the event that no joints are detected. This situation could arise if the structure was monolithic (a single structural component) and radar sampling was started just after the start-of-deck (SOD) abutment joint and was terminated just before the end-of-deck (EOD) joint. In observed data sets, no GPR data from any bridge deck excluded both the start and end of deck joints. In this eventuality, the system assumes all data is aligned.

Once data alignment has been accomplished for each data line, the system updates the system blackboard to indicate the correct data set offset from the deck start abutment. This offset value can be either positive or negative and is added to the LINE:OFFSET member slot, making it available to all subnodes through the frame inheritance mechanism. Following alignment, all spatial references include the base level data offset ($Pos_{actual} = Pos + offset$).

This completes all phases of system preprocessing and as illustrated, all operations are controlled by the expert system inferencing to provide effective data abstraction and cross-sectional model generation.

5.5 Pre-Analysis

Prior to detailed cell analysis inferencing, the system examines the entire data set in the context of a three dimensional entity. This examination attempts to identify data set phenomena which could result in interpretation errors due to extraneous sources. This pre-analysis operation lead to the identification of several global events.

5.5.1 Cross-Section Identification

System cross-sectional analysis of available data sets attempt to correlate possible site specified cross-sections with available data sets. Information produced by the data alignment operation (identifying absolute structural joint positions) and the LAYER data structures allow the identification of the diversity of cross-sections represented by the recorded data sets. Layer position and amplitude are compared against the system generated cross-section models. As bridge sections are identified, the SEG are tagged. Through frame-based inheritance, both the appropriate cross-section and unique segment identity is available for cell level inferencing. This segmentation inferencing is shown in Figure 5.16. Examining the figure reveals a lack of segment registration, which physically must exist for the structure (ie. joints are linear and typically perpendicular to the longitudinal axis of the structure). This phenomena arises from two effects. The first is cell size, if a joint occurs at some point inside a cell, then the cell will be tagged according to the majority of the sample (WAVE units) type contained within. A second more severe problem is the positional information recorded with the original analog data. After digitization, it was found that deck structural events (physically verifiable events) were not accurately positioned. The system compensates for this data related problem through the data alignment operation where maximum alignment to structural phenomena is achieved.

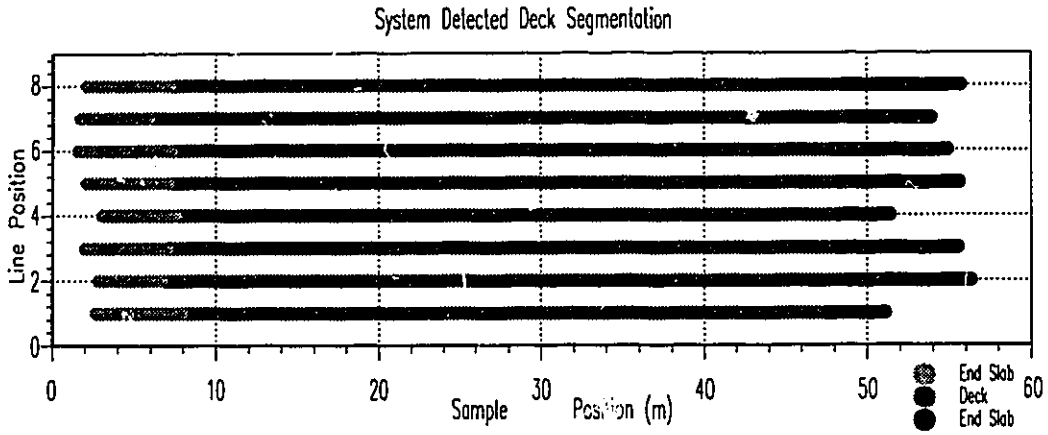

Figure 5.16: System Detected Cross-Sections
Prior to actual processing the system determines the nature of each bridge cell, grouping cross-sections into the segments which allow physical model change according to deck position. Line positions (in meters from curb) are [1.0 2.0 3.0 4.0 5.0 6.0 7.0 7.7].

5.5.2 Thin Asphalt Layer Events

Of significant interest to reflection amplitude reliability, is the inter-reflection effects from thin layers. Given the non-ideal transmit wavelet, thin layer effects may occur beyond layers which are nominally of single wavelet thickness. The system scans the interface layer separations based on default material permitivitties and flags any cells containing layer separations corresponding to less than 1.5 transmit wavelet period. Thin layer awareness is exploited during inferencing as a possible cause for thickness related reflection amplitude variation observations. The areas for the Cobbledick Road bridge structure identified from the data as thin layer events are shown in Figure 5.17.

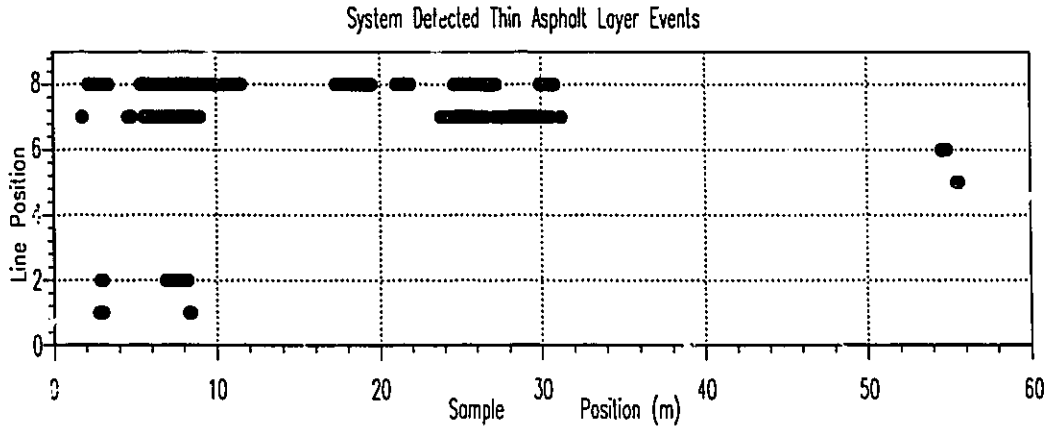

Figure 5.17: System Detected Thin Asphalt Events
In order to properly anticipate amplitude variations due to the sidelobe effects of the transmit wavelet and interwavelet interference, the system flags areas where the second interface reflection is separated by less than 1.5 transmit wavelets. Line positions (in meters from curb) are [1.0 2.0 3.0 4.0 5.0 6.0 7.0 7.7].

5.5.3 Rough Surface Effects

Through surface texture analysis (based partially on user indicated Pavement Condition Index (PCI) rating) the system attempts to correlate global surface reflection patterns with known surface distress phenomena. Principally, the system identifies two related surface reflection disturbances. The first is effects stemming from the road crown (the longitudinal peak in the center of the deck surface to promote drainage) representing a strip down the center of the deck exhibiting a generally decreased surface reflection amplitude due to convex scattering. The second is wheel rut effects; these would generally be identified as two separate strips of increased surface reflection amplitude due to concave surface reflection. These two events are closely related, and accurate identification may be difficult. For the Cobbledick Road data, this surface amplitude inferencing identified the areas of increased amplitude as wheel rut effects based on: the driven lane positions, the positional skew to the data (LINE 8 is

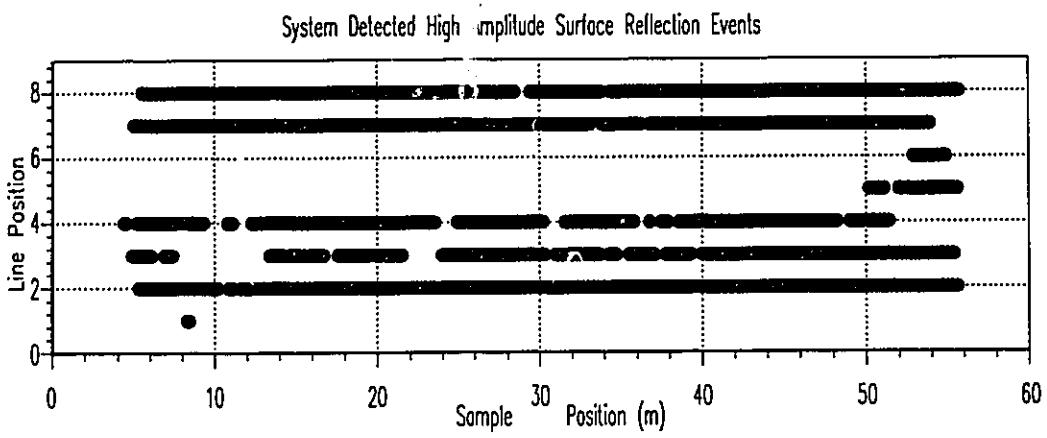

Figure 5.18: System Detected Elevated Surface Amplitude Events
System detected surface amplitude changes attributed to transverse surface concavity in both driven lanes (attributed to wheel rutting due to asphalt compaction). Line positions (in meters from curb) are [1.0 2.0 3.0 4.0 5.0 6.0 7.0 7.7].

not actually in the curb lane) and the nominal surface reflection amplitudes observed in LINE 1 data (curb lane). The system identified areas of increased reflection amplitude which are shown in Figure 5.18. Identification of these effects allow the system to compensate for wheel rut effects when inferencing in affected cells. Currently, the system compensates by applying a global correction to all identified lines which reduces the surface reflections. To perform this correction, the average line amplitude is determined, and a line scaling factor is calculated relative to the average amplitude for all non-wheel rut lines. This scaling factor is then applied to the wheel rut data line. This simplistic approach arose from recognition of the phenomena but a lack of actual radar equipment to quantify these undulating surface scattering effects. Actual experimental results could be included in the rule system if they existed.

5.5.4 Vehicle Acceleration Effects

Using the facts that the radar data logging vehicle used a forward mounted cantilever antenna system and that the method for data acquisition required the vehicle to proceed from a standing start at one end of the deck and stop at the other, the system is capable of identifying the related antenna position variation associated with vehicle acceleration. As a vehicle accelerates, driven wheel torque causes a sudden positive (upward) deflection of the front of the vehicle with respect to the horizon. The sharp upward motion is followed by a slow return to the relaxed suspension position (and perhaps a slight stabilizing oscillation) as a constant velocity is achieved. For the radar detected surface reflection, this would cause a sudden decrease in amplitude followed by a return to the correct surface reflection amplitude. Similarly, at the end of a longitudinal sample line, the vehicle will decelerate to a stopped position under braking. This braking causes the front of the vehicle to deflect downward (towards the horizon). The increased proximity of the radar to the reflecting surface decreases scattering losses and results in increased surface reflection amplitude. Both of these events are significant for any amplitude based parameter estimates. The system analyses surface amplitude over an area at the start and end of each data run for acceleration/deceleration effects. Normal acceleration/deceleration events are heuristically identified as having a duration of approximately 3 seconds. Vehicle velocity causes acceleration events to appear shorter (spatially) than deceleration (when vehicle speed is much higher); these observations are verified in data obtained from Cobbledick Road. If these effects are detected, the system tags the affected cells. During inferencing, these areas of amplified (attenuated) surface reflection amplitude are compensated for by approximating the true amplitude. In this case an approximation is applied based on the nominal surface reflection amplitude in a stable area near the affected area; again if experimental results were known they could be added to the rule system. Figure 5.19 shows the acceleration/deceleration

affected cells and the surface amplitude for the data line corresponding to LINE 6. It is apparent that these effects are significant, and field notes available for this data indicate that the driver of the vehicle acknowledges that during LINE 1 sampling the vehicle was accelerated significantly, attaining a high speed run.

These pre-analysis results represent the first level of spatial inferencing for the data. The following chapter presents the results of the detailed interpretation of the complete Cobbledick Road data set.

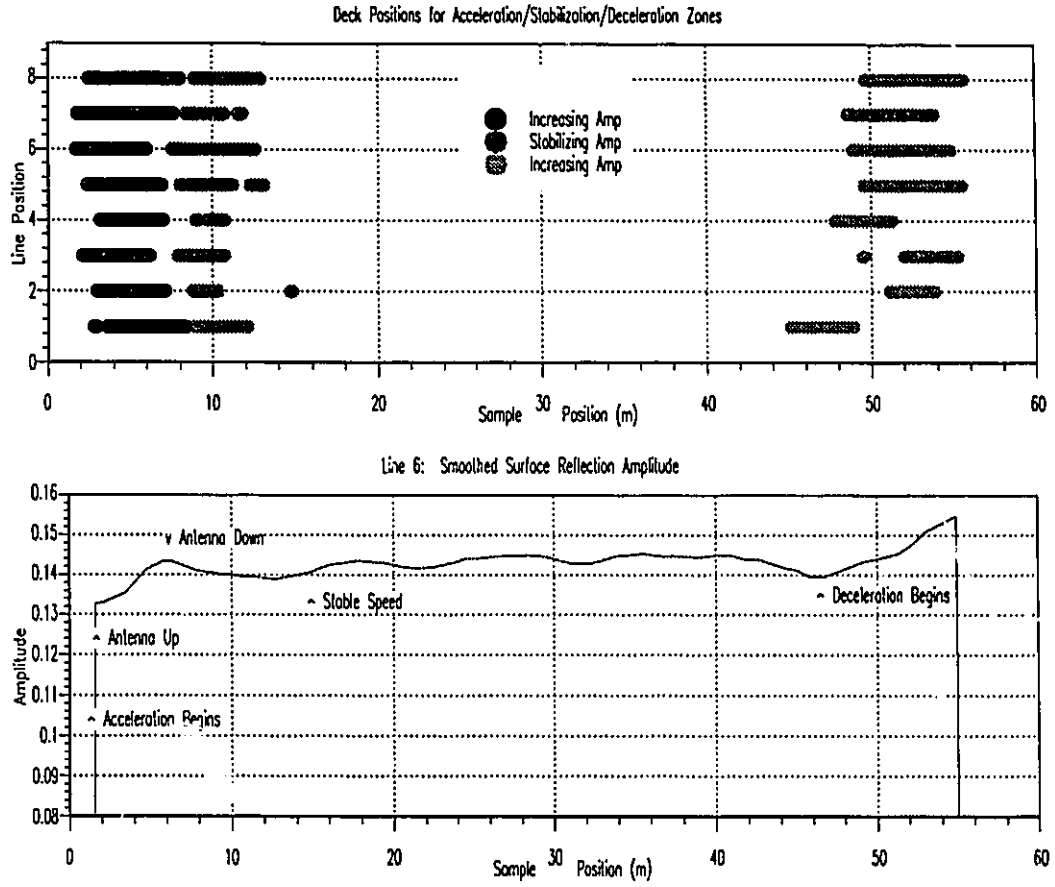

Figure 5.19: System Detected Antenna Displacement Events
System detected surface amplitude changes attributed to antenna height variations caused by a cantilever mounted antenna structure mounted at the front of the data acquisition vehicle. Line positions (in meters from curb) are [1.0 2.0 3.0 4.0 5.0 6.0 7.0 7.7].

Chapter 6

Discussion

6.1 Introduction

Perhaps the most difficult task is the presentation of results which cannot be directly verified. Such is the case with *nondestructive evaluation*, which by definition has no detailed physical means for verification. However, the successful operation of the mechanism developed for knowledge management can be confirmed by corroboration with available data and alternate analyses. Also, the presentation of the results will attempt to indicate system produced justifications where applicable.

The reader is urged to consult the raw radar data presented in Appendix C during discussions of system produced results and identification of interface anomalies.

6.2 Modeling Capabilities

The modeling capabilities of the system are demonstrated through the detailed identification of the two fundamental cross-sections the system will encounter while inferencing across the deck slab. The ability to identify the areas where the bottom

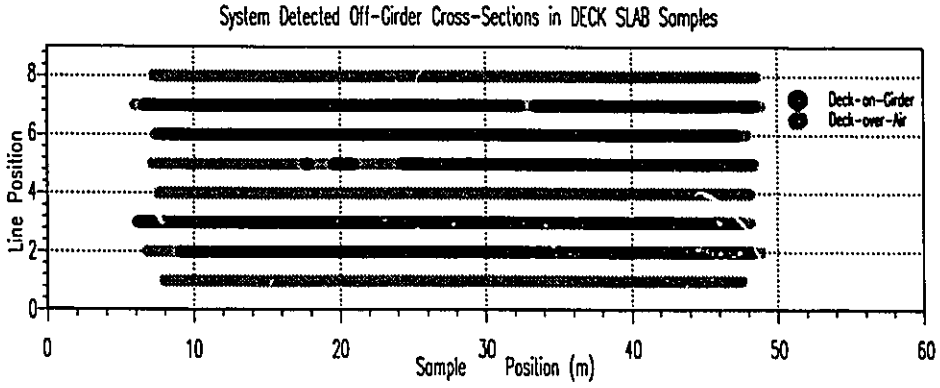

Figure 6.1: System Detected Deck-On-Air Events
The system is able to identify areas of the bridge which match the DECK-ON-AIR cross-sectional model and therefore allow accurate deck thickness estimates.

of deck reflection is *reliably* identified also determines where accurate deck thicknesses can be approximated. Figure 6.1 represents the areas the system has identified as producing a strong bottom of deck (concrete/air) reflection. In areas where the bottom of deck is not apparent, the deck thickness estimates are typically greater than actual layer thicknesses. This overestimation is due to deck slab/girder interface (concrete/concrete), electrical similarity and the difficulty in distinct bottom of deck reflection identification. The lack of bottom reflection is noted by the system and affects the reliability of the deck slab thickness estimates used for velocity and permittivity determinations. It is interesting to note that the casual data collection approach taken by the MTO field staff raises many position credibility questions. In addition to start-of-line registration errors (discussed in Section 5.4), examining Figure 6.1 reveals a substantial traversal displacement during data collection for LINE 5. Examining physical site specifications for girder placement, the lateral displacement from 0 to 25 meter point exceeds 0.7 meters. The Slab-on-Girder rule base identifies this phenomena (as well as the case of uniform cross-section for the entire slab) as data set anomalies.

6.3 MTO Data Analysis System

As indicated in the original problem statement, interpretation systems currently in use which implement the individual sequential processing of the radar data sets perform with limited success. As a means of comparison, data analysis from one such system used at MTO was available for the Cobbledick Road bridge site data presented throughout this work. This data will be presented here, in a graphical form, based on the internal site evaluation report resulting from a detailed bridge survey performed in November, 1989.

As standard procedure, the analog data which was recorded onto magnetic tape at the time of the survey were retained in MTO archives. Through the cooperation of MTO, this analog data was obtained and redigitized in 1991 to be used as input for the expert system. Although the actual analog-to-digital conversion (ADC) hardware differed, it is assumed that the data used as inputs for the two systems is comparable. Scaling errors arising from the use of different ADC hardware were minimized since all reflection amplitudes are analyzed as ratios against the ideal flat plate reflection. The flat plate signal was recorded at the site and therefore digitized with the same systems. Under these considerations, the different ADC system effects are considered negligible.

In order to obtain a foundation for comparision, an attempt was made to defeat all inferencing capabilities of the expert system. It was hoped that this would allow a comparison of non-active expert system interpretation of the data with the original MTO results. However, the base level preprocessing of the expert system, which produces the LAYER structures for the data sets in conjunction with the cross-sectional modeling capabilities (which are fundamental to the system and cannot be defeated), proved to be substantially better than the sequential analysis system. This dramatic improvement may be attributed to the effectiveness of the modeling operation. The

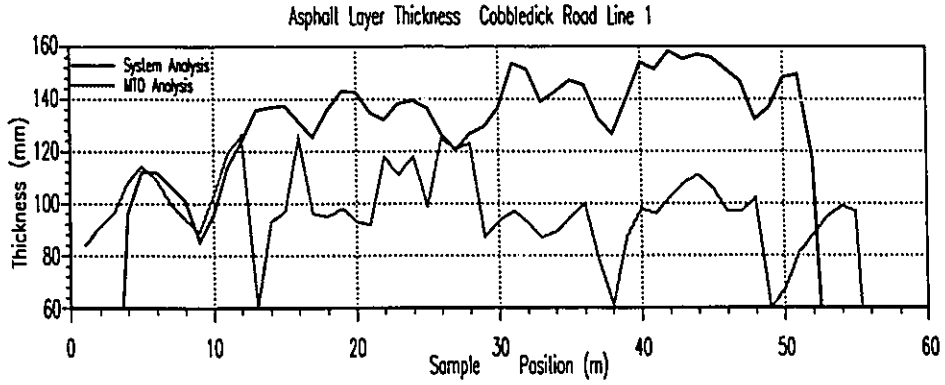

Figure 6.2: MTO Analysis Error
The figure illustrates the effects of incorrectly identifying interface reflections. The MTO analysis software incorrectly tracked a false asphalt/concrete interface reflection over most of the radar data line (the interpretaion was correct only in the range [0..12] and [26..28] meters). These errors are extremely covert and only surface during subsequent ground truthing operations.

expert system successfully identifies the major interface layers and, therefore, is better able to track layer changes across the structure. By way of an illustration of this phenomena, Figure 6.2 shows the comparision of the interpretations of the asphalt layer thickness (of Cobbledick Road LINE 1) from the two systems. There is a close correlation between results until approximately the 13 meter point. At that point in the interpretation the MTO system incorrectly construed a sudden model change and began tracking a false reflection (a sidelobe of the surface reflection wavelet). The MTO system continued until the 26 meter point when it correctly resumed tracking the asphalt concrete layer and then reverted back to the incorrect layer interpretation. The transition at the 11 meter point represents a highly unlikely physical phenomena (without some form of visible surface distress) and an intelligent interpretation approach would recognise it as highly improbable.

6.3.1 MTO Analysis

Figure 6.3 presents the tabular surface asphalt layer thickness and concrete cover over the top layer of reinforcing steel in contour plot format. The resolution of the contour plot is dictated by available data result resolution of 1 meter. Examining these surfaces reveals numerous locations where apparent layer thicknesses change suddenly. At one point on the structure, this variation corresponds to an asphalt layer thickness change of 70mm/meter (LINE 2 10-16 meter range). The approach used by the MTO system to compensate for poor modeling is to incorporate extensive averaging.

6.3.2 Expert System Analysis

The comparable expert system analysis of the raw radar data (no compensation for observed physical phenomena) is shown in Figure 6.4. The expert system interpretation also includes the concrete layer estimates for the deck cross-section. The gross dissimilarity in the two interpretations can be attributed to the inability of the MTO system to properly track the layer changes, and the cross-sectional model variation across the structure. The correct identification of interfaces provides a more physically realizable interpretation with no disjoint layer thickness variations.

Subsequent Figures 6.5 and 6.6 present data interpretations resulting from the application of compensations for surface distresses recognized by the system. Figure 6.5 is produced as a result of the system compensating for surface amplitude variations attributed to driven lane wheel ruts (or potentially road crown effects). Figure 6.6 further compensates the radar data set for acceleration and deceleration effects at the beginning and ends of the lines. The final contour plot (Figure 6.7) presents the permittivity estimates for the asphalt and concrete layers based on the analysis presented in Figure 6.6.

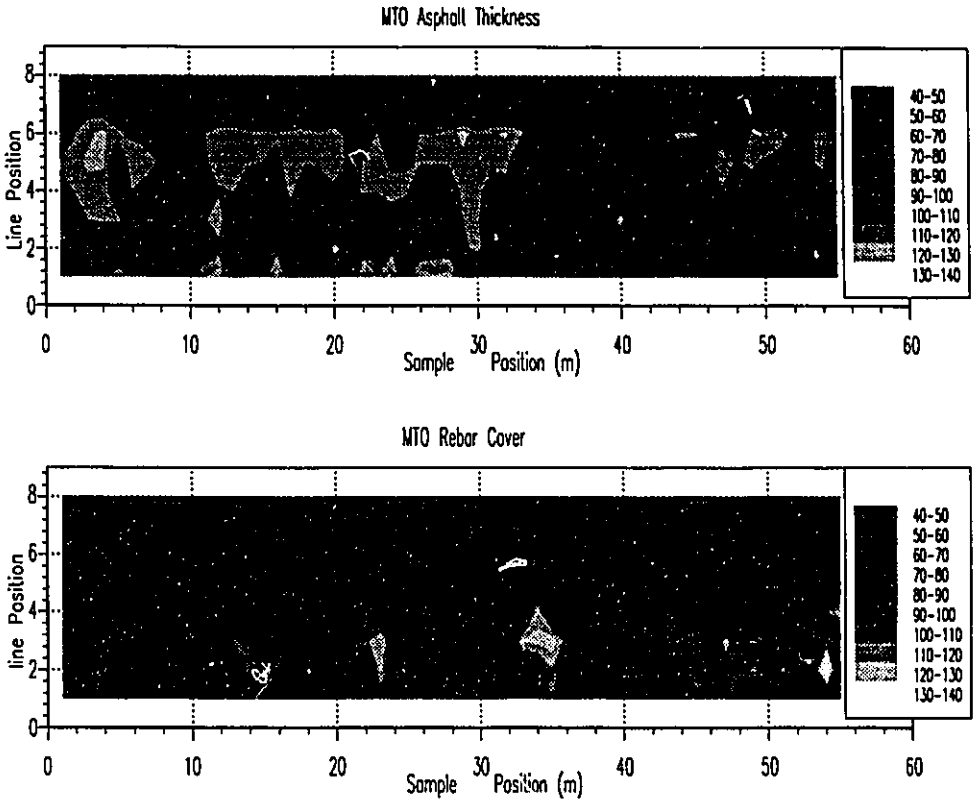

Figure 6.3: MTO Radar Analysis Software Results
MTO analysis results for asphalt(top) and concrete rebar cover(bottom) layer thickness estimates from Cobbledick Road bridge structure survey.

6.4 Spatial and Temporal Analysis

The potential of the qualitative relationships in supplementing system reasoning facts for parameter resolution in the case of the underdetermined problem has been demonstrated. During the course of inferencing, the system examines the current inferencing point temporal relationships in an attempt to identify the responsible parameter for any observed variations. The practical application of these concepts raised many important issues for the success of the qualitative analysis concept.

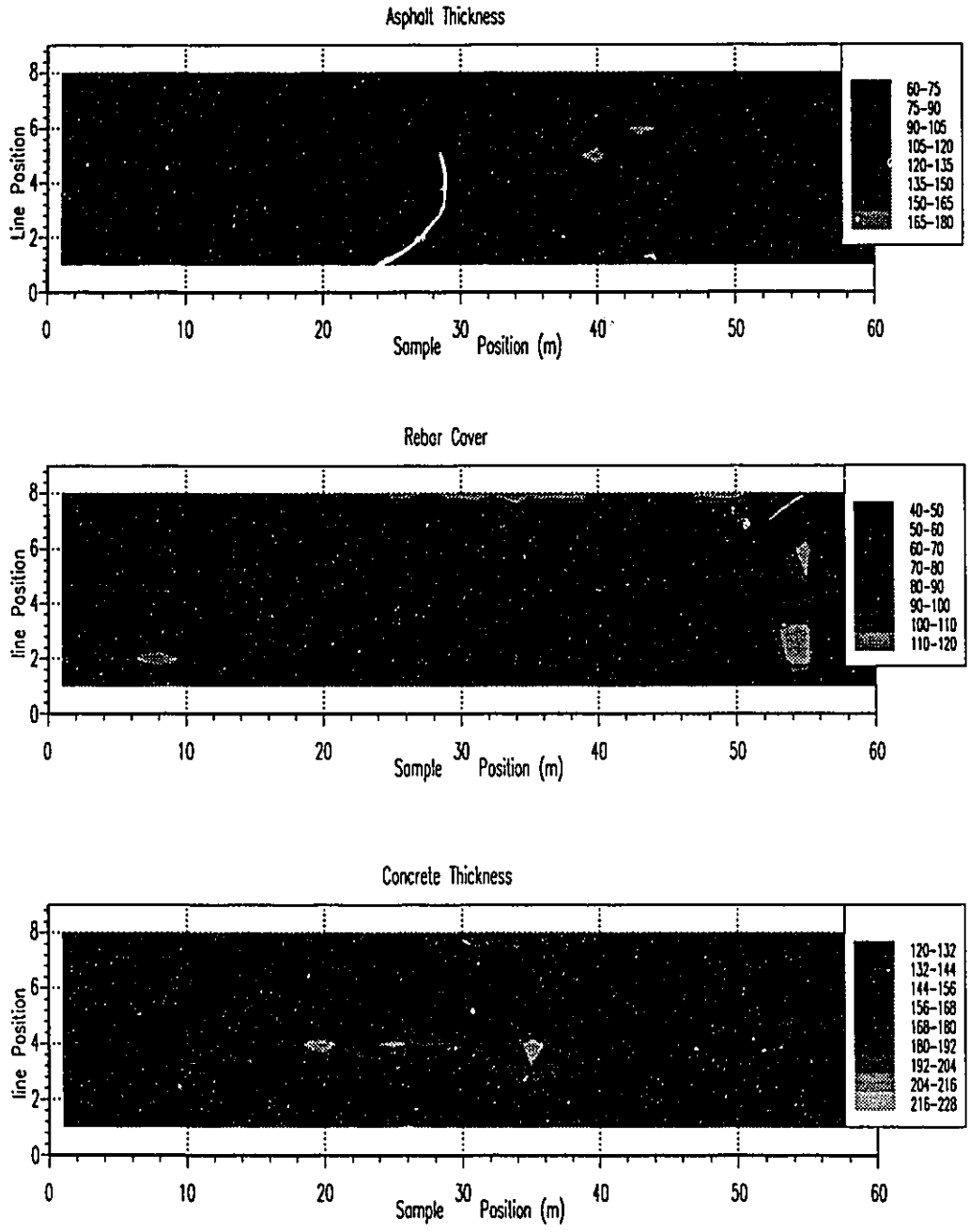

Figure 6.4: Expert System Results: ORIGINAL DATA INTERPRETATION
Contour Plot of expert system estimates for asphalt(top), concrete rebar cover(middle) and concrete(bottom) layer thicknesses from Cobbledick Road bridge structure survey. These results are based on the original data.

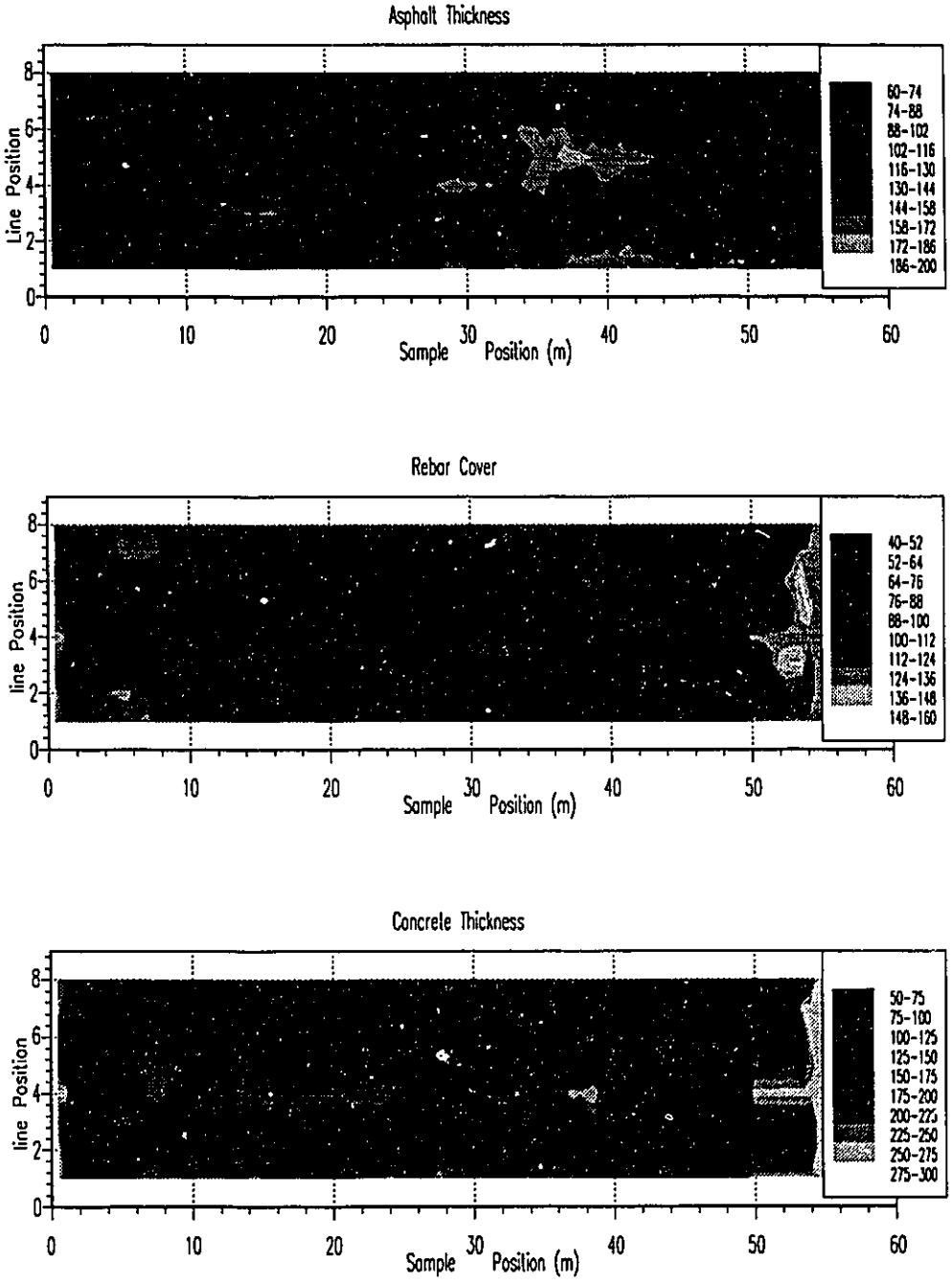

Figure 6.5: Expert System Results: WHEEL RUT COMPENSATION
Contour Plot of expert system estimates for asphalt(top), concrete rebar cover(middle) and concrete(bottom) layer thicknesses from Cobbledick Road bridge structure survey. These results are based on wheel-rut compensated data.

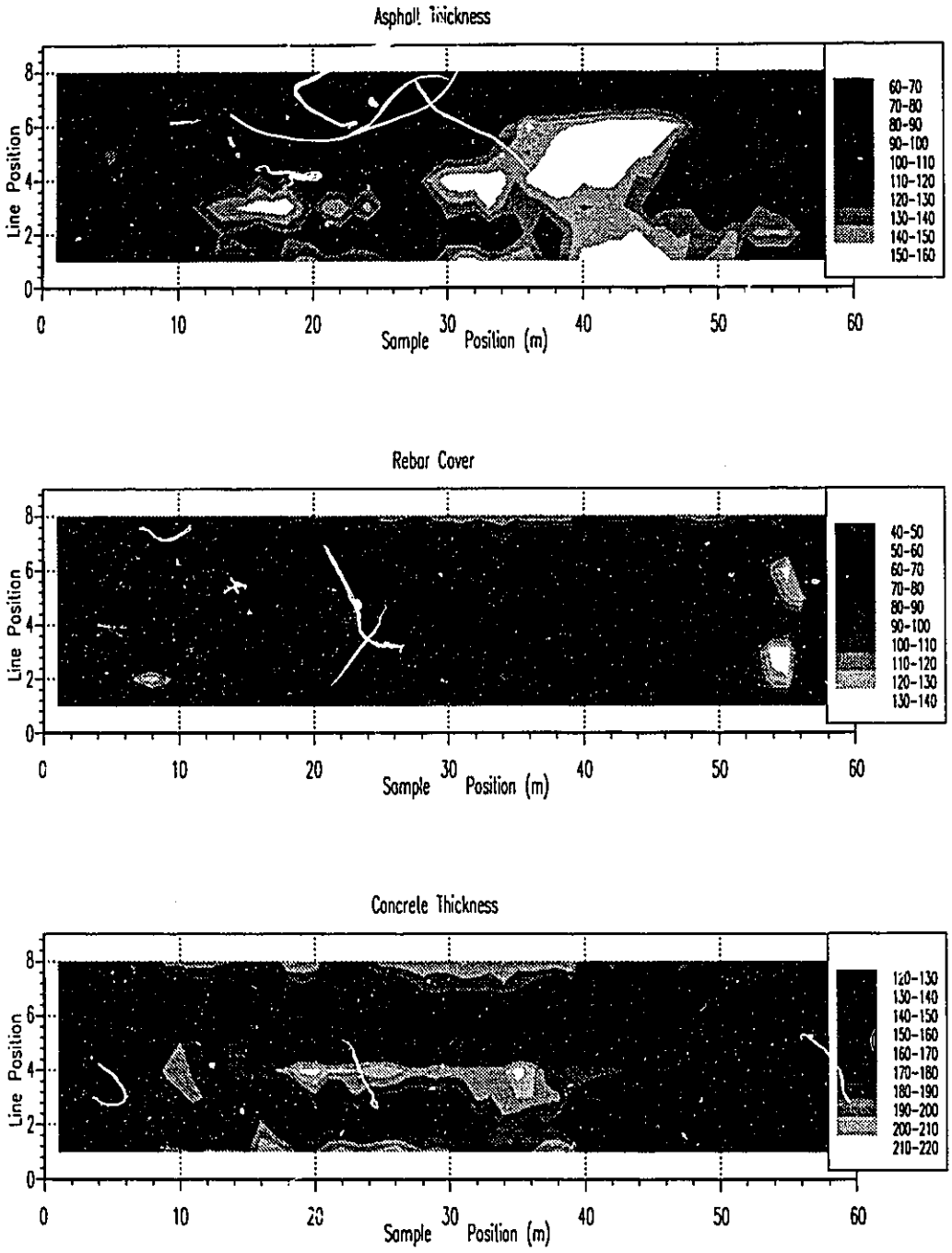

Figure 6.6: Expert System Results: WHEEL RUT and ACCELERATION COMPENSATION Contour Plot of expert system estimates for asphalt(top), concrete rebar cover(middle) and concrete(bottom) layer thicknesses from Cobbledick Road bridge structure survey. These results are based on wheel-rut and antenna-displacement compensated data.

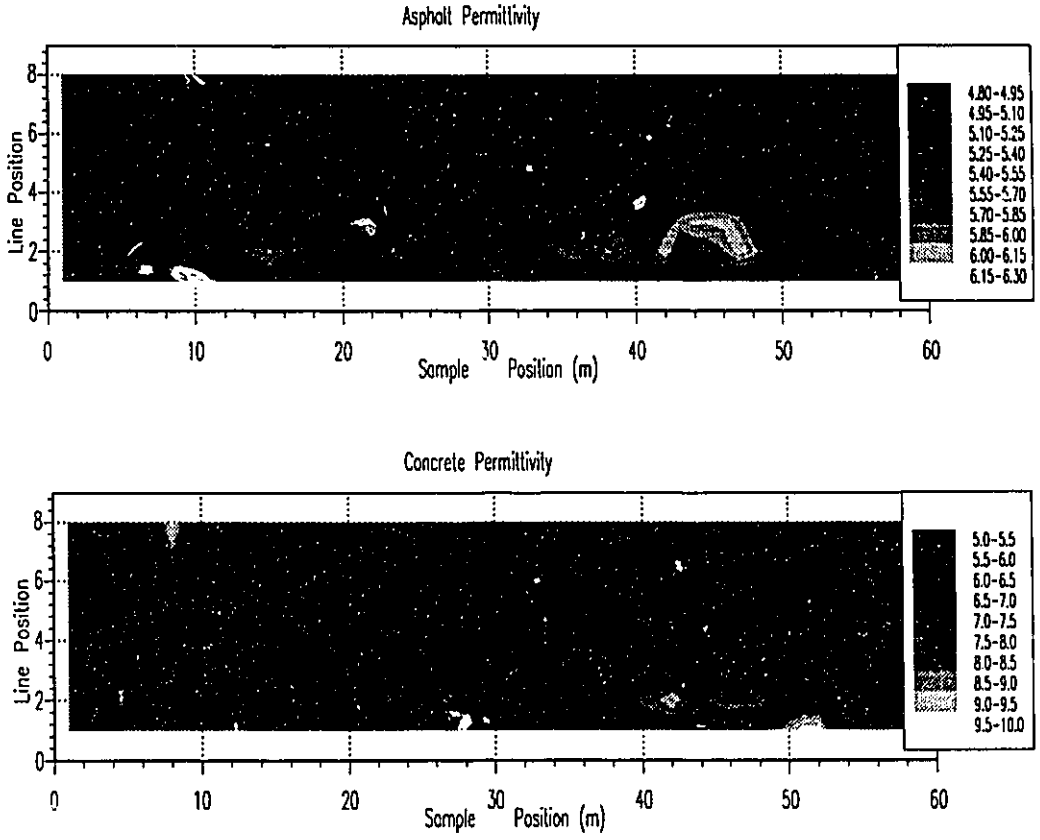

Figure 6.7: Expert System Results - Layer Permittivities
Contour Plot of expert system estimates for asphalt(top) and concrete(bottom) permittivity estimates for the entire bridge structure.

- Neighborhoods used for the analysis have an effective upper bound for separation. At present, the usefulness of neighbouring observations at 1 meter separations is dubious. In terms of physical cross-sections, dramatic variations over 1 meter displacments are possible and these would lead to local inferencing errors.

- Qualitative analysis relies on the notion of INCREASING, CONSTANT, and DECREASING ([+],[0],[-]) parametric observations. In practical data situations, plagued with noise and error sources, a correct method for selecting the bounds of the CONSTANT[0] is not intuitively obvious. Currently, the system bounds are selected through data set observation and are parameter dependent.

- Parameter oscillations are effectively managed through the use of two level qualitative analysis. Wide area spatial smoothing allows qualitative analysis in a structural sense. This allows system identification of general trends, such as extended areas of layer thickness increase or decrease despite local parameter oscillations. The system currently incorporates both sample and cell level qualitative analysis.

Based on the causal relationships presented in Section 4.4.3, two examples of the qualitative analysis information are presented. Figure 6.8 reveals areas in the Cobbledick Road data set where the qualitative relationship between subsequent layers indicate observed interface layer position changes attributed to a permittivity change of the surface layer. Conversely, Figure 6.9 shows areas where qualitative analysis indicate layer position change attributed to layer thickness variations.

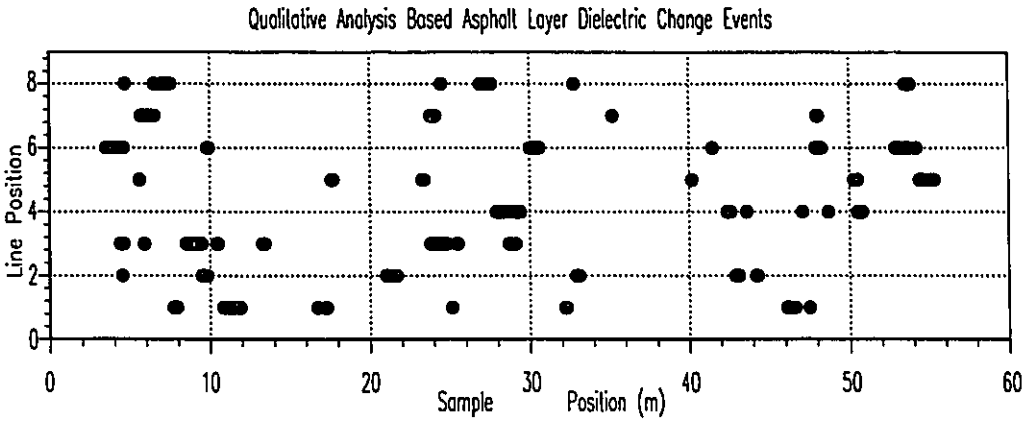

Figure 6.8: Qualitative Reasoning: Layer Perimittivity Variations
Points on the deck surface where the system qualitative reasoning suggests a surface layer dielectric change.

6.4.1 Spatial Analysis and Fault Identification

Combining all aspects of the system allows the identification of candidate fault locations. These areas arise from anomalies recognised by the system which are inexplainable by physical phenomena.

The spatial derivative and neighbourhood cell reasoning capabilities are demonstrated by the identification of observed physical parameter variation. In the event the system detects a spatial derivative threshold violation, the system tags the location as faulted. The thresholds are maximum physical parameter change limits arising from material and structural constraints. Of primary interest in bridge deck analysis is the identification of asphalt/concrete interface distress. The system identifies two layer interface faults;

1. Layer thickness variations. Layer position faults are identified based on structure PCI (pavement condition index) and severe position displacements. The displacement threshold is determined by building codes and bridge design type.

2. Layer permittivity variations. Extreme interface permittivity ratio variations

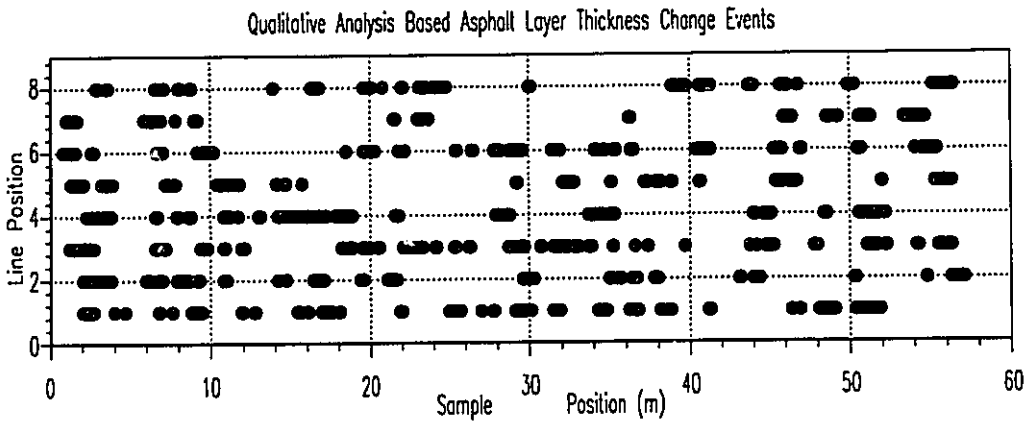

Figure 6.9: Qualitative Reasoning: Layer Thickness Variations
Points on the deck surface where the system qualitative reasoning suggests a surface layer thickness change.

are indicative of interface faults such as debonding, aqueous ponding or scaling. Permittivity variations not coinciding with appropriate interface position shifts are identified as unexplainable and therefore indicative of faults.

Two such spatial variation analyses are presented here. Figure 6.10 identifies concrete surface interface violations based on sudden permittivity (derived from reflection amplitudes) changes. Figure 6.11 identifies concrete surface interface violations based on sudden layer postion changes. These parameter variations represent anomalies which are currently attributed to general interface faults.

The reinforcing steel layer reflection amplitude analysis presents a unique challenge for interpretation. Due to the variable rebar placement strategies found in Ontario bridge structures prior to 1978, it is not inconceivable to experience areas of no detectable reinforcing steel. In the MTO system, a uniform steel concentration is assumed and variations are perceived as delamination faults. System analysis of the rebar layer reflection amplitude produces elevated levels as shown in Figure 6.12.

Structural awareness allows the system to identify these events with joints and diaphragms where reinforcing concentrations are high.

Bridge structure based layer analysis allows the recognition of two lift asphalt delaminations. Separate layer detection implies dissimilar asphalt layers, and requires multiple asphalt layer permittivity approximations for accurate layer estimates. Figure 6.13 shows areas on the bridge which are identified as second lift asphalt delaminations. Examination of raw radar data presented in Appendix C and the interpretation data presented here indicates the effectiveness of the system in detecting points of physical distress associated with structural faults. Without a detailed destructive structural evaluation there are no absolute methods for result verification.

All inferencing capabilities are combined to produce the final analysis results presented in contour plots of Figures 6.14 and 6.15.

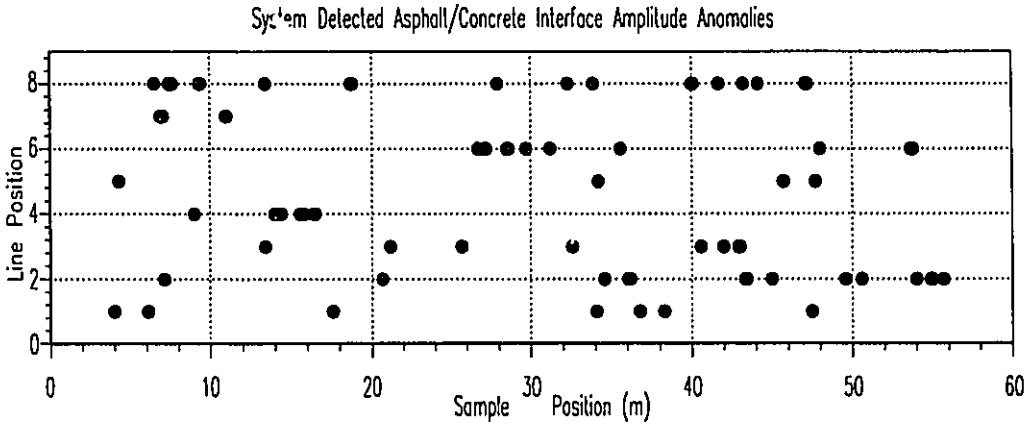

Figure 6.10: Asphalt/Concrete Interface Amplitude Faults
Faulted points on the deck surface where the system detects reflection amplitude based spatial parameter violations of the asphalt/concrete interface.

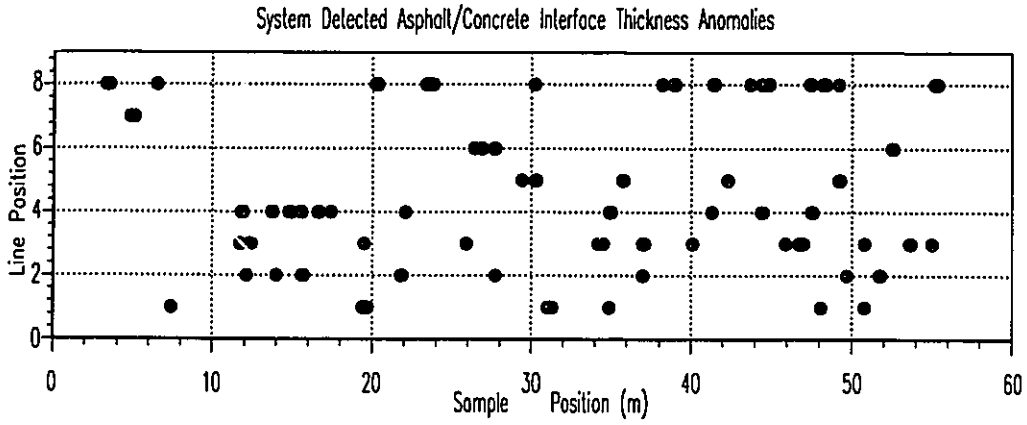

Figure 6.11: Asphalt/Concrete Interface Position Faults
Faulted points on the deck surface where the system detects reflection position based spatial parameter violations of the asphalt/concrete interface.

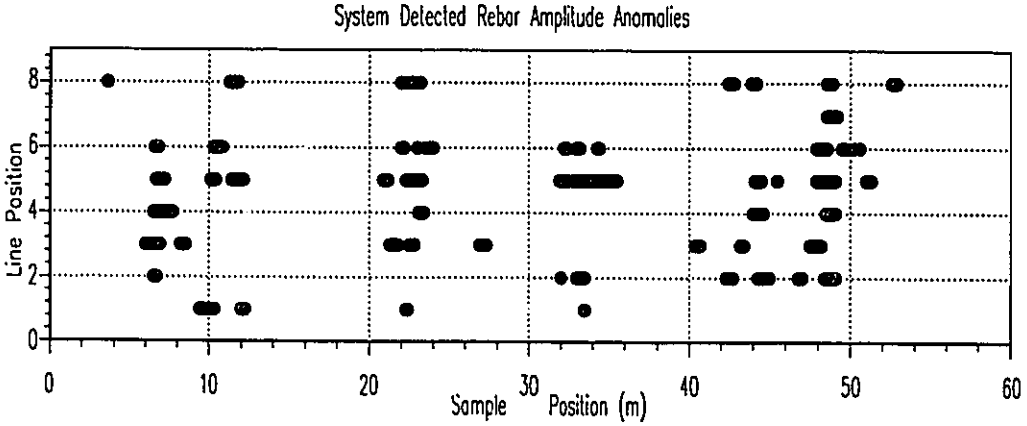

Figure 6.12: Elevated Rebar Reflection Amplitudes
The figure shows locations of rebar reflection amplitudes which are detected above ambient level. All events correspond to high concentrations of reinforcing steel in the vicinity of joints and diaphragms.

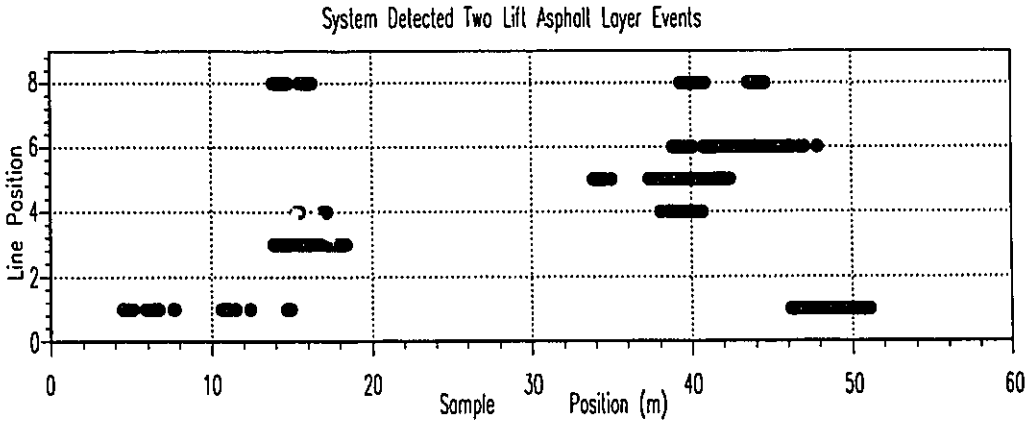

Figure 6.13: System Classified Intra-Asphalt Layer Distress

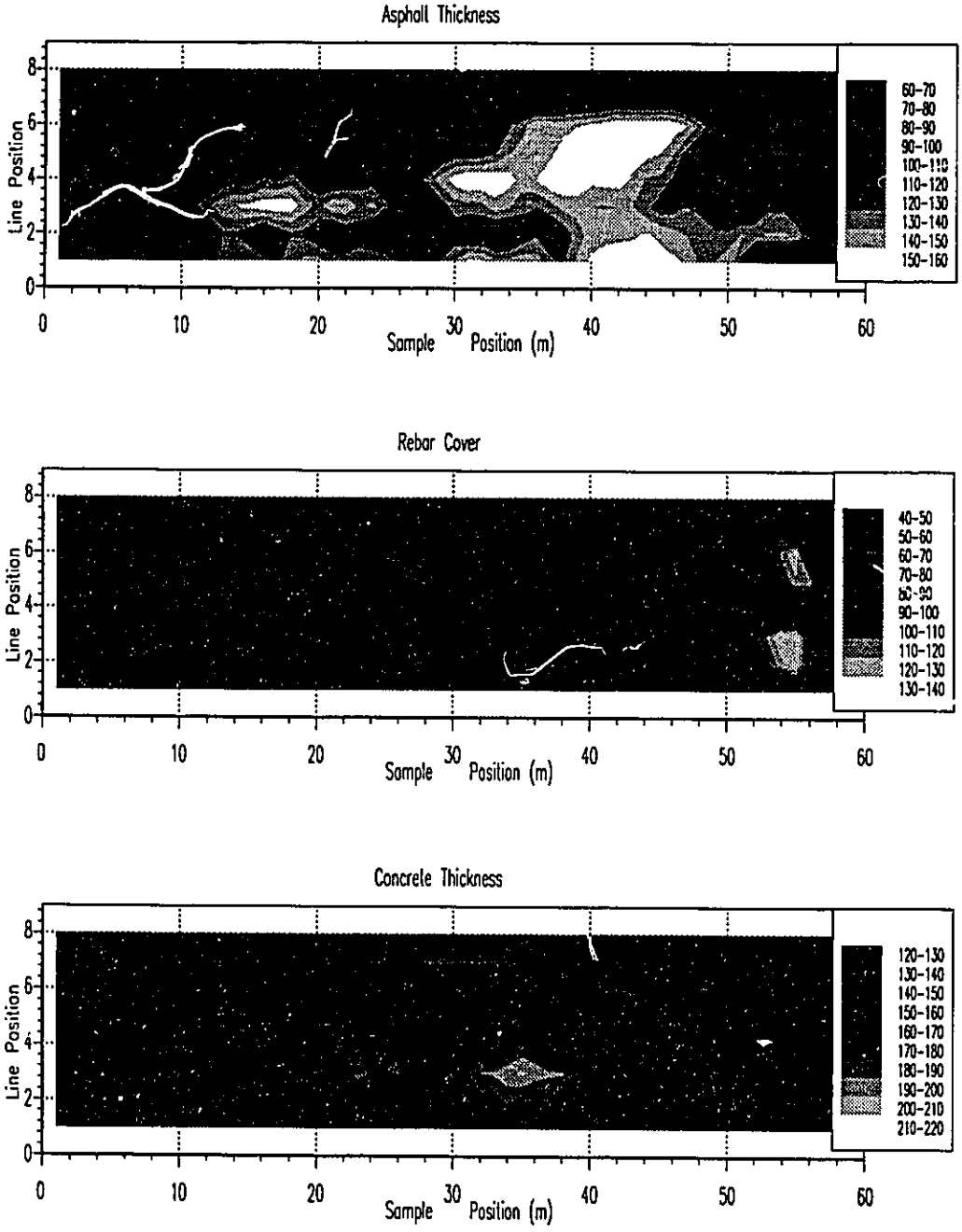

Figure 6.14: Expert System Results: Final Analysis
Contour Plot of expert system final estimates for asphalt(top), concrete rebar cover(middle) and concrete(bottom) layer thicknesses from Cobbledick Road bridge structure survey.

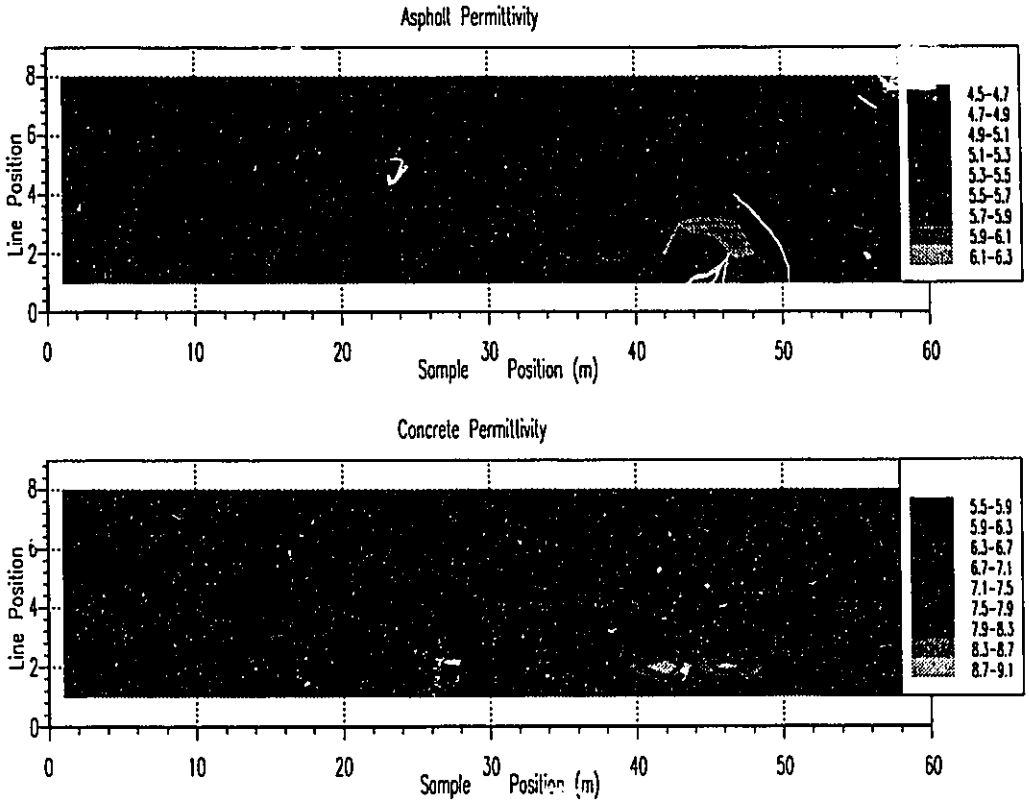

Figure 6.15: Expert System Results Final Analysis
Contour Plot of expert system final estimates for asphalt(top) and concrete(bottom) permittivity estimates for the entire bridge structure.

Chapter 7

Conclusions and Recommendations

7.1 Summary

The focus of this work addressed the potential of knowledge based systems for application to the arduous task of bridge deck radar analysis. It was shown that an interpretation task of this complexity requires significant detailed background pseudo-knowledge from diverse engineering disciplines. The embodiment of the necessary multi-disciplinary expertise has been effectively realized through the adaptation of expert system technology. The limited success of the described pioneering work in expert system development for radar signature analysis has been extended considerably through the cross-sectional modeling and qualitative analysis methods presented here. The foundation of the modeling capabilities for the system originate from the autonomous creation and training of a neural network based wavelet filter. Expert system based data analysis techniques broaden inverse solution methods through the use of both spatial and temporal relationships. This spatial awareness allows the definition of parameter variation thresholds which facilitate differentiation between

model variation and defect manifestations. Top-level inferencing control allows the processing of data in an agenda determined by data and site specifications. It was demonstrated that the interpretation problem is not a simple pattern matching problem as there is not generally a direct mapping of cross-sectional structural geometry to radar reflection waveform. The expert system presented in this work effectively interprets actual radar data, providing layer thickness estimates and indicating areas of anomalous interface charateristics attributed to faults.

7.2 Conclusions

Based on this research, the expert system approach is a viable technology for the large data set, multi-domain deep reasoning problem. General conclusions about the performance of such a system can be drawn. Frame based data structures are capable of efficiently managing the extremely large data sets (both raw and processed) produced by bridge radar surveys. Additionally, frame based systems provide an efficient hierarchical data structure which allows unlimited data fusion capabilities. These data units are viewed by the system as a subset of the entire system blackboard. As information is added, it can be included both globally and locally, allowing the reasoning scope to be limited. This focusing of the inferencing process dramatically improves the performance of the system. The modular design of the knowledge based system allows incremental refinement and modification. As new and different entities are encountered (bridge design types, materials, radars etc.) they need only to be added to the appropriate system knowledge base. The system can coherently focus the knowledge of disparate domains (electrical and civil engineering etc.) to generate an automated and sophisticated (as in multi-model) reasoning system.

From a signal processing standpoint, several observations are significant. The autonomous generation of data/radar specific neural network filters is both plausible

and novel. Expert system controlled topology definition and training set generation was accomplished. Through the use of a high performance modified backpropagation training method, the nonconvergence training scenario is detectable, and network training times were acceptable. This nonconvergence detection allows system controlled modification of the network topology and retraining to ensure final convergence. The performance of the neural network based filter was shown to be superior to the classical sum-squared-error similarity measure for the task of generalised wavelet identification [ANDE88]. The ability to dynamically define and train neural network based filters allows the system to interpret various data formats from different radar units.

Based on peak detection and wavelet filter preprocessing, the system is able to achieve data reduction of several orders of magnitude while preserving the essential interface information content of the raw data. This data abstraction (and the considerable data reduction it represents) is mandatory in addressing the real-time requirements of high data rate systems such as impulse radar in the future.

Using the bridge design, materials and building codes knowledge bases, the system is capable of generating all possible cross-sectional models for the particular bridge type. These models are then used to identify the cross-sectional variations detected in the raw data during the analysis operation. Accurate cross-section models allow the identification, and the migration of the correct wavelet filtered peak segments to the data abstraction level of interface LAYERS. This data abstraction (consisting of sequences of amplitude and position pairs) forms an effective foundation for the remaining system inferencing.

The system effectively overcomes data registration problems through physical event recognition in the data sets and alignment without human intervention. Previous systems were not concerned with positional registration and overcame gross data anomalies through raw data set averaging. Correctly aligned data sets provide

the capability for spatial analysis. This spatial analysis relies on neighbourhoods and provides a mechanism to define rate of change relationships for the parameters associated with the layered structure backscatter problem. Violations of realistic parameter thresholds constitute physical faults. The effectiveness of the inter-line neighbourhoods was limited by the 1 meter separation of the lines. Closer longitudinal radar survey lines would prove beneficial for future applications employing cell-based spatial analysis. Also, data gathering methodology must ensure accurate traversal positioning to ensure consistent line separation distances.

Surface effects were ignored prior to this system. Such effects have been shown to be real, explainable and traditionally the source of interpretation inaccuracies. The effects of vehicle mounted airborne antennas present a significant source of error for systems relying solely on amplitude ratios for surface layer permittivity estimates. Ancillary methods for permittivity determination would allow such a system to focus on interpretation of interface faults. Based on single source data, the expert system based data surface analysis provides a means for identifying various surface effects and producing reasonable corrections.

The temporal relationships provided by the qualitative physics developed here, allow increased confidence for the estimation of parameters in an undetermined problem. The examination of the layered media physics and the complex parameter relationships allow the formulation of causal relationships. Using these temporal based causal relationships facilitates the identification of the most likely layer physical parameter change for the observed interface changes.

By circumventing traditional sequential processing of the radar data sets through the creation of a data processing agenda, available physical data (arising from core samples) may be used as the nucleus of the reasoning process. These physical data/radar data synergism provides the system with the capability for determining physical radar system properties such as surface scattering losses which are crucial

for remaining parameter estimation.

7.2.1 Recommendations

Due to the multi-domain problem which is bridge radar interpretation, the areas of further research are truely extensive. The detailed examination of the radar interpretation problem consistently revealed areas of much needed investigation. Several of these issues are presented here.

Most knowledge engineering for the operating parameters used by the system was derived through observation (due to a lack of access to the actual air-mounted radar units or the data acquisition vehicle) and therefore demand experimental verification[1]. These parameters include:

- amplitude variation with antenna height above a surface. It should be possible to accurately establish an analytic relationship for height variation and spreading losses based on antenna type. This relationship would be antenna/radation pattern dependent. Also, related studies for cantilever mounted radar antenna effects and antenna position deflection with vehicle acceleration or deceleration.

- concave and convex surface effects. These road surface undulations (both traversal and longitudinal) should also be investigated to allow their accurate differentiation and recognition.

- rough surface effects as they apply to cracked and low PCI pavements at road radar frequencies.

- sub-fraction of wavelength layer thickness effects such as produced by membrane and dry delamination effects. Modeling efforts reveal a large variation

[1]Some of this experimental work has been done by Texas Transport Institute but due to political sensitivities access to this important information was denied.

in observed reflections from thin interfaces. These models require experimental verification.

- physical property limits. The spatial derivatives developed here rely on threshold violations based on material properties. These require further quantification to establish practical limits.
  - determine the validity of the isotropic material assumption on which this system is based, ie. determine working permittivity variations of the form $(\Delta\epsilon_{material}/meter)$
  - construction based physical variations. Examination of the validity of structural component tolerances based on active building codes (for example slab thickness variations).

The diversity of rebar concentrations in bridge structures requires the detailed examination of various dielectric encapsulated reinforcing steel configurations. The study should include the effects of rebar density in concrete at depth, as well as the issue of manifestation and resolution of multiple reflections from parallel bars.

Ideally, an analysis system confronted with previously unseen events should provide an update capability to allow inclusion of this new knowledge. This learning capability should automatically identify the related causal relationships for any detected anomalous or unusual events.

The system should have in place a detailed explanation facility. As the system is a prototype, only the raw results are presented to the user. The user must manually examine cells of interest to determine slot values leading to observed results.

From an architectural standpoint, the system should be moved from the realm of expert system shell based application to embedded expert system. This would allow substantial performance improvements as well as the potential for a multiprocessing architecture. Expert system shells are excellent for development and rapid

prototyping, however, a practical near real-time expert system should not be forced to suffer under the development-tool-overhead penalty. Although capable, the LISP based KEE system is a huge monolith which suffers in inferencing performance in comparison to currently available dedicated shell tools which run on high performance engineering workstations. The multiprocessing paradigm for such a system could exploit separate neural, numeric and symbolic processors. Currently available neural hardware could be configured dynamically under expert system control. Such dedicated neurocomputing would allow all numerical raw data preprocessing to be performed outside of the expert system.

Appendix A

Ontario Bridge Building Code

A.1 Ontario Building Codes; Pre-1958 to Present

With the widespread acceptance of prestressed concrete as a bridge design material in the mid-1950's the building code governing construction practices was changed extensively. These changes were motivated by changes in materials, construction techniques and decreasing design tolerances. The construction material and design philosophy effects of these changes are outlined here [MANN83a].

Prior to 1958

- concrete was not air-entrained, therefore prone to salt penetration and scaling due to freeze-thaw cycle
- no waterproofing
- condition varies considerably

1958-1961

- poorly air entrained
- ineffective short-term sprayed silicone waterproofing
- condition is generally better than group 1

1962-1964

- properly air entrained concrete
- mastic asphalt or glass fibre/asphalt emulsion waterproofing. These became brittle and ineffective after several years of service
- variable condition but generally good

1965-1972

- generally good quality, properly air entrained concrete exposed concrete deck with 40 mm top cover
- later waterproofed and asphalted due to corrosion distress
- generally good condition

1973-1978

- good quality air entrained concrete
- mastic asphalt waterproofing on rigid frames, otherwise rubberized membrane with 7 mm protection board after 1975
- generally good condition

After 1978

- good quality air entrained concrete
- rubberized membrane waterproofing with protective board
- top matte of reinforcing steel epoxy-coated with a specified cover of 70 ± 20 mm
- isotropic reinforcing steel
- good condition

Appendix B

Cobbledick Road Bridge-Physical Plan

B.1 Physical Specifications

Physical specifications based on structural drawings and site measurement for the Cobbledick Road Bridge, located at the junction of Highway 115 and Highway 401. The bridge was constructed in 1958 and appears (visually) in excellent condition.

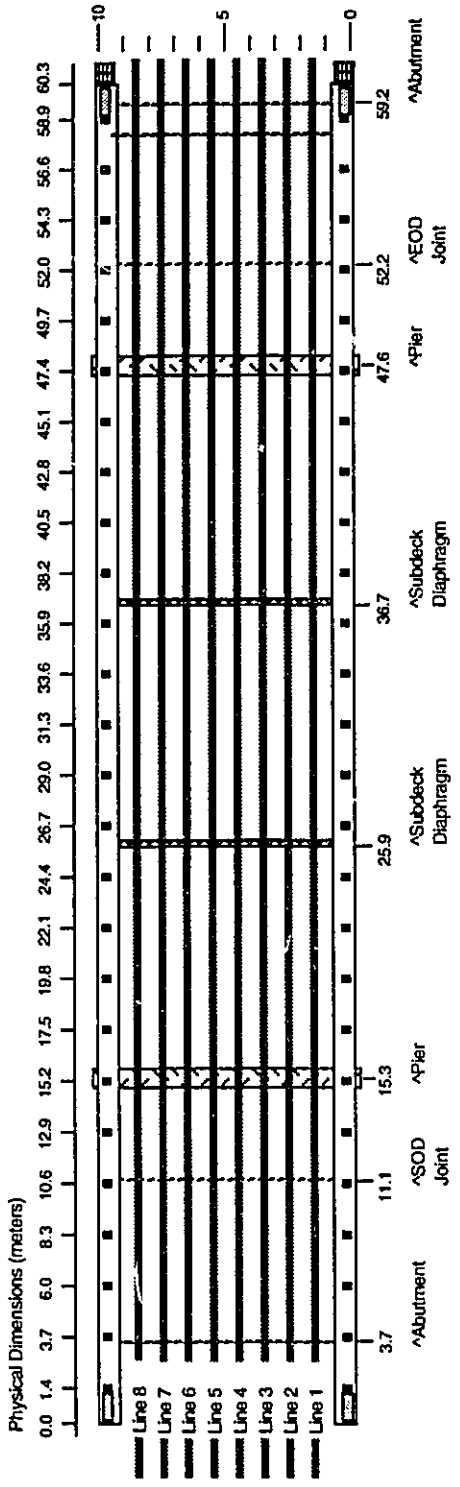

Figure B.1: Cobbledick Road Physical Site Plan- Top view and Data Line Positions

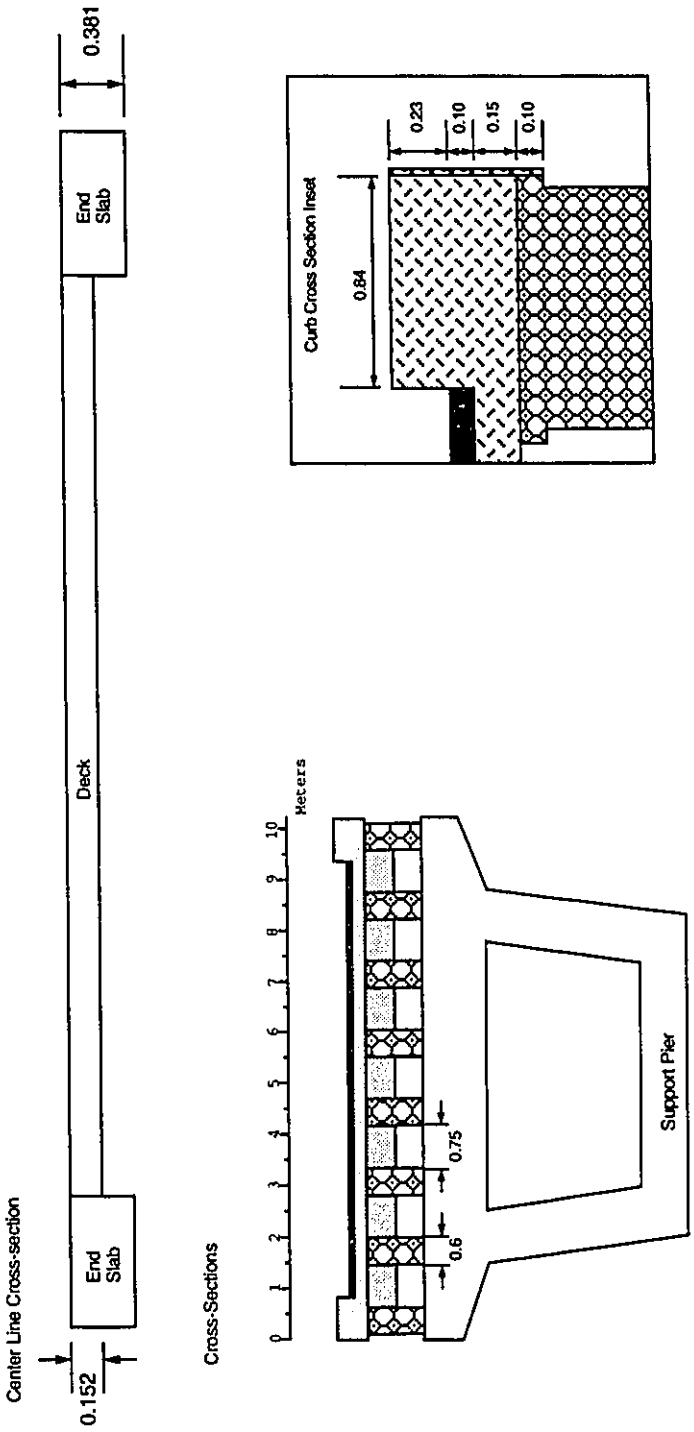

Figure B.2: Cobbledick Road Physical Site Plan- Cross-Sections

Appendix C

Bridge Radar Data

This appendix presents the various stages of processing for the raw data collected by MTO at the Cobbledick Road bridge site during November of 1989. This radar produced data was recorded to an instrumentation quality multichannel magnetic tape device which allowed off-line digitization of the analog signals. Positional synchronization was provided through a fifth-wheel system which generated boolean signal transitions for 10cm and 1m intervals. These transitions were recorded concurrently with the free running radar signals (approximately 50 samples per second) on the same physical tape device. The digitization was accomplished with a 12bit ADC system and provided the binary data as input to the GPR expert system.

The raster images use 256 gray levels to represent the approximate signal range of [-0.1 to +0.1] of the surface reflection amplitude with image offset (gray scale level= 128) adjusted for best fine detail reproduction. The significant white band at the top of the window is the surface reflection, and subsequent bands indicate positive (shown as white) reflections and negative (shown as black) reflections. The strong negative reflection at approximately 6ns seen in some data lines is the concrete/air reflection of the bottom of the deck.

C.1 Raw Data

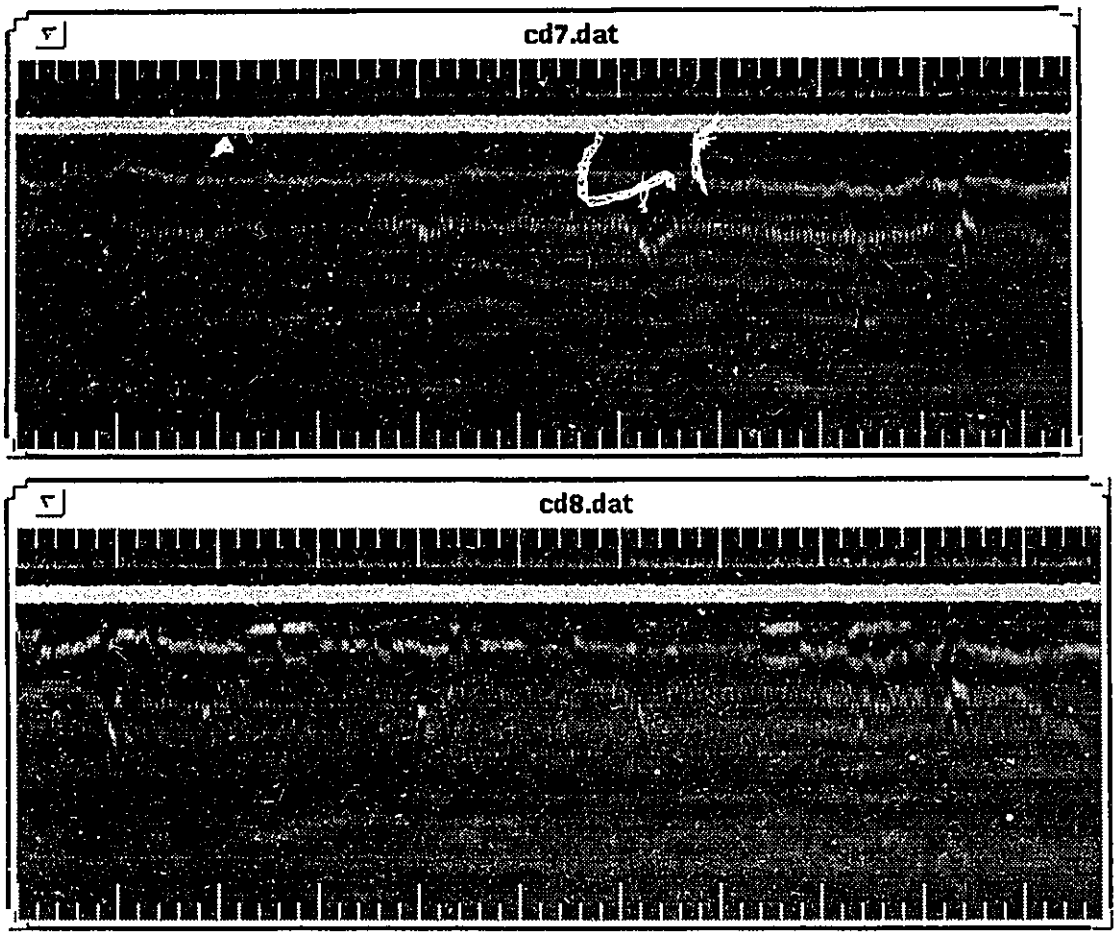

Figure C.3: Cobbledick Road Raw Data Dump (Lines 7 and 8) These 256 gray scale raster image dumps of the raw radar data represent approximately 54 meters of bridge deck in the horizontal direction (one sample taken every 10cm) with each visible tick corresponding to a meter mark. The vertical direction is linear with the entire distance representing approximately 10.8ns.

C.2 Segmented Data

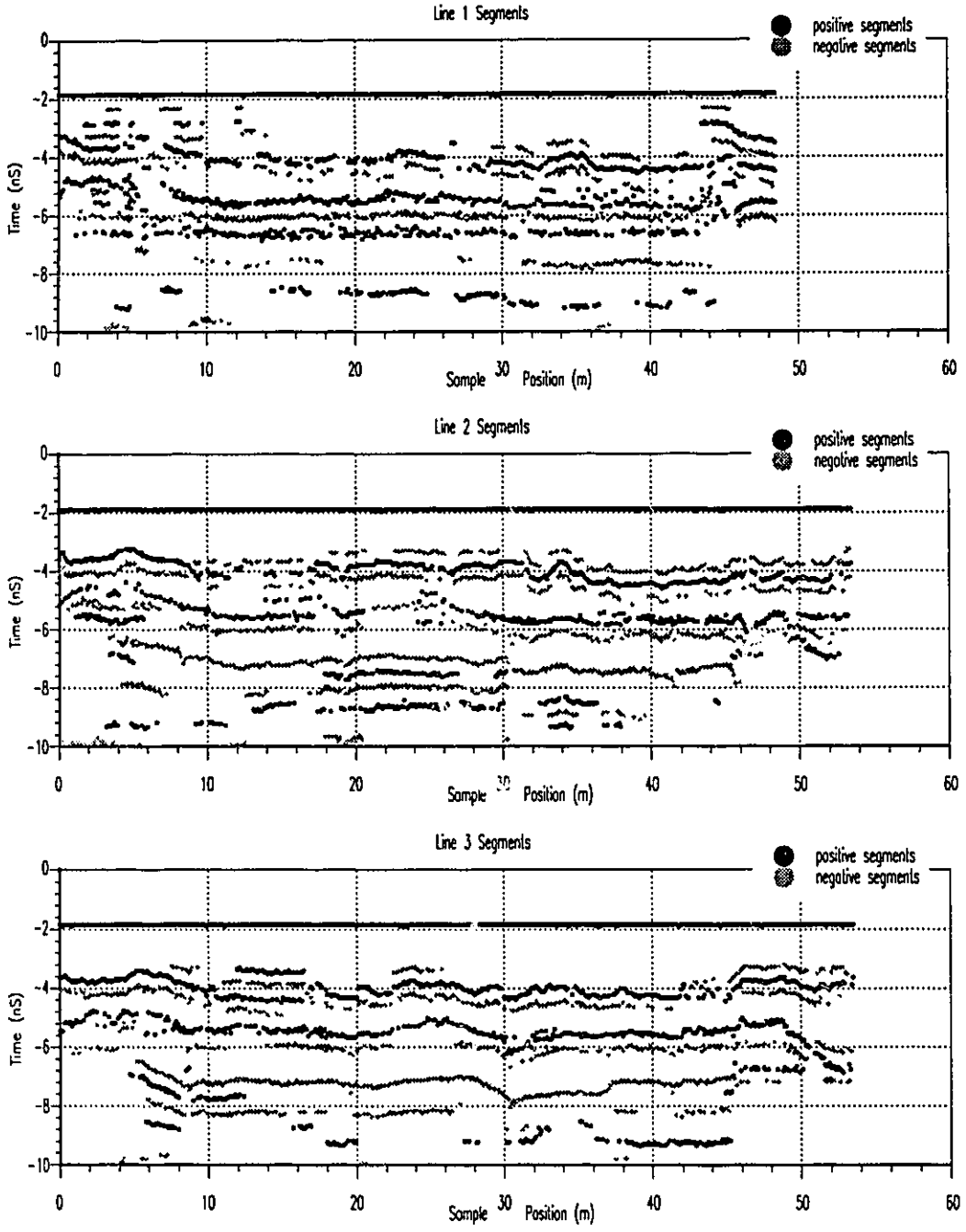

Figure C.4: Cobbledick Road Segmented Data: (Lines 1 to 3)
System generated neural-network segmentation operation output.

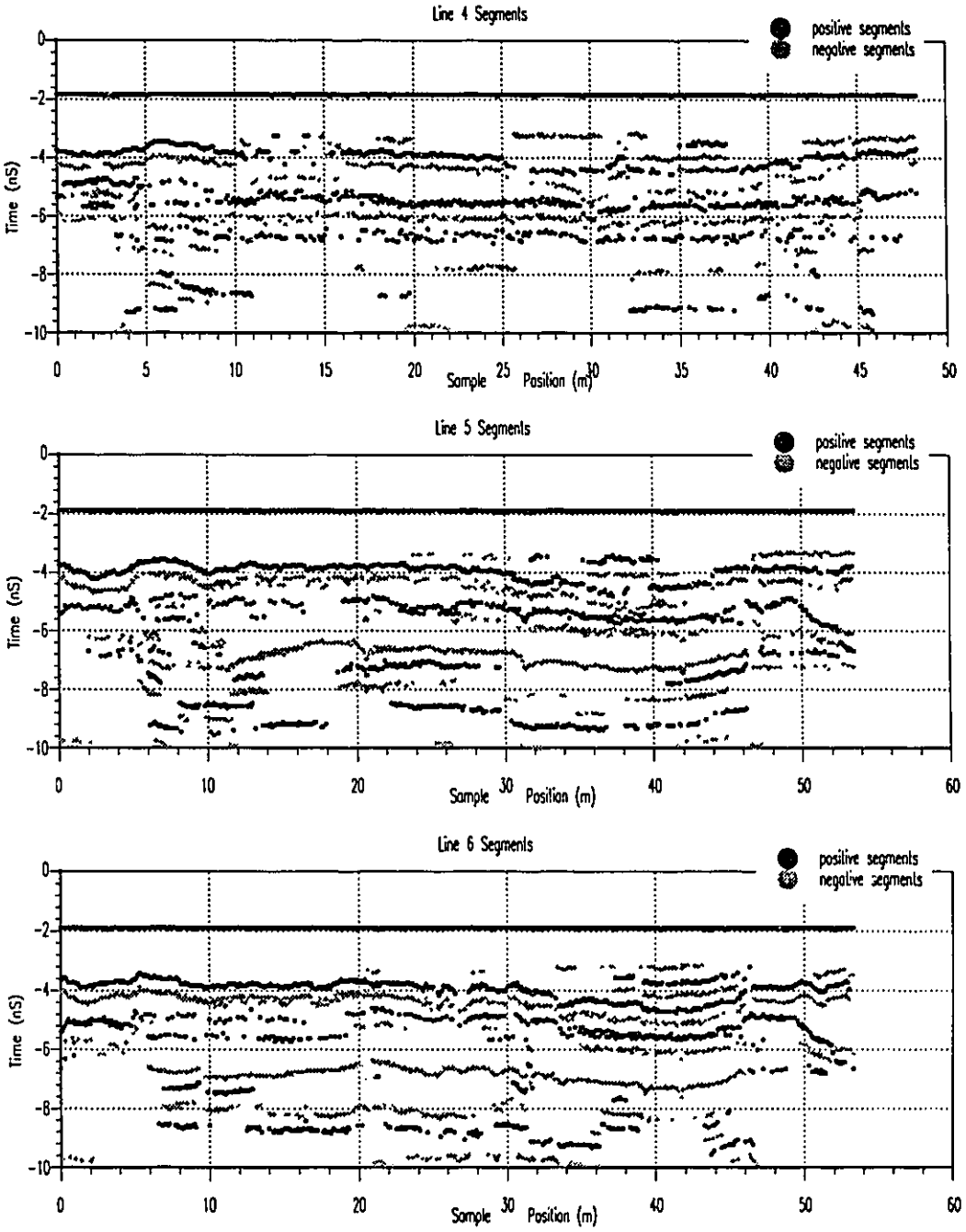

Figure C.5: Cobbledick Road Segmented Data: (Lines 1 to 3)
System generated neural-network segmentation operation output.

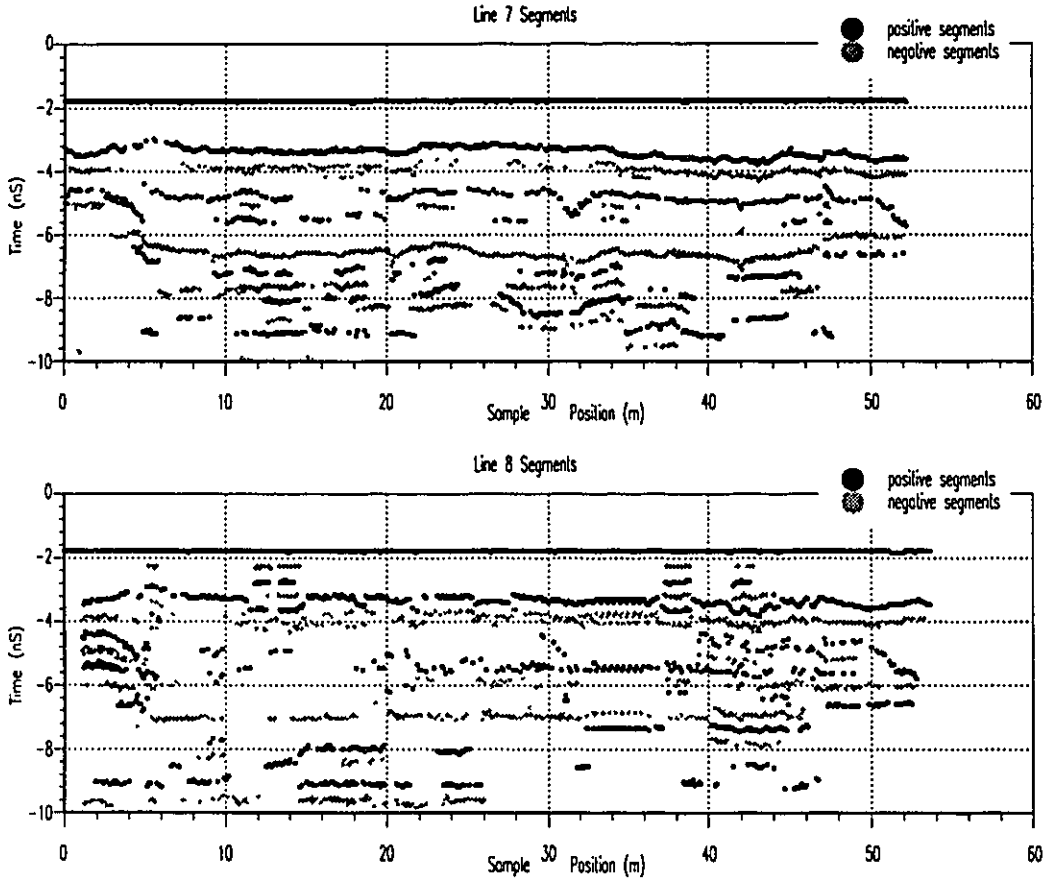

Figure C.6: Cobbledick Road Segmented Data: (Lines 7 and 8)
System generated neural-network segmentation operation output.

C.3 Layered Data

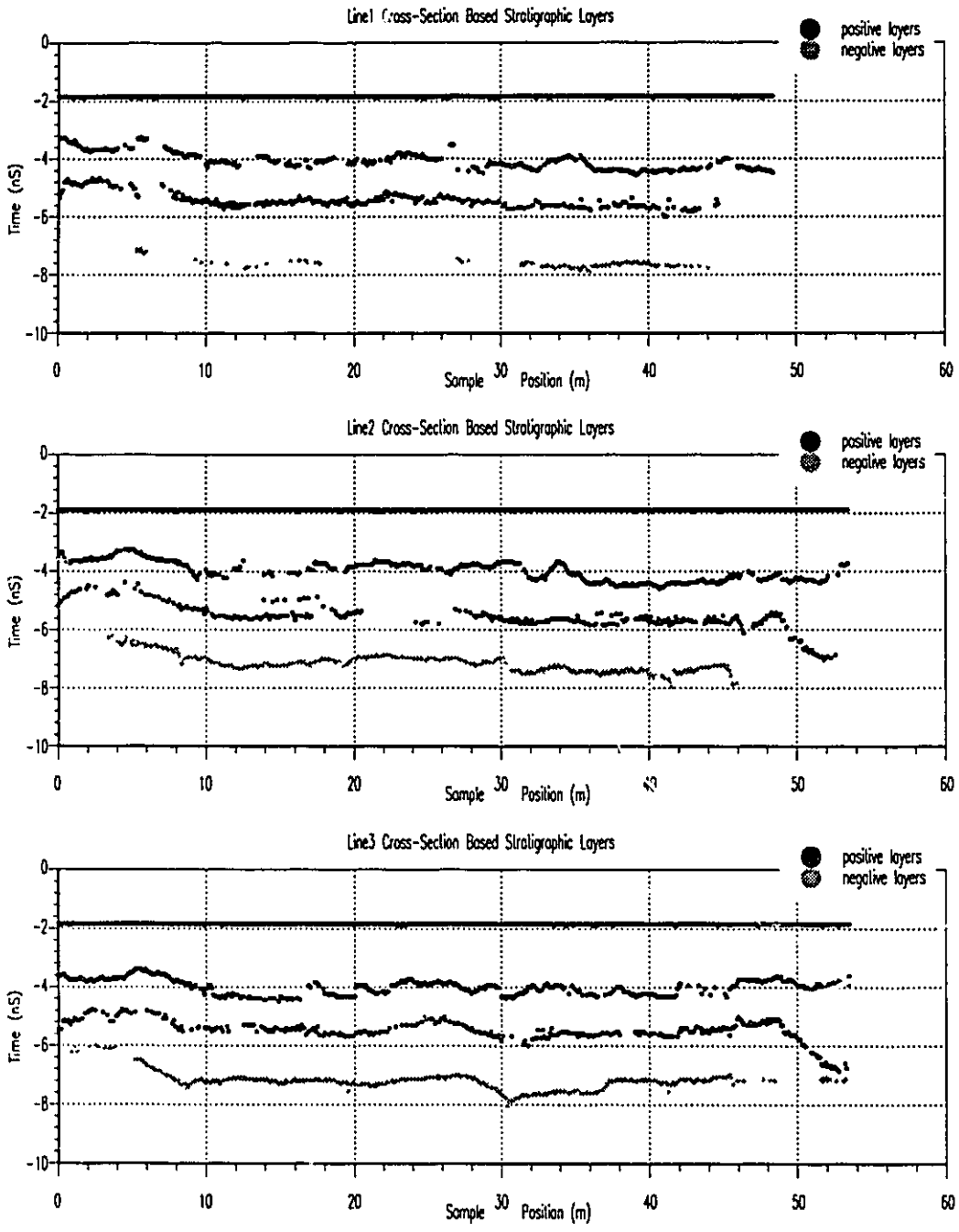

Figure C.7: Cobbledick Road Layered Data: (Lines 1 to 3)
System knowledge-based layering operation output.

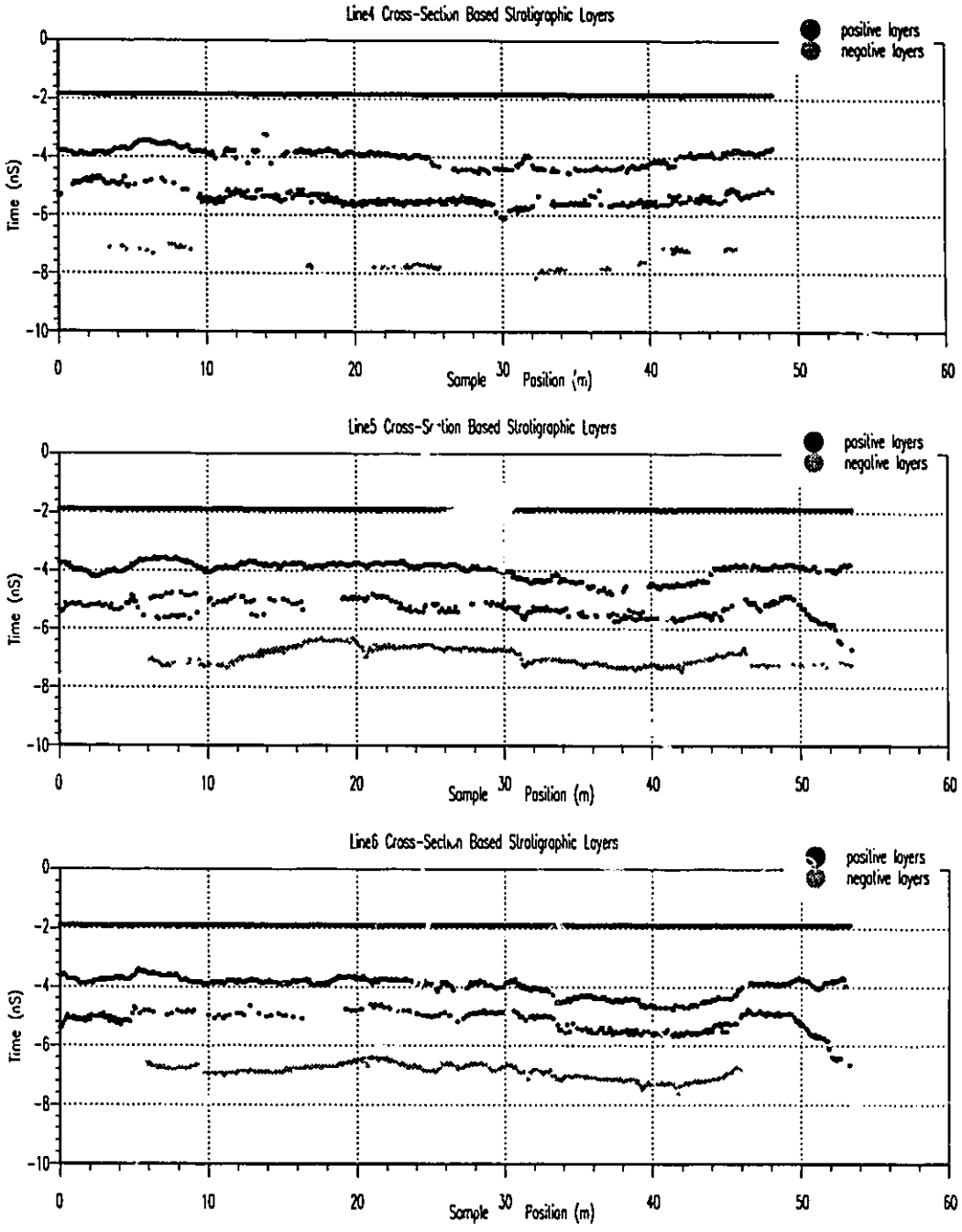

Figure C.8: Cobbledick Road Layered Data: (Lines 4 to 6)
System knowledge-based layering operation output.

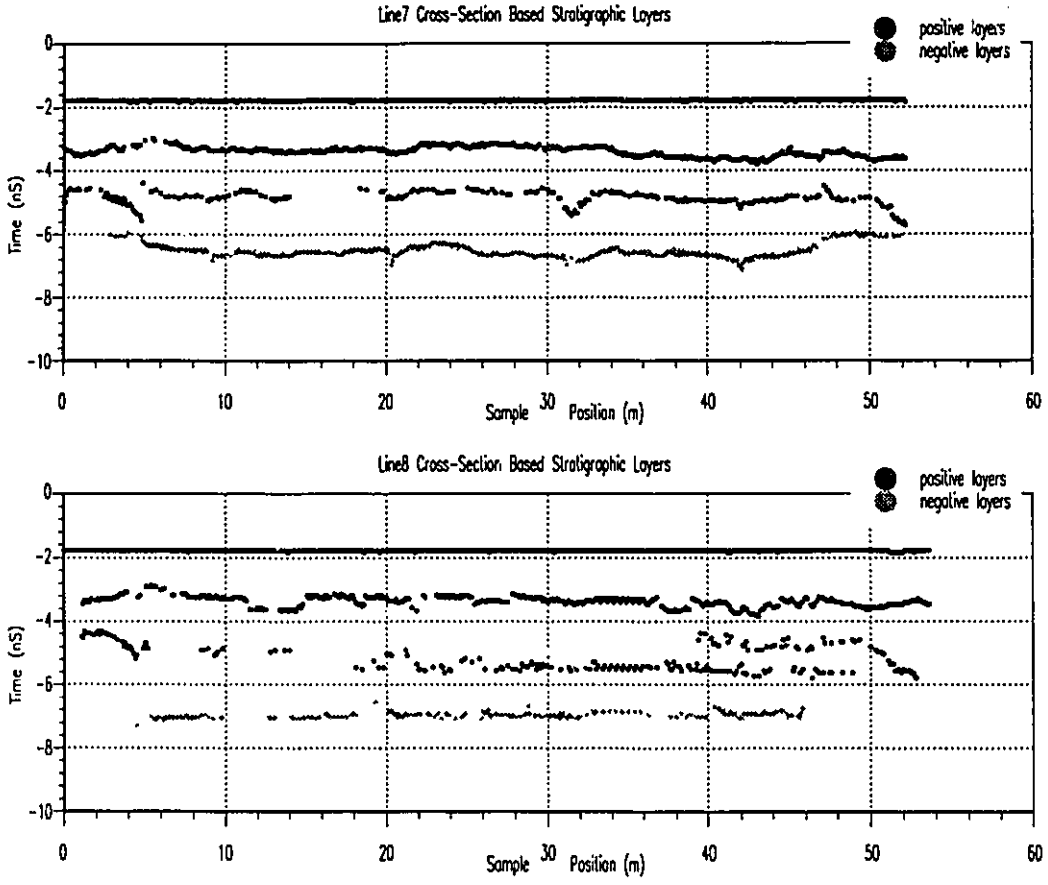

Figure C.9: Cobbledick Road Layered Data: (Lines 7 and 8)
System knowledge-based layering operation output.

Appendix D

Expert System Dialogs

A sequence of dialogs is presented for the user interaction necessary for system starup. The user interface to the system is closely coupled to the Texas Instruments MicroExplorer windowing system.

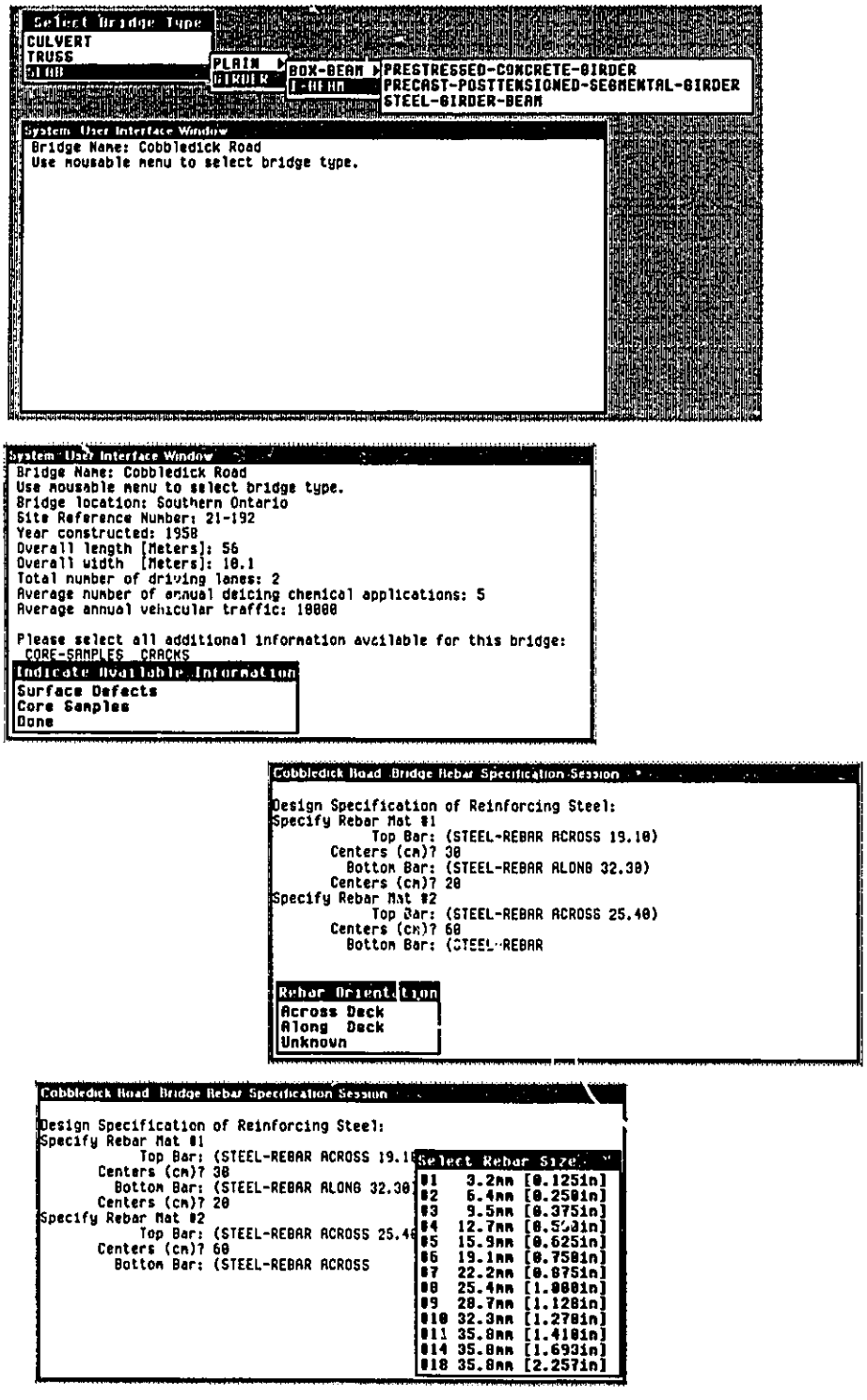

Figure D.1: System Site Configuration and Initialization Dialog
The expert system allows configuration of site physical parameters for the particular bridge structure.

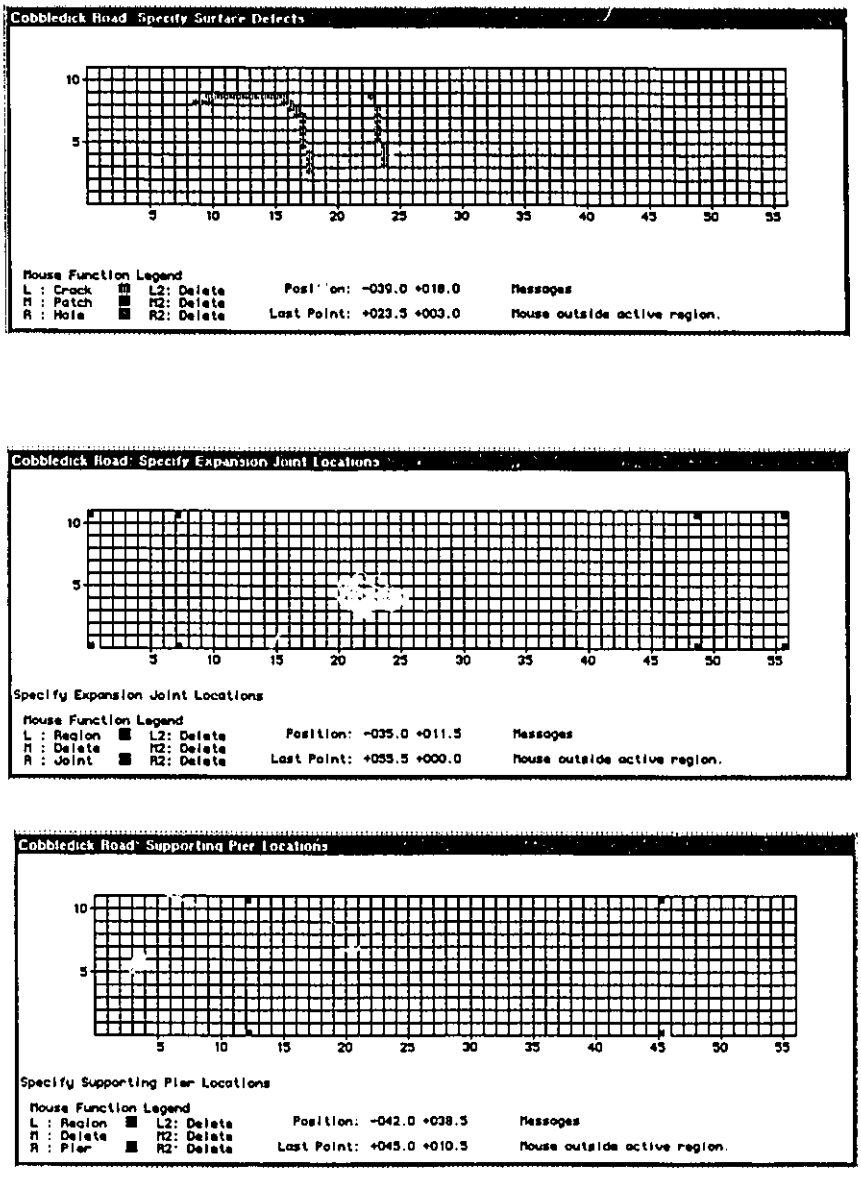

Figure D.2: System Site Configuration and Initialization Dialog
System configuration includes user specification of Pavement Condition Index parameters and observable structural events.

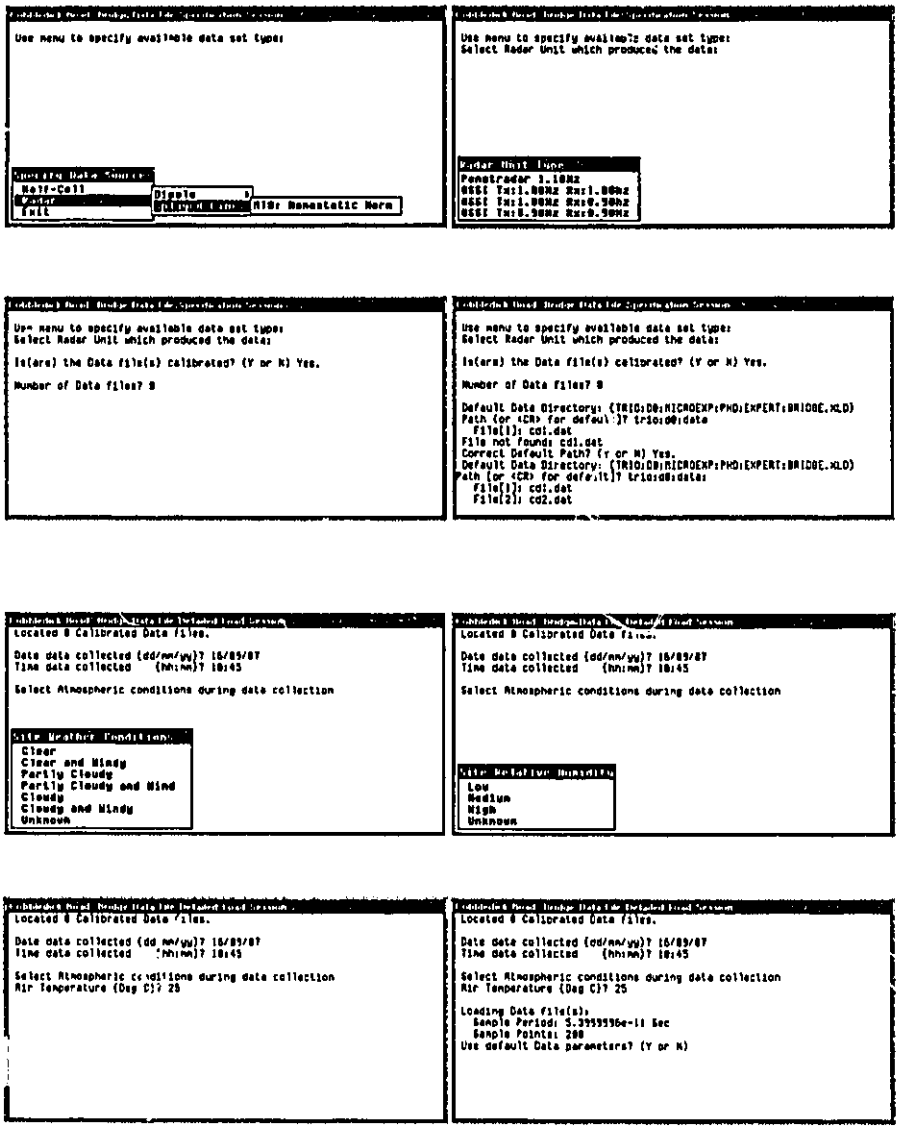

Figure D.3: System Data File Configuration and Initialization Dialog Sequence
The expert system allows configuration of both data file specification as well as ancillary information regarding conditions at the time of data acquisition.

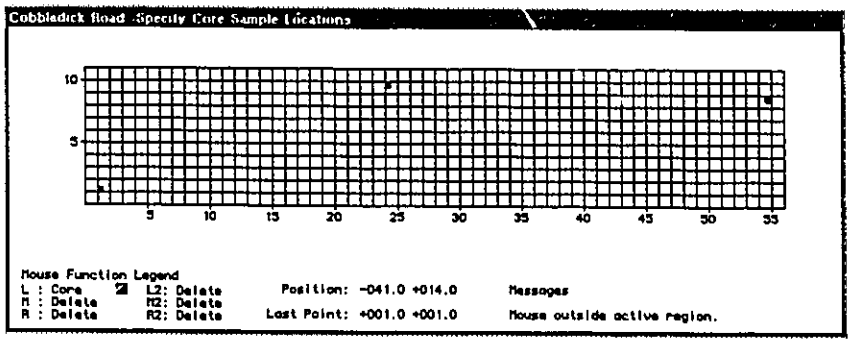

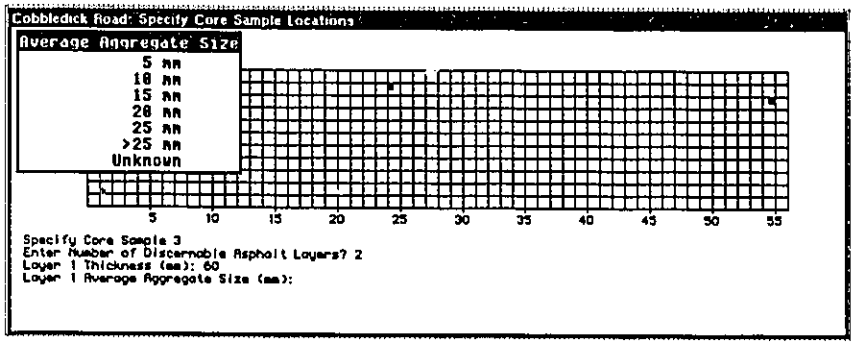

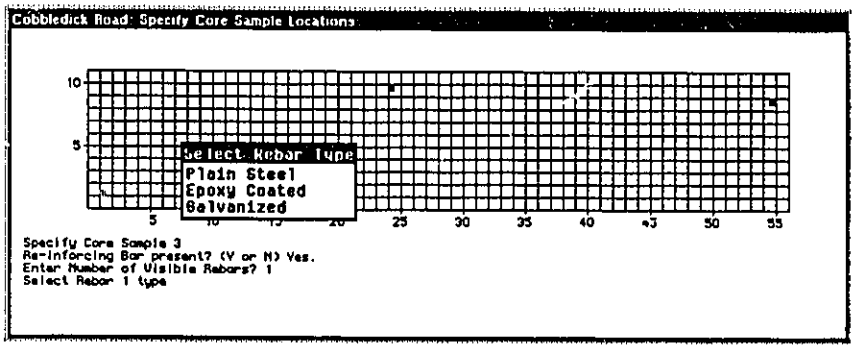

Figure D.4: System Core Sample Specification Dialog
Core sample specification defines the number and location sample extraction sites.

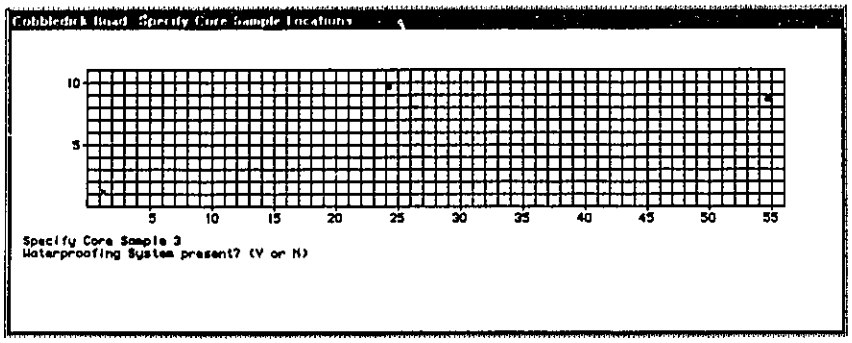

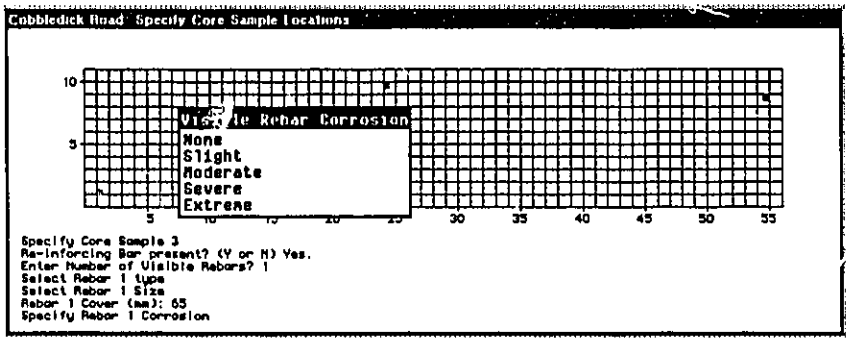

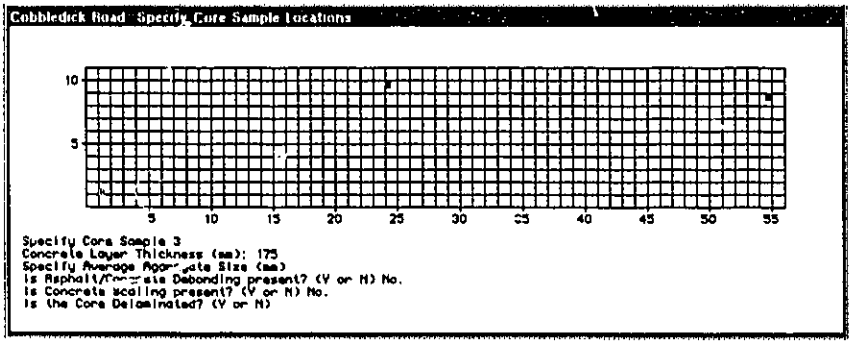

Figure D.5: System Core Sample Specification Dialog
Core sample details include composition, cross-section and visible defects.

Appendix E

Expert System Inferencing Samples

E.1 Cross-Sectional Modeling Output

System generated cross-sections for default physical specifications for a 1958 constructed slab-on-girder design. This cross-section information is contained as part of the system blackboard and is printed here in a readable format.

System Layer Structures for models shown in Figure 5.3:

```
(get.value 'abutment.basic.1 'default.cross-section)
([LYR: GENERIC-ASPHALT Thk=0.10m Str=0.00m e=7.00 Att=-6.00 Emb:NIL]
 [LYR: GENERIC-CONCRETE Thk=1.00m Str=0.10m e=10.00 Att=-20.00
        Emb:
         (([RBR: STEEL-REBAR Dia=0.02m Cov=0.08m e=-.21 Att=-2.76
             Mtx:[MAT: TBC=0.30m LBC=0.30m]]
           [RBR: STEEL-REBAR Dia=0.02m Cov=0.50m e=-.21 Att=-2.76
             Mtx:[MAT: TBC=0.30m LBC=0.30m]]))]
 [LYR: SUBGRADE Thk=1000.00m Str=1.10m e=3.50 Att=-10.00 Emb:NIL])

(get.value 'approach.unsupported.2 'default.cross-section)
([LYR: GENERIC-ASPHALT Thk=0.10m Str=0.00m e=7.00 Att=-6.00 Emb:NIL]
 [LYR: GENERIC-CONCRETE Thk=0.40m Str=0.10m e=10.00 Att=-20.00
        Emb:
         (([RBR: STEEL-REBAR Dia=0.01m Cov=0.03m e=-.16 Att=-1.93
             Mtx:[MAT: TBC=0.30m LBC=0.30m]]
           [RBR: STEEL-REBAR Dia=0.01m Cov=0.32m e=-.16 Att=-1.93
             Mtx:[MAT: TBC=0.30m LBC=0.30m]]))]
 [LYR: AIR Thk=1000.00m Str=0.50m e=1.00 Att=0.00 Emb:NIL])

(get.value 'deck.on.air.3 'default.cross-section)
([LYR: GENERIC-ASPHALT Thk=0.10m Str=0.00m e=7.00 Att=-6.00 Emb:NIL]
 [LYR: GENERIC-CONCRETE Thk=0.20m Str=0.10m e=10.00 Att=-20.00
        Emb:
         (([RBR: STEEL-REBAR Dia=(0.015875 0.0127)m Cov=0.08m e=-.26 Att=-3.51
             Mtx:[MAT: TBC=0.31m LBC=0.46m]]
           [RBR: STEEL-REBAR Dia=(0.015875 0.0127)m Cov=0.12m e=-.26 Att=-3.51
             Mtx:[MAT: TBC=0.15m LBC=0.37m]]))]
 [LYR: AIR Thk=1000.00m Str=0.30m e=1.00 Att=0.00 Emb:NIL])

(get.value 'deck.on.conc.girder.4 'default.cross-section)
([LYR: GENERIC-ASPHALT Thk=0.10m Str=0.00m e=7.00 Att=-6.00 Emb:NIL]
 [LYR: GENERIC-CONCRETE Thk=0.20m Str=0.10m e=10.00 Att=-20.00
        Emb:
         (([RBR: STEEL-REBAR Dia=(0.015875 0.0127)m Cov=0.08m e=-.13 Att=-1.58
             Mtx:[MAT: TBC=0.15m LBC=0.46m]]
           [RBR: STEEL-REBAR Dia=(0.015875 0.0127)m Cov=0.12m e=-.13 Att=-1.58
             Mtx:[MAT: TBC=0.31m LBC=1.37m]]))]
 [LYR: CONCRETE Thk=0.50m Str=0.30m e=10.00 Att=-25.00 Emb:NIL]
 [LYR: AIR Thk=1000.00m Str=0.30m e=1.00 Att=0.00 Emb:NIL])

(get.value 'roadway.basic.0 'default.cross-section)
([LYR: GENERIC-ASPHALT Thk=0.10m Str=0.00m e=7.00 Att=-6.00 Emb:NIL]
 [LYR: SUBGRADE Thk=1000.00m Str=0.10m e=3.50 Att=-10.00 Emb:NIL])
```

E.2 Acceleration Related Amplitude Analysis

```
Bridge structure
  data lines  : 8
  deck length : 60 meters

Default Acceleration/Stabilization/Deceleration [ A: | S: | D: ] Zones
  Line[1]:  A:[2.6 -> 8.6] S:[8.6 -> 14.6] D:[45.1 -> 51.1]
  Line[2]:  A:[2.8 -> 8.8] S:[8.8 -> 14.8] D:[50.3 -> 56.3]
  Line[3]:  A:[1.9 -> 7.9] S:[7.9 -> 13.9] D:[49.5 -> 55.5]
  Line[4]:  A:[3 -> 9] S:[9 -> 15] D:[45.4 -> 51.4]
  Line[5]:  A:[2 -> 8] S:[8 -> 14] D:[49.6 -> 55.6]
  Line[6]:  A:[1.5 -> 7.5] S:[7.5 -> 13.5] D:[48.9 -> 54.9]
  Line[7]:  A:[1.6 -> 7.6] S:[7.6 -> 13.6] D:[47.9 -> 53.9]
  Line[8]:  A:[2 -> 8] S:[8 -> 14] D:[49.7 -> 55.7]

Percentage of Zone Experiencing Amplitude Variations

Line[1]:  A:83%   S:55%   D:62%
  Assert: '(the ACC.ZONE of LINE01 is
      '(CELL00002 CELL00003 CELL00004 CELL00005 CELL00006 CELL00007 CELL00008)
  Assert: '(the STB.ZONE of LINE01 is '(CELL00008 CELL00009 CELL00010 CELL00011 CELL00012)
  Assert: '(the DEC.ZONE of LINE01 is '(CELL00045 CELL00046 CELL00047 CELL00048)
Line[2]:  A:68%   S:29%   D:45%
  Assert: '(the ACC.ZONE of LINE02 is '(CELL01003 CELL01004 CELL01005 CELL01006 CELL01007)
  Assert: '(the STB.ZONE of LINE02 is '(CELL01008 CELL01009 CELL01010 CELL01014)
  Assert: '(the DEC.ZONE of LINE02 is '(CELL01051 CELL01052 CELL01053)
Line[3]:  A:68%   S:47%   D:50%
  Assert: '(the ACC.ZONE of LINE03 is '(CELL02002 CELL02003 CELL02004 CELL02005 CELL02006)
  Assert: '(the STB.ZONE of LINE03 is '(CELL02007 CELL02008 CELL02009 CELL02010)
  Assert: '(the DEC.ZONE of LINE03 is '(CELL02049 CELL02052 CELL02053 CELL02054 CELL02055)
Line[4]:  A:57%   S:21%   D:59%
  Assert: '(the ACC.ZONE of LINE04 is '(CELL03003 CELL03004 CELL03005 CELL03006 CELL03007)
  Assert: '(the STB.ZONE of LINE04 is '(CELL03009 CELL03010)
  Assert: '(the DEC.ZONE of LINE04 is '(CELL03047 CELL03048 CELL03049 CELL03050 CELL03051)
Line[5]:  A:75%   S:60%   D:98%
  Assert: '(the ACC.ZONE of LINE05 is
      '(CELL04002 CELL04003 CELL04004 CELL04005 CELL04006)
  Assert: '(the STB.ZONE of LINE05 is
      '(CELL04008 CELL04009 CELL04010 CELL04011 CELL04012 CELL04013)
  Assert: '(the DEC.ZONE of LINE05 is
      '(CELL04049 CELL04050 CELL04051 CELL04052 CELL04053 CELL04054 CELL04055)
Line[6]:  A:72%   S:75%   D:98%
  Assert: '(the ACC.ZONE of LINE06 is
      '(CELL05001 CELL05002 CELL05003 CELL05004 CELL05005 CELL05006)
  Assert: '(the STB.ZONE of LINE06 is
      '(CELL05007 CELL05008 CELL05009 CELL05010 CELL05011 CELL05012)
  Assert: '(the DEC.ZONE of LINE06 is
      '(CELL05048 CELL05049 CELL05050 CELL05051 CELL05052 CELL05053 CELL05054)
Line[7]:  A:93%   S:37%   D:86%
  Assert: '(the ACC.ZONE of LINE07 is
      '(CELL06001 CELL06002 CELL06003 CELL06004 CELL06005 CELL06006 CELL06007)
  Assert: '(the STB.ZONE of LINE07 is '(CELL06008 CELL06009 CELL06010 CELL06011)
  Assert: '(the DEC.ZONE of LINE07 is
      '(CELL06048 CELL06049 CELL06050 CELL06051 CELL06052 CELL06053)
Line[8]:  A:91%   S:62%   D:93%
  Assert: '(the ACC.ZONE of LINE08 is
      '(CELL07002 CELL07003 CELL07004 CELL07005 CELL07006 CELL07007 CELL07008)
  Assert: '(the STB.ZONE of LINE08 is '(CELL07008 CELL07009 CELL07010 CELL07011 CELL07012)
  Assert: '(the DEC.ZONE of LINE08 is
      '(CELL07049 CELL07050 CELL07051 CELL07052 CELL07053 CELL07054 CELL07055)
```

E.3 Wheel Rut Related Amplitude Analysis

```
Bridge structure
  data lines  : 8
  deck width  : 8.6 meters
  driven lanes: 2

Mean Amplitude and Deck Position Analysis [amp, pos]
  Line[1]:  [0.1423,0.8]
  Line[2]:  [0.1546,1.8]
  Line[3]:  [0.1512,2.8]
  Line[4]:  [0.1508,3.8]
  Line[5]:  [0.1444,4.8]
  Line[6]:  [0.1431,5.8]
  Line[7]:  [0.1527,6.8]
  Line[8]:  [0.1525,7.4]

Default Lane Usage Parameters
  curb width          : 1 meters
  median width        : 1 meters
  effective lane width: 2.8 meters

  lane[1]: [1 -> 3.8] meters
  lane[2]: [4.8 -> 7.6] meters

Default Orientation:
  Line[1] normal
  Line[2] over wheel track
  Line[3] over wheel track
  Line[4] normal
  Line[5] normal
  Line[6] over wheel track
  Line[7] over wheel track
  Line[8] over wheel track

Found bimodal distribution of mean data line amplitudes.
Low amp lines
 [1] [6] [5]
High amp lines
 [4] [3] [8] [7] [2]

Expected low amplitude lines: [1] [4] [5]
Found: [1] [5] [6]
Assert: '(the LINE.POSITION.OFFSET of dbg is LOW-SHIFT)

Tagging high amplitude lines for wheel track amplitude adjustment
Nominal amplitude adjustment= 0.9402
Adjusted Mean Line Amplitudes:
Assert: '(the WHEEL.TRACK.ADJ of LINE01 is  1.0)
  Line[1]:  [0.1423,0.8]
Assert: '(the WHEEL.TRACK.ADJ of LINE02 is 0.9402)
  Line[2]:  [0.1454,1.8]
Assert: '(the WHEEL.TRACK.ADJ of LINE03 is 0.9402)
  Line[3]:  [0.1422,2.8]
Assert: '(the WHEEL.TRACK.ADJ of LINE04 is 0.9402)
  Line[4]:  [0.1418,3.8]
Assert: '(the WHEEL.TRACK.ADJ of LINE05 is  1.0)
  Line[5]:  [0.1444,4.8]
Assert: '(the WHEEL.TRACK.ADJ of LINE06 is  1.0)
  Line[6]:  [0.1431,5.8]
Assert: '(the WHEEL.TRACK.ADJ of LINE07 is 0.9402)
  Line[7]:  [0.1436,6.8]
Assert: '(the WHEEL.TRACK.ADJ of LINE08 is 0.9402)
  Line[8]:  [0.1434,7.4]
```

Appendix F

System Tangle Graphs

This appendix presents a sequence of system data structure *Tangle Graphs*. These graphs allow visual inspection of the class/subclass relationships associating various units in the system hierarchical structure. Solid lines indicate class/subclass links and broken lines indicate class membership relationships.

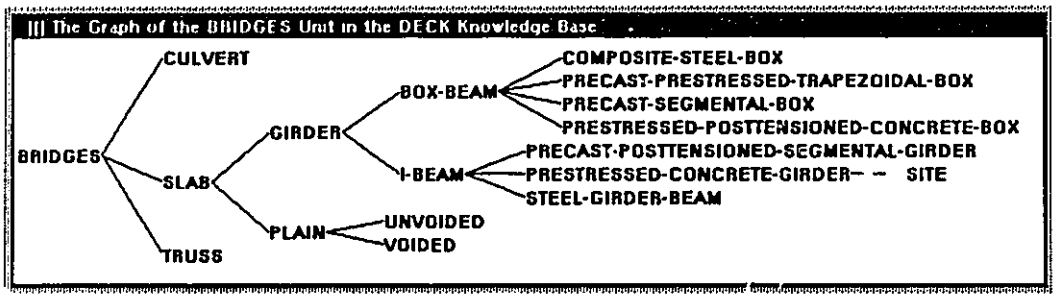

Figure F.1: BRIDGES KB Tangle Graph

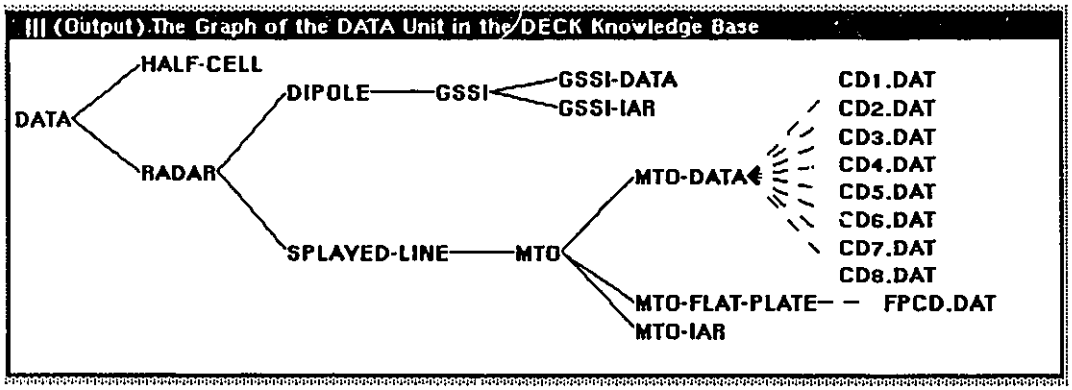

Figure F.2: DATA KB Tangle Graph

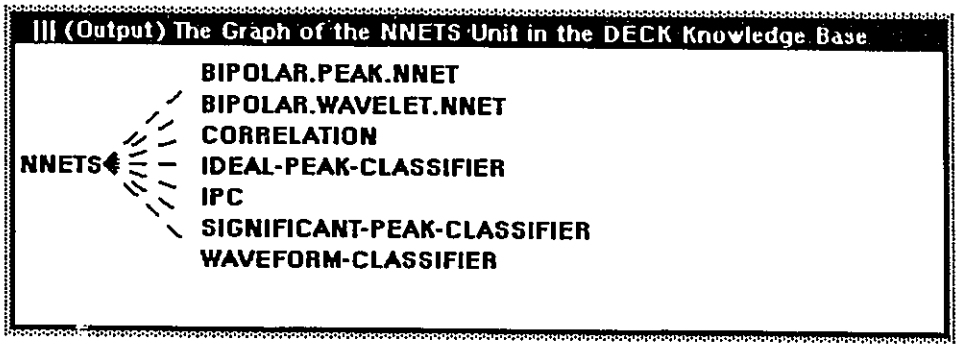

Figure F.3: NNET KB Tangle Graph

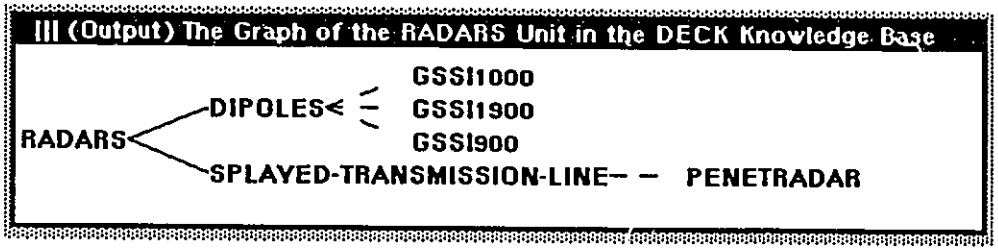

Figure F.4: RADARS KB Tangle Graph

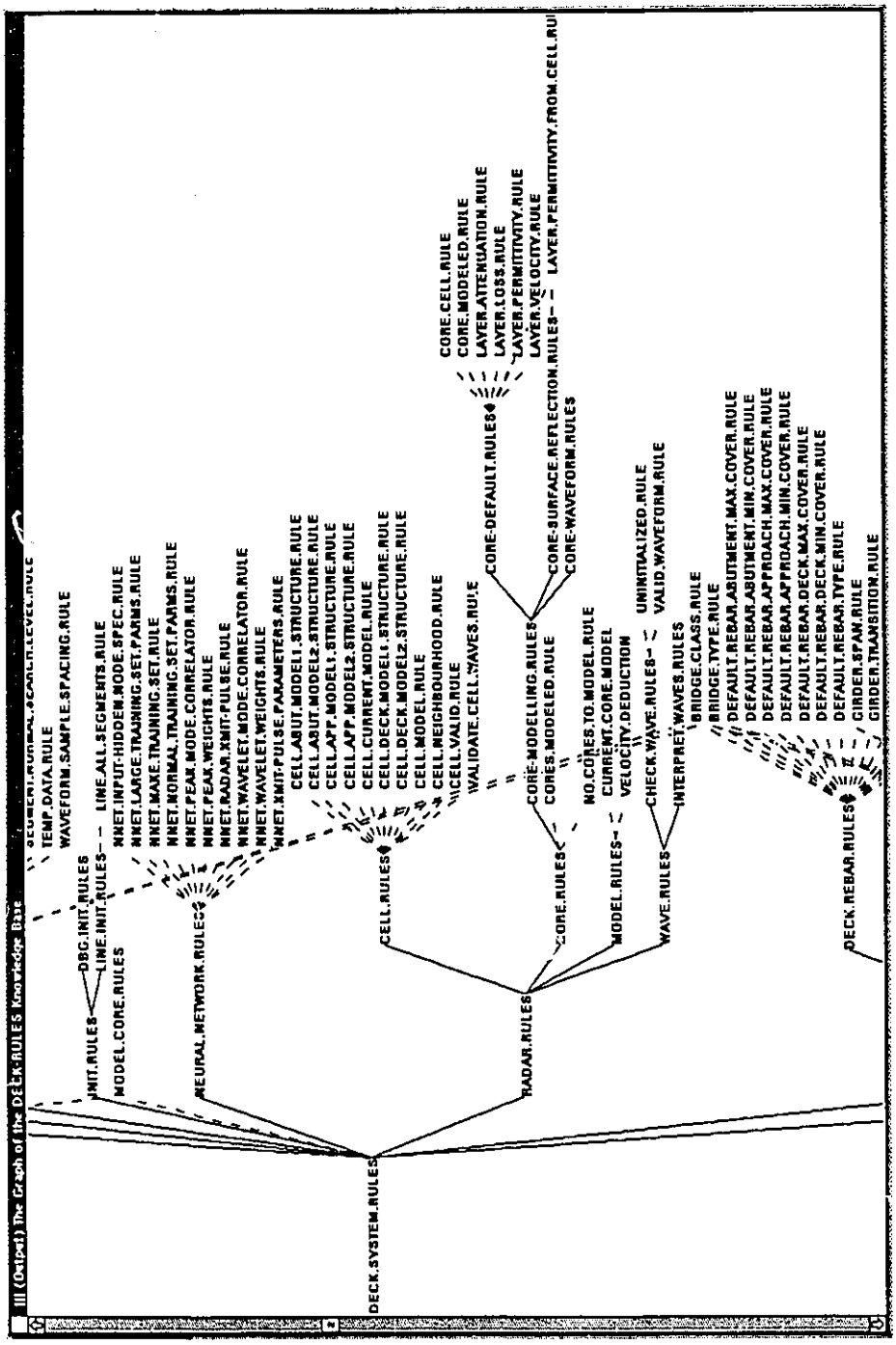

Figure F.5: Rule Base Fragment Tangle Graph
This figure shows a small portion of the entire system rule base.

Bibliography

[ADAM72] Adamson, B. (1972), "Joint Failures in Concrete Pavements of Ontario", Report IR-46, Ontario Ministry of Transportation and Communications, February.

[ALON77] Alongi, A.V. and Alongi, A.J. (1977), "Design Considerations for a Short-Pulse, High-Resolution Radar", Report PTR-0677, Penetradar Corporation, Niagara Falls, New York.

[AMAR67] Amari, S. (1967), "A Theory of Adaptive Pattern Classifiers", IEEE Trans. Electronic Computers, EC-16(3), 299-307.

[AMIN87] Aminzadeh, F. (1987), *Handbook of Geophysical Exploration, Section 1, Seismic Exploration, Volume 20, Pattern Recognition and Image Processing*, Geophysical Press.

[ANDE88] Anderson, J.A. and Rosenfeld, E. [Eds.] (1988), *Neurocomputing: Foundations of Research*, MIT Press.

[ANTO91] Antognetti, P. and Milutinovic, V. (1991), *Neural Networks: Concepts, Applications, and Implementations*, Volume II, Prentice Hall, Inc.

[BALA89] Balanis, C.A. (1989), *Advanced Engineering Electromagnetics*, John Wiley and Sons.

[BARH89] Barhen, J., Gulati, S. and Zak, M. (1989), "Neural Learning of Constrained nonlinear Transformations", IEEE Computer, 22, 67-76.

[BARR86] Barr, A. and Feigenbaum, E.A. (1986), *The Handbook of Artificial Intelligence*, Volumes I-IV, Addison-Wesley Publishing Company, Inc.

[BARR82] Barr, A. and Feigenbaum, E.A. (1982), *The Handbook of Artificial Intelligence*, Volume II, Addison-Wesley Publishing Company Inc.

[BART53] Barton, D.K. (1953), *Radar Resolution and Multipath Effects*, Radar Systems Volume 4, Raytheon Company.

[BATH84] Bath, M. and Berkhout, A.J. (1984), *Handbook of Geophysical Exploration, Section 1, Seismic Exploration, Volume 17, Mathematical Aspects of Seismology*, Geophysical Press.

[BECK63] Beckmann, P. and Spizzichino, A. (1963), *The Scattering of Electromagnetic Waves from Rough Surfaces*, The MacMillan Company.

[BLAC90] Personal Communication, Mike Black (1990), October.

[BLUM72] Blum, W. (1972), "Bridge Deck Waterproofing in Ontario", Report IR-50, Ontario Ministry of Transportation and Communications, July.

[BOER81] Boerner, W-M, Jordan, A.K. and IKay, I.W. (1981), "Introduction to the Special Issue on Inverse Methods in Electromagnetics", IEEE Transactions on Antennas and Propagation, Vol. AP-29, No. 2, March.

[BOWM69] Bowman, J.J., Senior, T.B.A. and Uslenghi, P.L.E. (1969), *Electromagnetic and Acoustic Scattering by Simple Shapes*, North-Holland Publishing Company.

[BRUC87] Bruckstein, A.M. and Kailath, T. (1987), "An Inverse Scattering Framework for Several Problems in Signal Processing", IEEE ASSP Magazine, January.

[CALD79] Calderwood, J.H. and Scaife, B.K.P. (1979), "On the Estimation of the Relative Permattivity of a Mixture", Dielectric Materials, Measurement and Applications, IEE Conference Publication No. 177.

[CANT77] Cantor, T.R. and Kneeter, C.P. (1977), "Radar and Acoustic Emission Applied to the Study of Bridge Decks, Suspension Cables and a Masonry Tunnel", The Port Authority of New York and New Jersey, Engineering Department, Research and Development Division, Report No. 77-13, December.

[CART86] Carter, C.R., Chung, T., Holt, F.B. and Manning, D.G. (1986), "An Automated Signal Processing System for the Signature Analysis of Radar Waveforms from Bridge Decks", Canadian Electrical Engineers Journal, Vol. 11, No. 3.

[CHEN82] Chen, C.H. (1982), *Seismic Signal Analysis and Discrimination*, Elsevier Scientific Publishing Company.

[CHOM86] Chommeloux, L., Pichot, C. and Bolomey, J-C (1986), "Electromagnetic Modeling for Microwave Imaging of Cylindrical Buried Inhomogeneities", IEEE Transactions on Microwave Theory and Techniques, Vol. MTT-34, No. 10, October.

[CHUN84] Chung, T., Carter, C.R., Manning, D.G. and Holt, F.B. (1984), "Signature Analysis of Radar Waveforms Taken on Asphalt Covered Bridge Decks", Report ME-84-01, Ontario Ministry of Transportation and Communications, June.

[CHUN89] Chung, T. and Carter, C.R. (1989), "Radar Signal Enhancement for DART", Report MAT-89-05, Ontario Ministry of Transportation and Communications, June.

[CHUN90] Chung, T. and Carter, C.R. (1990), "Upgrading of DART Software to 386 Computer Specifications", Report MAT-90-15, Ontario Ministry of Transportation and Communications, December.

[CHYC62] Chyc, H., Langhammer, K. and Smith, P. (1962), "Epoxy Resins for Concrete Construction and Restoration", Report RR-026, Ontario Ministry of Transportation and Communications, April.

[COEN81] Coen, S., Mei, K.K., Angelakos, D.J. (1981), "Inverse Scattering Technique Applied to Remote Sensing of Layered Media", IEEE Transactions on Antennas and Propagation, Vol. AP-29, No. 2, March, pp. 298-306.

[COPE87] Cope, R.J. (1987), *Concrete Bridge Engineering: Performance and Advances*, Elsevier Applied Science Publishers Ltd.

[CORK64] Corkill, J.T. and Lee, G.R. (1964), "Effectiveness of Bridge Deck Waterproofing", Report RR-057, Ontario Ministry of Transportation and Communications, September.

[CORK75] Corkill, J.T. (1975), "A Field Study of the Performance of Bridge Deck Waterproofing Systems in Ontario", Report ME-75-01, Ontario Ministry of Transportation and Communications, September.

[DAVI69] Davies, J. and Walker, R. (1969), "An Investigation on the Permeability of Asphalt Mixes", Report RR-145, Ontario Ministry of Transportation and Communications, May.

[DAVI92] Personal Communication, Les Davis (1992), March.

[DEKI 84A] de Kleer, J. and Bobrow, D.G. (1984), "Qualitative Reasoning With Higher Order Derivatives", Proceedings of the National Conference on Artificial Intelligence.

[DEKL84B] de Kleer, J. and Brown, J.S. (1984), "Qualitative Physics Based On Confluences", Artificial Intelligence, 24:7-83.

[DEKL84C] de Kleer, J. (1984), "How Circuits Work", Artificial Intelligence, 24:205-280.

[DEKL79] de Kleer, J. (1979), "The Origin and Resolution of Ambiguities in Causal Arguments", Proceedings of the International Joint Conference on Artificial Intelligence, Cambridge, Mass.

[DORT73] Dorton, R. and Csagoly, P. (1973), "Proposed Ontario Bridge Design Load", Report RR-186, Ontario Ministry of Transportation and Communications, November.

[DORT83] Dorton, R.A., Bakht, B. et al. (1983), "Ontario Highway Bridge Design Code", Report OHBDC-83-01, Ontario Ministry of Transportation and Communications.

[DUDA79] Duda, R., Goschnig, J. and Hart, P.E. (1979), "Model design in the PROSPECTOR consultant system for mineral exploration", In D. Michie (Ed.), Expert systems in the microelectronics age. Edinburgh: Edinburgh University Press, pp 153-167.

[FORB83] Forbus, D.K. (1983), "Measurement Interpretation in Qualitative Process Theory", Proceedings of the Eighth International Joint Conference on Artificial Intelligence, Karlsruhe, West Germany: 315-320.

[FORB84] Forbus, D.K. (1984), "Qualitative Process Theory", Artificial Intelligence 24:85-168.

[FRAN87] Franklin, J. (1987), "Thermal Characteristics of Rock Aggregate Materials", Report RR-241, Ontario Ministry of Transportation and Communications, October.

[FROM72] Fromm, H.J. and Phang, W. (1972), "A Study of Transverse Cracking of Bituminous Pavements", Report RR-176, Ontario Ministry of Transportation and Communications, January.

[GAUN81] Gaunaurd, G.C. and Uberall, H. (1981), "Solution of the Inverse Electromagnetic Scattering Problem in the Resonance Case", IEEE Transactions on Antennas and Propagation, Vol. AP-29, No. 2, March.

[GROS88] Grossberg, S. (1988), "Nonlinear Neural Networks: Principles, Mechanisms and Architectures", Neural Networks, 1(1), 17-61.

[GULA87] Gulati, S., Iyengar, S.S., Toomarian, N., Protopopescu, V. and Barhen, J. (1987), "Nonlinear Neural Networks for Deterministic Scheduling", IEEE First Int. Conf. on Neural Networks, IV, 745.

[HAJE86] Hajek, J.J, Phang, G.A., Wrong, A. and Prakash, G.M.S. (1986), "Pavement Condition Index (PCI) for Flexible Pavements", Report PAV-86-02, Ontario Ministry of Transportation and Communications, August.

[HECH87] Hecht-Nielsen, R. (1987), "Nearest Matched Filter Classification of Spatiotemporal Patterns", Applied Optics, 26(10), 1892-1899.

[HECH90] Hecht-Nielsen, R. (1990), *Neurocomputing*, Addison-Wesley Publishing Company.

[HOLT80] Holt, F.B. and Manning, D.G. (1980), "Deterioration of Bridge Substructures – Phase I", Report ME-80-03, Ontario Ministry of Transportation and Communications, January.

[HOLT82] Holt, F.B. (1982), "Detection of Delamination Below Asphalt Wearing Courses on Concrete Bridge Decks (Interim Report)", Report ME-82-02, Ontario Ministry of Transportation and Communications, May.

[JONE86] Jones, P.H., Jeffrey, B.A., Walter, P.K. and Hutchon, H. (1986), "Environmental Impact of Road Salting – State of the Art", Report RR-237, Ontario Ministry of Transportation and Communications, July.

[KAME82] Kamel, N., Musgrove, G.R. and Rutka, A. (1982), "Design and Performance of Bituminous Friction Course Mixes", Report ME-82-02a, Ontario Ministry of Transportation and Communications.

[KEE88] — (1988), "KEE User's Guide, KEE Version 3.1", Intellicorp Inc., Mountain View, California, USA, May.

[KING59] King, R.W.P. and Wu, T.T. (1959), *The Scattering and Diffraction of Waves*, Harvard University Press.

[KNOT85] Knott, E.F., Shaeffer, J.F. and Tuley, M.T. (1985), *Radar Cross Section*, Artech House.

[KRAU73] Kraus, J.D. and Carver, K.R. (1973), *Electromagnetics*, McGraw-Hill, Second Edition.

[CUN85] Le Cun, Y. (1985), "A Learning Scheme for Asymmetric Threshold Networks", Proc. Congitiva 85, 599-607.

[LEE88] Lee, S., Milos, E., Greiner, R. and Rossiter, J. (1988), "An Expert System for Automated Interpretation of Ground Penetrating Radar Data", Proceedings of Workshop on Ground Penetrating Radar, J.A. Pilon (Ed.), Ottawa.

[LEE87] Lee, S.R. (1987), *Machine Analysis of Impulse Radar Signals for Ice Profiling*, Masters Thesis, University of Toronto.

[LIND80] Lindsay, R., Buchanan, B.G., Feigenbaum, E.A. and Lederberg, J. (1980), *DENDRAL*, New York: McGraw-Hill.

[LIPP87] Lippmann, R.P. (1987), "An Introduction to Computing With Neural Nets", IEEE ASSP Magazine, April.

[LONG83] Long, M.W. (1983), *Radar Reflectivity of Land and Sea*, Artech.

[MANN86a] Manning, D. and Reel, R. (1986), "Maintenance of the Highway Infrastructure, Bridge Management", Report ONT-86-11, Ontario Ministry of Transportation and Communications, March.

[MANN86b] Manning, D. and Ryell, J. (1986), "Durable Bridge Decks", Report RR-203, Ontario Ministry of Transportation and Communications, April.

[MANN83a] Manning, D.G. and Bye, D.H. (1983), "Bridge Deck Rehabilitation Manual, Part One: Condition Survey", Report SP-016, Ontario Ministry of Transportation and Communications, November.

[MANN83b] Manning, D.G. and Bye, D.H. (1983), "Bridge Deck Rehabilitation Manual, Part Two: Contract Preparation", Report SP-017, Ontario Ministry of Transportation and Communications, November.

[MANN83c] Manning, D.G. and Bye, D.H. (1983), "Bridge Deck Rehabilitation Manual - Supplement", Report SP-018, Ontario Ministry of Transportation and Communications, September.

[MANN82] Manning, D.G. and Holt, F.B. (1982), "Detecting Deterioration in Asphalt-Covered Bridge Decks", Report ME-82-03, Ontario Ministry of Transportation and Communications, September.

[MANN85] Manning, D.G. et al. (1985), "The Development of DART (Deck Assessment by Radar and Thermography)", Report ME-85-03, Ontario Ministry of Transportation and Communications, November.

[MARS86] Marsalek, J. (1986), "Road and Bridge Deck Drainage Systems, Part II: Laboratory Investigations", Report RR-238, Ontario Ministry of Transportation and Communications, August.

[MASE86] Maser, K. (1986), "Automated Interpretation of Sensor Data for Evaluating In-Situ Conditions", Applications of Artificial Intelligence in Engineering Problems, 1st International Conference, Southampton University, UK, April.

[MASE91] Maser, K. (1991), "BRIDGE DECK CONDITION SURVEYS USING RADAR", Transportation Research Board 70th Annual Meeting, Washington D.C., January.

[MASL87] Masliwec, T. and Manning, D.G. (1987), "Bridge Condition Surveys Using the DART Prototype Vehicle", Report ME-87-12, Ontario Ministry of Transportation and Communications, December.

[MASL90a] Personal Communication, Tony Masliwec (1990), October.

[MASL90b] Masliwec, T. (1990), "Optimizing Infrared Detection for Bridge Deck Deterioration", Report ME-88-10, Ontario Ministry of Transportation and Communications, April.

[MEND80] Mendel, J.M. and Habibi-Ashrafi, F. (1980), "A Survey of Approaches to Solving Inverse Problems for Lossless Layered Media Systems", IEEE Transactions on Geoscience and Remote Sensing, Vol. GE-18, No. 4, October.

[MERL92] Personal Communication, Tony Merlo (1992), March.

[MINS75] Minsky, M. (1975), "A Framework for Representing Knowledge", In P.H. Winston (Ed.), The Psychology of Computer Vision, McGraw- Hill, 211-277.

[MUSI86] Musil, J. and Zacek, F. (1986), *Microwave Measurements of Complex Permittivity by Free Space Methods and Their Applications*, Elsevier.

[ODRI88] O'Driscoll, K.F. and Suddaby, K.G. (1988), "Property Modification of a De-icing Agent", Report MAT-88-05, Ontario Ministry of Transportation and Communications, July.

[NACE72] — (1972), *Coatings and Linings for Immersion Service*, TPC Publication 2, National Association of Corrosion Engineers.

[RTAC77] — (1977), *Concrete Bridge Decks: Guide to Construction, Maintenance and Repair*, Roads and Transportation Association of Canada.

[NACE87] — (1987), *Corrosion of Metals in Concrete*, Proceedings of the Corrosion/87 Symposium on Corrosion of Metals in Concrete, National Association of Corrosion Engineers.

[NACE83] — (1983), *Solving Rebar Corrosion Problems in Concrete*, National Association of Corrosion Engineers.

[OMTC83] — (1983), "World Trends in the Design and Construction of Bridges", Report STRUC-83-02, Ontario Ministry of Transportation and Communications, July.

[OPPE75] Oppenheim, A.V. and Schafer, R.W. (1975), *Digital Signal Processing*, Prentice-Hall, Inc.

[PAO89] Pao, Y. (1989), *Adaptive Pattern Recognition and Neural Networks*, Addison-Wesley Publishing Company, Inc.

[PARR92] Parry, N.S., Davis, J.L. and Rossiter, J.R. (1992), "GPR Systems for Roads and Bridges", Fourth International Conference on Ground Penetrating Radar, June.

[PHAN74] Phang, W. and Chong, G. (1974), "Thin Asphalt Pavements – A Performance Study", Report IR-53, Ontario Ministry of Transportation and Communications, February.

[POWE77] Powell, M.J.D. (1977), *Restart Procedures for the Congugate Gradient Method*, Mathematical Programming, Vol. 12, April.

[RICH67] Richardson, B.S. (1967), "Report on Highway Bridge Design in Ontario", Report IR-10, Ontario Ministry of Transportation and Communications.

[ROBI75] —— (1975), "Dynamic predictive deconvolution", Geophys. Prospecting, Vol. 23, pp 779-797.

[ROBI67] Robinson, E.A. (1967), "Predictive decomposition of time-series with application to siesmic exploration", Geophysics, Vol. 32, pp 418-484.

[ROSS89] Personal Communication from Dr. J.R. Rossiter: Inkster, D.R., Rossiter, J.R., Goodman, R., Galbraith, M., Davis, J.L. (1989), "Ground Penetrating Radar for Subsurface Environmental Applications", Presented at the Seventh Annual Thematic Conference on Remote Sensing for Exploration Geology, Calgary, Alberta, Canada, October.

[ROSS91] Personal Communication, Dr. J.R. Rossiter (1991), April.

[RUME86a] Rumelhart, D.E., Hinton, G.E. and Williams, R.J. (1986), *Parallel Distributed Processing: Explorations in the Microstructure of Cognition*, Vol. I and II, MIT Press.

[RUME86b] Rumelhart, D.E., McClelland, J.L. and the PDP Research Group (1986), *Parallel Distributed Processing*, Vol. I and II, MIT Press.

[RYEL72] Ryell, J. and Richardson, B. (1972), "Cracks in Concrete Bridge Decks and their Contributions to Corrosion of Reinforcing Steel and Prestressing

Cables", Report IR-51, Ontario Ministry of Transportation and Communications, September.

[RYEL67] Ryell, J. and Smith, P. (1967), "Case Histories of Poor Durability of Concrete in Ontario Highway Structures", Report IR-03, Ontario Ministry of Transportation and Communications, June.

[SAND78] Sander, K.F. and Reed, G.A. (1978), *Transmission and Propagation of Electromagnetic Waves*, Cambridge University Press.

[SHOR76] Shortliffe, E.M. (1976), *Computer-based medical consultations: MYCIN*, New York: American Elsevier.

[SKOL90] Skolnik, M. (1990), *Radar Handbook*, Second Edition, McGraw-Hill Publishing Company.

[SMIT62] Smith, P. (1962), "Observations on Protective Surface Coatings for Exposed or Asphaltic Surface Concrete", Report RR-027, Ontario Ministry of Transportation and Communications.

[STEI81] Steinway, W.J., Echard, J.D. and Luke, C.M. (1981), "Locating Voids Beneath Pavement Using Pulsed Electromagnetic Waves", National Cooperative Highway Research Program Report 237, Transportation Research Board, National Research Council, Washington, D.C., November.

[STOL86] Stolt, R.H. and Benson, A.K. (1986), *Handbook of Geophysical Exploration, Section 1, Seismic Exploration, Volume 5, Seismic Migration Theory and Practice*, Geophysical Press.

[STON90] Stone, W.R. (1990), *Radar Cross Sections of Complex Objects*, IEEE.

[TIEX87] —— (1987), "MicroExplorer Technical Summary", Texas Instruments Inc., Austin, Texas, USA, June.

[BEEK67] Van Beek, L.K.H. (1967), "Dielectric Behaviour of Heterogeneous Systems", Progress in Dielectrics, No. 7, pp 69-114, Heywood Books, London, England.

[VINC67] Vincent, P. (1967), "Deterioration of Reinforcing Steel in Concrete Structures", Report ME-67-01, Ontario Ministry of Transportation and Communications, September.

[WAIT81] Wait, J.R. (1981), *Wave Propagation Theory*, Pergamon Press.

[WOOD91] Personal Communication, Dave Wood (1991), November.

[YOLL67] Yolles, M.S. and Smith, P. (1967), "Unknown Properties of Your Concrete", Report IR-16, Ontario Ministry of Transportation and Communications, April.

[ZAHN79] Zahn, M. (1979), *Electromagnetic Field Theory: A Problem Solving Approach*, John Wiley and Sons.